UNIVERSITY OF CALIFORNIA, SAN DIEGO

Self-assembling Functionalized Single-walled Carbon Nanotubes

A Dissertation submitted for partial satisfaction of the requirement for the degree

Doctor of Philosophy

in

Engineering Sciences (Mechanical Engineering)

by

Yan Gao

Committee in charge:

Professor Sia Nemat-Nasser, Chair
Professor Yitzhak Tor
Professor Gaurav Arya
Professor Prabhakar R. Bandaru
Professor Richard K. Herz

2011

The Dissertation of Yan Gao is approved and it is acceptable in quality and form for publication on microfilm and electronically:

Chair

University of California, San Diego

2011

DEDICATION

To my wife, Yifeng Zhang, for everything she has done for me.

To my parents and my sister who consistently supported me in my life.

TABLE OF CONTENTS

LIST OF ABBREVIATIONS

$CDCl_3$	Deuterated Chloroform
CEAM	Center of Excellence for Advanced Materials
CNT	Carbon Nanotube
CVD	Chemical Vapor Deposition
DCM	Dichloromethane
DMAP	4-dimethylaminopyridine
DMF	N,N-dimethylformamide
DMSO-d_6	Dimethyl-d6 Sulfoxide
EtOAc	Ethyl Acetate
EtOH	Ethanol
ESI-MS	Electrospray Ionisation-Mass Spectrometry
FT-IR	Fourier Transform Spectroscope
HEG	Hexa-ethylene Glycol
HER	Hydrophilic End Region
HSR	Hydrophobic Sidewall Region
IPMC	Ionic Polymer Metal Composite
MC	Monte Carlo
MWCNT	Multi-walled Carbon Nanotube
NMR	Nuclear Magnetic Resonance
NVT	Canonical Ensemble
OPLS	Optimized Potentials for Liquid Simulations

PdC	Palladium on carbon catalyst
PEG	Polyethylene Glycol
PME	Particle Mesh Ewald Algorithm
PMF	Potential of Mean Force
PPh_3	Triphenylphosphine
SEM	Scanning Electron Microscope
SWCNT	Single-walled Carbon Nanotube
TEM	Transmission Electron Microscope
THF	Tetrahydrofuran
TsCl	4-toluenesulfonyl Chloride
VDW	Van Der Waals
VE	Volume Element

LIST OF FIGURES

LIST OF TABLES

LIST OF SCHEMES

ACKNOWLEDGEMENT

First and foremost, I thank my advisor, Professor Sia Nemat-Nasser. Without his academic passion and selfless support, I could not have achieved what I have today. I have been inspired by his dedication to teaching, and the numerous contributions he continues to make in many diverse fields of science. Through working with him, I have been exposed to a wide range of research frontiers which are more than the materials included in this dissertation. I also thank my committee members Prof. Yitzhak Tor, Prof. Gaurav Arya, Prof. Prabhakar Bandaru and Prof. Richard Herz for their personal commitments and technical contributions.

I would like to express my gratitude to all with whom I have worked at the Center of Excellence for Advanced Materials, especially Prof. Yitzhak Tor's lab, and Prof. Gaurav Arya's lab, over the course of my research. In particular, I am grateful to Dr. Tam Victor and Dr. S. G. Srivatsan for the many helpful discussions regarding chemical synthesis. I wish to acknowledge Mason Mackey for many helpful discussions regarding the electron tomography procedure. I am very appreciative toward Dr. Alireza V. Amirkhizi for many helpful discussions regarding the Gibbs free energy analysis. I am indebted to Dr. Arijit Maitra for providing his molecular simulation codes for me to build the Monte Carlo integrator upon, and for many helpful discussions regarding the molecular modeling and numerical simulations. I would also like to acknowledge Jon Isaacs and Lauri Jacobs-Cohantz who went to

extraordinary efforts to assist me every time I looked for help. Finally, I am grateful to all my friends for their unwavering support and confidence in me.

Chapter 2 is prepared for publication by S. Nemat-Nasser, Y. Gao and Y. Tor. The dissertation author was the primary investigator and author of this paper. This work has been conducted at the Center of Excellence for Advanced Materials, CEAM, Department of Mechanical and Aerospace Engineering, University of California, San Diego, and has been supported by the Air Force Office of Scientific Research Grant Number N0001404M0164.

Chapter 3 is prepared for publication by S. Nemat-Nasser, Y. Gao and Y. Tor. The dissertation author was the primary investigator and author of this paper. This work has been conducted at the Center of Excellence for Advanced Materials, CEAM, Department of Mechanical and Aerospace Engineering, University of California, San Diego, and has been supported by the Air Force Office of Scientific Research Grant Number N0001404M0164.

Chapter 4 is prepared for publication by S. Nemat-Nasser, Y. Gao and Y. Tor. The dissertation author was the primary investigator and author of this paper. This work has been conducted at the Center of Excellence for Advanced Materials, CEAM, Department of Mechanical and Aerospace Engineering, University of California, San Diego, and has been supported by the Air Force Office of Scientific Research Grant Number N0001404M0164.

VITA

2002	Bachelor of Science in Mechanical Engineering, Tsinghua University, Beijing, P.R.CHINA
2005	Master of Science in Engineering Sciences, Materials Science, Tsinghua University, Beijing, P.R.CHINA
2008	Master of Science in Engineering Sciences, Mechanical Engineering, University of California, San Diego
2010	Doctor of Philosophy in Engineering Sciences, Mechanical Engineering, University of California, San Diego

PUBLICATIONS

ARCHIVAL JOURNALS

Y. Gao, Z. Wang, Q. Ma, G. Tang and J. Liang (2004). "A study on the wear resistance of nano-material/E51." Mater. Sci. Technol., Vol.20(3), 340-343.

Z. Wang, Y. Gao, Q. Ma and L. Wang (2004). "Study on the wear resistance of MWCNTs/E51 composite coating." Surf. Tchnol., Vol.5, 30-32. (In Chinese)

Y. Gao, Z. Wang, R. Wang, J. Liang and L. Wang (2006). "Preparation and characterization of MWCNTs/E44." J. Mater. Sci. Technol., Vol.22(1), 117-122.

OTHER PROCEEDINGS

Y. Gao, S. Nemat-Nasser and Y. Tor (2009). "Self-assembling single-walled carbon nanotubes." SPIE Proc. on Smart Structures/NDE, 7287-90.

ABSTRACT OF THE DISSERTATION

Self-assembling Functionalized Single-walled Carbon Nanotubes

by

Yan Gao

Doctor of Philosophy in Engineering Sciences (Mechanical Engineering)

University of California, San Diego, 2011

Professor Sia Nemat-Nasser, Chair

Single-walled carbon nanotubes (SWCNTs) are promising bottom-up building materials due to their superior properties. However, the lack of an effective method to arrange large quantities of SWCNTs poses an obstacle toward their applications. Existing studies to functionalize, disperse, position, and assemble SWCNTs provide a broad understandings regarding SWCNTs behavior, especially in aqueous electrolyte solution. Inspired by ionic polymer metal composite (IPMC) materials, this dissertation envisions fabrication of orderly SWCNTs network structure via their ionic clustering-mediated self-assembly. SWCNTs tend to bundle together due to inter-

nanotube VDW attractions, which increase with nanotube length. The author seeks short SWCNTs with long chain molecules bearing ionic termini to facilitate debundling and self-assembly in aqueous electrolyte solution through end-clustering. First, a simple model was applied based on essential physical factors. The results indicated that SWCNTs must be shorter than ~100 nm to achieve stable network structures. Experiments were then carried out based upon the results. Short SWCNTs (50-100 nm) were end-functionalized with hexaethylene glycol (HEG) linkers bearing terminal carboxylate anions. Both 2D and 3D network structures were observed after placing the functionalized SWCNTs in aqueous electrolyte (sodium ion). The network structures were characterized by microscopic and spectroscopic methods. A novel approach was applied via electron tomography to study the 3D structures of SWCNTs structure in aqueous electrolyte. Free energy analysis of the SWCNTs network structure was implemented with the assistance of both analytical tools and molecular simulations. The results indicate that, when a cluster is formed by three functionalized SWCNTs ends, the resulting network structure is most stable. Indeed, 72% of the clusters/joints were formed by three nanotubes, as observed in experiments. Finally, Monte Carlo simulations of coarse-grained SWCNTs were implemented to understand the behavior of SWCNTs. SWCNTs clusters were observed as a result of this simulation.

Chapter 1

Introduction

1.1. A review of single-walled carbon nanotubes (SWCNTs) and their self-assembly

1.1.1 Single-walled carbon nanotubes

Carbon nanotubes (CNTs) are carbon-based tubular materials. Their diameters vary from sub-nanometer to tens of nanometers, while their lengths can be as long as millimeters. The single-walled carbon nanotube (SWCNT), simple in structure, is composed of a single graphene sheet rolled up into a tube approximately one millionth the diameter of a human hair. A multi-walled carbon nanotube (MWCNT), as named, contains multiple coaxial layers of rolled-up graphene sheets. From an application point of view, in comparison to MWCNTs, SWCNTs have more uniform structures. SWCNTs can be either metallic or semiconducting depending on the chiralities.

1.1.2 SWCNTs synthesis

SWCNTs have been produced via three major approaches (Figure 1.1): chemical vapor deposition (CVD) (Kong *et al*., 1998), arc-discharge (Ebbesen and

Ajayan, 1992), and laser ablation (Thess *et al*., 1996). In the CVD method, reaction of amorphous carbon with transition metals is known to generate stable or metastable carbides, which graphitize at higher temperatures (Oberlin *et al*., 1976; Bethune, 2002; Sinclair *et al*., 2002). This reaction involves the dissolution of carbon in the metal to form a supersaturated solution, followed by the precipitation of crystalline graphite. The reaction temperature varies depending on the transition metal. Fe, Ni and Co, for example, graphitize amorphous carbon at 400–500 ºC. The graphite forms sheets when the metal is a thin film. When the metal is in the form of nano-sized particles, carbon nanotubes grow (Iijlma, 1991; Bethune *et al*., 1993; Yudasaka *et al*., 1993). The growth mechanism has been studied extensively and remains an active research field (Charlier *et al*. 2001). In a study of carbon nanotube growth from methane decomposition at 500–540 ºC on Ni nanocrystals (5–20 nm diameters), Helveg *et al*. (2004) observed that nucleation and growth of the graphene layers occurred during a dynamic formation and restructuring of mono-atomic step edges on the Ni surface. The observation was enabled using an *in situ* transmission electron microscope (TEM).

In the arc-discharge approach, a carbon source is evaporated in helium plasma ignited by high currents passed through the carbon anode and carbon cathode. The nanotube diameter depends on the composition of helium and argon, due to their different thermal conductivities and diffusion coefficients.

In the laser-ablation approach, a short and intense laser is employed to ablate a target in an oven heated to approximately 1200 ºC. The target carbon source usually

contains 0.5%–2.5% metallic catalysts such as nickel and cobalt. Inert gas flow is applied to ensure the collection of produced nanotubes on the cold finger of the oven. The laser ablation has similar characteristics with arc-discharge. The catalyst metals can be sputtered onto a substrate, followed by either chemical etching or thermal annealing to induce the catalysts nucleation.

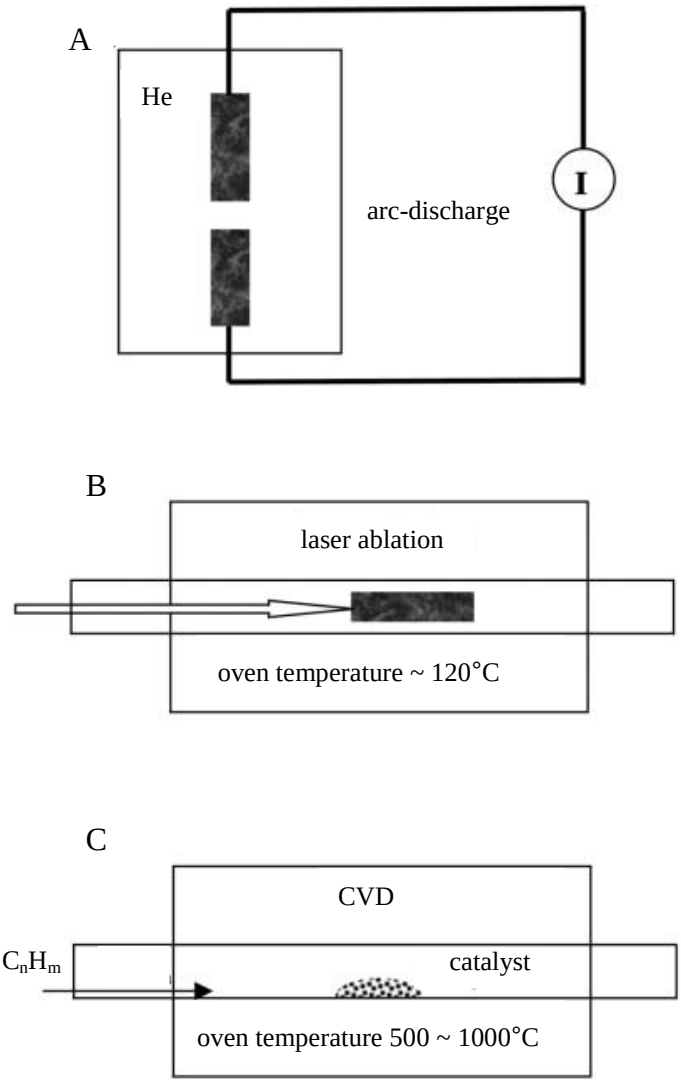

Figure 1.1. Schematic experimental setups for nanotube growth methods (Dai, 2001).

As-synthesized SWCNTs usually contain impurities, such as metal catalyst particles and amorphous carbon. Various purification procedures have been developed to remove these impurities. Popular methods include acid treatment, annealing, ultrasonication and microfiltration. The mass yield of nanotubes after purification varies from 10% to 50%, according to the literature (Rinzler *et al*., 1998; Dillon *et al*., 1999). SWCNT characterization can be performed using various established methods, such as electron microscopy, X-ray, thermogravimetry analysis, Fourier transform spectroscopy (FTIR), Raman spectroscopy, etc.

One of the most significant morphological characteristics of carbon nanotubes is their strong van der Waals aggregation. As-synthesized CNTs are 3–5 μm long (Liu *et al*., 1998). SWCNTs with lengths exceeding 10 mm are obtained in certain chemical vapor deposition (CVD) methods of growing on substrates (Doorn *et al*., 2005). The nanotubes aggregate within the growth chamber, forming random networks of hexagonal packed structures, together with residual amorphous carbon and metal particles (Liu *et al*., 1998). High order aggregation is observed as precipitation of purified nanotubes from stable dispersions (Gennett *et al*., 2000; Sano *et al*., 2002). The intertube interaction between CNTs is weaker than the interlayer interaction within a MWCNT (Kataura *et al*., 2000; Zacharla *et al*., 2004).

1.1.3 SWCNTs structure and properties

The molecular structure of the carbon nanotube determines its properties. The molecular structure of a single-walled carbon nanotube is described by its chirality, as

illustrated in Figure 1.2 (Iijima and Ichihashi, 1993; Hamada *et al*., 1992). Rolling up the sheet to superimpose the lattice point (n , m) on the origin (0,0) generates the SWCNT structure of chirality (n , m), where m and n are indicated as the chiral indices. A chiral vector, $\vec{\mathbf{C}}$, is defined with m and n.

$$\vec{\mathbf{C}} = n\vec{\mathbf{a}}_1 + m\vec{\mathbf{a}}_2 \tag{1}$$

$\vec{\mathbf{a}}_1$ and $\vec{\mathbf{a}}_2$ are unit vectors with equivalent magnitude equal to the lattice constant a =0.246 nm. Note that $\vec{\mathbf{C}}$ is perpendicular to the axis of the rolled up single-walled carbon nanotube.

The diameter of a single-walled carbon nanotube is a function of m and n. For example, a (10,10) SWCNT has a diameter of 1.357 nm.

$$D = \frac{a}{\pi}\sqrt{n^2 + mn + m^2} \tag{2}$$

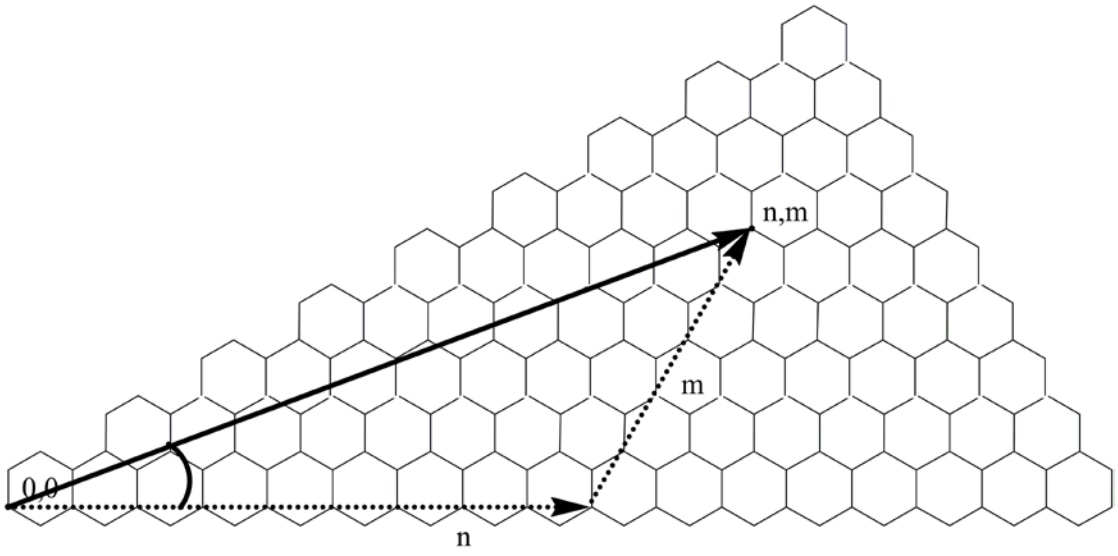

Figure 1.2. A graphene sheet segment. A lattice point (m,n) is noted with respect to the origin (0,0). Superimposing the lattice point and the origin results in the structure of a (m,n) SWCNT.

According to the rolling directions, SWCNTs are referred to as zigzag, armchair or chiral. If m =0, the nanotube is called 'zigzag'. If $m = n$, the nanotube is called 'armchair'. Otherwise, the nanotube is called 'chiral'. Schematic SWCNT models of different chiralities are drawn in Figure 1.3.

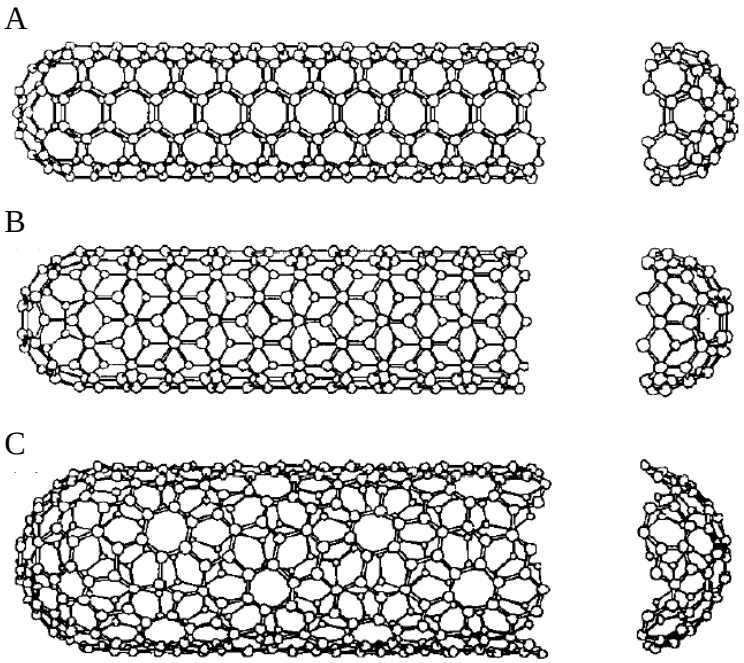

Figure 1.3. By rolling up a graphene sheet as a cylinder and capping each end of the cylinder with half of a fullerene molecule, a "fullerene-derived tubule," one layer in thickness, is formed. Shown here is a schematic theoretical model for a SWCNTs with chiralities (n,m) of (A) (5,5), armchair, (B) (9,0), zigzag, and (C) (10,5), chiral (Dresselhaus *et al*., 1995).

The special topological structure of SWCNTs results in interesting electronic band structures. Consider the band structure of a graphene sheet, the conducting properties follow from the nature of its electronic states near the Fermi energy, which is the energy of the highest occupied quantum state at absolute zero temperature. The electronic band structure of graphene lies between that of metals and semiconductors.

Metals have many states that can freely propagate through the crystal lattice at Fermi energy. Semiconductors have an energy gap with no electronic states near Fermi energy. Graphene is a semi-metal, given its valence and conduction bands touch each other only at six corners (K_B) of the hexagonal first Brillouin zone (Figure 1.4). The Fermi surface of the graphene sheet is reduced to these six points. This structure is fundamental to the electronic properties of SWCNTs (Ouyang *et al*., 2002). One of the important outcomes of this structure is conductance criteria. When $(n-m)/3$ is an integer, the SWCNT is metallic; otherwise a SWCNT is semiconducting.

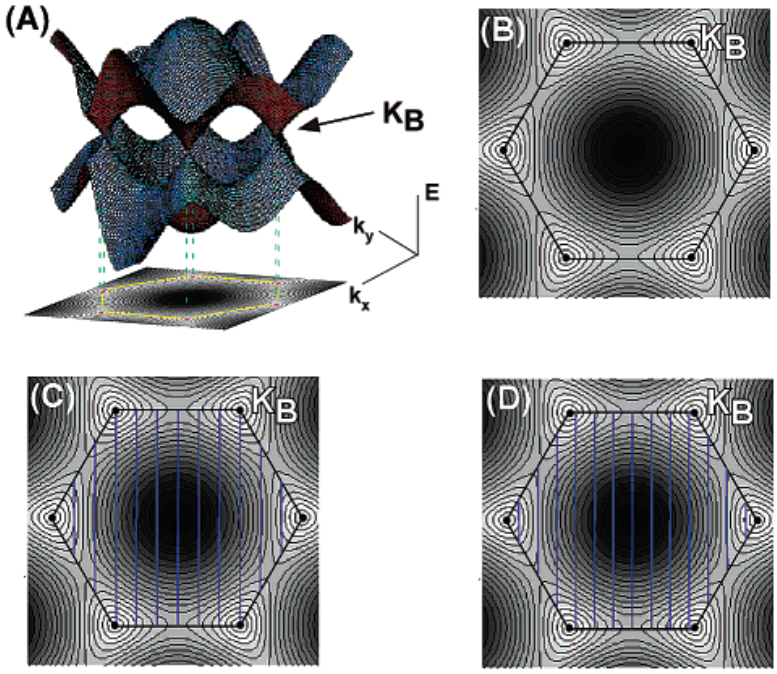

Figure 1.4. (A) Three-dimensional plot of the π and π* graphene energy bands and (B) a 2D projection. (C) Allowed 1D wavevectors for a metallic (9,0) SWNT. (D) Allowed 1D wavevectors for a semiconducting (10,0) tube. The black hexagons define the first Brillouin zone of a graphene sheet, and the black dots in the corners are the KB points. Blue lines represent allowed wavevectors, k, within the first Brillouin zone (Ouyang *et al*., 2002).

Density of state (DOS) for both metallic and semiconducting nanotubes has been derived by Mintmire and White (1998).

$$\rho(E) = \frac{\sqrt{3}}{\pi^2} \frac{1}{V_{pp\pi}} \frac{a_c}{r} \sum_{m=-\infty}^{+\infty} g(E, \varepsilon_m) \tag{3}$$

Here a_c =1.4 nm, the distance between carbon atoms, r is the nanotube radius, and $V_{pp\pi}$ =2.5 eV is the π-bond tight-binding parameter. The one-dimensional (1D) sub-bands are designated with index m and energy ε_m.

$$g(E, \varepsilon_m) = \begin{cases} |E| \Big/ \sqrt{E^2 - \varepsilon_m^2}, & |E| > |\varepsilon_m| \\ 0, & |E| > |\varepsilon_m| \end{cases} \tag{4}$$

Figure 1.5 shows the DOS for semiconducting and metallic nanotubes (Mintmire and White, 1998). The specific DOS characteristics result in SWCNTs rich optical properties, which have been used to identify the composition of bulk nanotube samples, and to evaluate SWCNTs purities (Bachilo *et al.*, 2002).

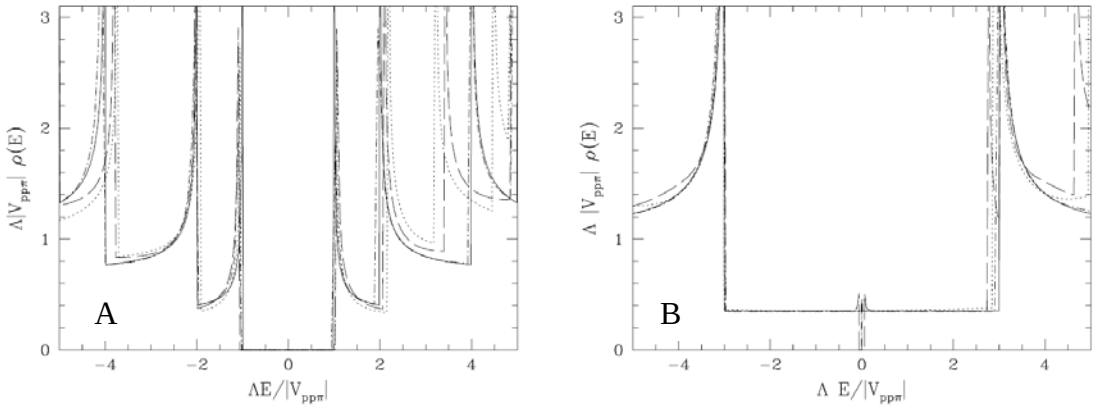

Figure 1.5. Comparison of scaled first-principles DOS results with universal relationship from equation (3). (A) Semiconducting SWCNT. (B) Mettalic SWCNT. Solid line depicts universal DOS for semiconducting nanotubes neglecting curvative effects (Mintmire and White, 1998).

At low temperatures, several interesting phenomena have been discovered for the 1D SWCNTs, such as Coulomb blockades and resonant tunneling (Ferry and Goodnick, 1997; Yao *et al*., 2001). Some fundamental questions remain under investigation regarding nanotube-nanotube contact barriers, nanotube-metal contact, and resistance scaling along nanotube length.

Aside from unique electronic properties and optical properties, SWCNTs have superior mechanical characteristics. SWCNTs are very stiff and strong, with Young's modulus ~ 1 TPa (Dujardin *et al*., 1998). Typically, a 1.4 nm diameter SWCNT has about 50 carbon atoms around its circumference. A similar number of covalent C-C bonds, which are very strong, must be broken to break a nanotube.

1.1.4 Applications and challenges

Due to the above-mentioned characteristic properties, SWCNTs have attracted tremendous interest. Many investigations have been carried out to explore their applications in multiple areas, such as electrochemical devices (Niu *et al*., 19997), field emission devices (Lee *et al*., 2001), drug delivery vehicles (Klumpp *et al*., 2006), electronic devices (Tans *et al*., 1998), sensors and actuators (Kong *et al*., 2000), and structural composites (Ramanathan *et al*., 2005).

Despite the attractive potential, several major challenges impede SWCNTs applications, such as mass production with controlled properties, effective purification and separation techniques, and effective mass manipulation methods. Among these

obstacles, an effective method for large-scale manipulation of SWCNTs is the most important step toward practical application in the factory.

1.1.5 Carbon nanotubes self-assembly

Due to SWCNTs small dimensions, it is very inefficient to manipulate nanotubes individually. Assembly or self-assembly of multiple SWCNTs into useful architectures, on the other hand, has attracted substantial attention. The SWCNTs assembly can be categorized into synthetic approaches and post-synthetic approaches (Yan *et al*., 2007).

In the synthetic approaches, assembled SWCNTs are fabricated by controlling the environments in which they grow. Introduction of an electric field to a CVD system has been demonstrated to promote the parallel growth of MWCNTs and SWCNTs on substrates (Zhang *et al*., 2001; Joselevich *et al*. 2002; Bandaru *et al*., 2004). For example, Joselevich *et al*. (2002) have synthesized electric field-induced SWCNTs arrays on a substrate by the CVD method using ethylene and methane as carbon sources. The electric-field-induced dipole moments, originating from high anisotropic polarizability of a long SWCNT, is believed to provide the aligning driving forces to the nanotubes (Nojeh *et al*., 2004). Template assisted SWCNT patterns have also been synthesized by Dai's group (Cassell *et al*., 1999; Franklin and Dai, 2000). They applied contact printing techniques to selectively deposit liquid Fe/Mo-based catalyst precursors on top of a silicon tower array. Calcination of the catalyst precursor, followed by CVD with methane, resulted in the SWCNTs

architectures that consist of suspended nanotube lines connecting adjacent silicon towers.

Post synthetic approaches typically manipulate SWCNTs after their fabrication. Nan *et al*. (2002) assembled carboxylic acid-functionalized SWCNTs onto a gold-particle-patterned substrate pretreated with $NH_2(CH_2)_{11}$. The linkage was established through amidation. Various other pattern-assisted approaches appear in the literature. In another approach, Garmestani and co-workers (2003) have demonstrated a polymer-mediated method for the parallel alignment of SWCNTs under a magnetic field. The nanotubes were dispersed ultrasonically in a liquid epoxy resin, and the mixture was subject to a magnetic field of 15 or 25 T for 2h at room temperature before it was cured. Flow-guided parallel alignment was also reported (Jin *et al*., 1998).

1.2. Motivation from ionic polymer metal composite (IPMC) materials and objectives for this dissertation

Existing SWCNTs assembly approaches, however, are generally unidirectional. Most methods applied a universal guiding force to drive all nanotubes to align in a certain direction. Individual nanotubes are independent of each other. An interconnected SWNTs network architecture, on the other hand, could better utilize the superior properties, such as strength, of the 1D material. However, the interconnection of nanotubes requires a local driving force capable of joining nanotubes together on

the nanoscale, which is very different for existing driving forces which were applied in a universal fashion.

Nemat-Nasser and co-workers (2000) fabricated ionic polymer metal composite (IPMC) materials as bending actuators and sensors. A typical IPMC consists of a thin (200 μm) polymer membrane with metal electrodes (5–10 μm thick) plated on both faces (Figure 1.6). The polyelectrolyte matrix is neutralized with a quantity of counter-ions, balancing the charge of anions covalently fixed to the membrane. When an IPMC in the solvated (i.e., hydrated) state is stimulated with a suddenly applied small step-potential (1–3 V, depending on the solvent), both the fixed anions and mobile counter-ions are subjected to an electric field, with the counter-ions capable of diffusion toward one of the electrodes. As a result, the composite undergoes an initial fast bending deformation, followed by a slow relaxation, either in the same or opposite direction, depending on the composition of the backbone ionomers and the nature of the counter-ion. The backbone amphiphilic ionomer can be perfluoro-sulfonate, e.g., Nafion-117® (DuPont, 0.18 mm thick, 1100 g/mol of equivalent weight), or it can be perfluoro-carboxylate, e.g., Flemion-1.44® (Asahi Glass, 0.14 mm thick, 690 g/mol of equivalent weight). The counter ions that have been used include alkali metals, i.e., Li^+, Na^+, K^+, Rb^+, and Cs^+, as well as multivalent cations such as Mg^{2+} and Al^{3+}.

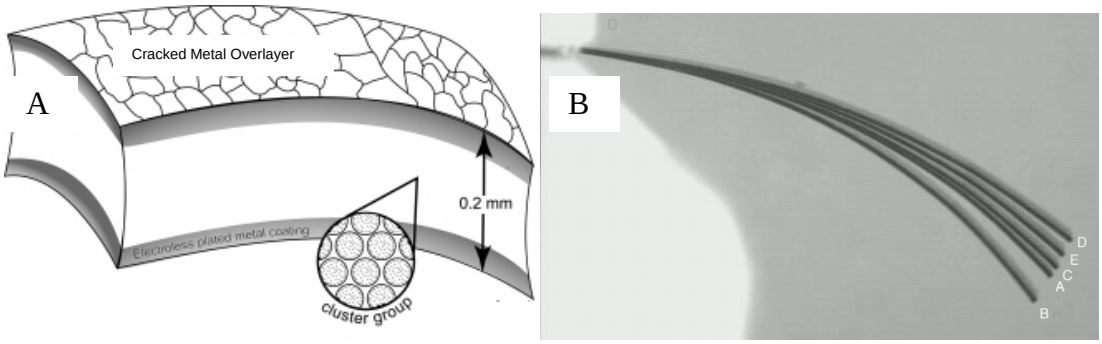

Figure 1.6. (A) IPMC schematics indicating surface morphology, interface, and cluster structure (Nemat-Nasser and Thomas, 2001). (B) Actuation of a K^+-form Nafion-based IPMC under 1V DC; from A to B fast initial motion, from B to C slow relaxation, from C to D fast motion upon shorting, and from D to E slow final relaxation (Nemat-Nasser, 2002).

The driving force of IMPC actuation and sensing comes from the electro-chemo-mechanical characteristics of the cluster units in the polyelectrolyte matrix. Nemat-Nasser (2002) modeled the mechanism in a cluster setting (Figure 1.7). The hydrophobic backbone fluorocarbon polymer is separated from the hydrophilic clusters. The anions within the clusters are attached to the fluorocarbon matrix, while under suitable conditions the associated unbound cations may move within the water that permeates the interconnected clusters. Under an electric field, cations redistribute and migrate toward the cathode. This redistribution produces several significant changes in the local properties of the composite that are specific to the anode and cathode. These changes form the basis for the model of IPMC actuation, and are suitable for explaining the observed actuation and subsequent relaxation of IPMC materials.

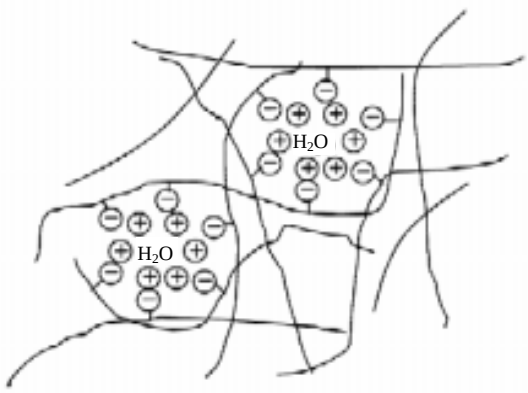

Figure 1.7. Schematic depiction of polymer domains within IPMC materials (Nemat-Nasser, 2002).

Motivated by the IPMC material, this dissertation seeks utilization of ionic force as the driving force to join SWCNTs into network structures in aqueous electrolyte. To promote SWCNTs self-assembly, this work focuses on fabrication of amphiphilic 1D SWCNTs having end-attached ions and a hydrophobic body.

1.3. Outline

Analytical tools, chemical fabrications and molecular modeling are used to predict, fabricate and analyze the SWCNTs self-assembly behavior, respectively. The reminder of the dissertation is organized as follows:

Chapter 2 discusses the SWCNTs behavior in aqueous electrolyte, suggesting that ionic clustering of end-functionalized SWCNTs is a key step in their assembly. A simple model is introduced to analyze the state change of SWCNTs from bundled status to clustered status.

Chapter 3 presents fabrication methods of SWCNTs' network via their self-assembly. Both two-dimensional (2D) and three-dimensional (3D) structures are observed. The characterization of the resulting network structure is then outlined, and the results are discussed.

Chapter 4 describes the material characterization methods used in Chapter 3, with an emphasis on the novel application of electron tomography method to study 3D structures of SWCNTs.

Chapter 5 presents a systematic free energy study of the network structure formed by SWCNTs. A numerical method using molecular models is applied to assist the study. The theoretical result is compared in high agreement with experimental observations.

Chapter 6 concludes the dissertation, and comments on the future work.

1.4. References

J. Kong, A. M. Cassella and H. Dai (1998). "Chemical vapor deposition of methane for single-walled carbon nanotubes." Chem. Phys. Lett., Vol.292, 567-574.

T. W. Ebbesen and P. M. Ajayan (1992). "Large-scale synthesis of carbon nanotubes." Nature, Vol.358, 220-222.

A. Thess, R. Lee, P. Nikolaev, H. Dai, P. Petit, J. Robert, C. Xu, Y. H. Lee, S. G. Kim, A. G. Rinzler, D. T. Colbert, G. E. Scuseria, D. Tomanek, J. E. Fischer and R. E. Smalley (1996). "Crystalline Ropes of Metallic Carbon Nanotubes." Science, Vol.273(5274), 483-487.

A. Oberlin, M. Endo and T. Koyama (1976). "Filamentous growth of carbon through benzene decomposition." Carbon, Vol.14, 335-349;

D. S. Bethune (2002). "Carbon and Metals: a Path to Single-Wall Carbon Nanotubes." Physica B, Vol.323, 90-96.

R. Sinclair, T. Itoh and R. Chin (2002). "In Situ TEM Studies of Metal–Carbon Reactions." Microsc. Microanal., Vol.8, 288-304.

S. Iijima (1991). "Helical microtubules of graphitic carbon." Nature, Vol.354, 56-58.

D. S. Bethune, C. H. Klang, M. S. de Vries, G. Gorman, R. Savoy, J. Vazquez and R. Beyers (1993). "Cobalt-catalysed growth of carbon nanotubes with single-atomic-layer walls." Nature, Vol.363, 605-607.

M. Yudasaka, R. Kikuchi, Y. Ohki, E. Ota and S. Yoshimura (1997). "Behavior of Ni in carbon nanotube nucleation." Appl. Phys. Lett. Vol.70(14), 1817-1818.

J. C. Charlier, S. Iijima (2001). "Topics in Applied Physics." Springer-Verlag, Berlin.

S. Helveg, C. Lopez-Cartes, J. Sehested, P. L. Hansen, B. S. Clausen, J. R. Rostrup-Nielsen, F. Abild-Pedersen and J. K. Norskov (2004). "Atomic-scale imaging of carbon nanofibre growth." Nature, Vol.427, 426-429.

H. Dai (2001). "Topics in Applied Physics." Springer-Verlag, Berlin.

A. G. Rinzler, J. Liu, H. Dai, P. Nikolaev, C. B. Huffman, F. J. Rodriguez-Macias, P. J. Boul, A. H. Lu, D. Heymann, D. T. Colbert, R. S. Lee, J. E. Fischer, A. M. Rao, P. C. Eklund and R. E. Smalley (1998). "Large-scale purification of single-wall carbon nanotubes. Process, product, and characterization." Appl. Phys. A, Vol.67(1), 29-37.

A. C. Dillon, T. Gennett, K. M. Jones, J. L. Alleman, P. A. Parilla and M. J. Heben (1999). "A Simple and Complete Purification of Single-Walled Carbon Nanotube Materials." Adv. Mater., Vol.11, 1354–1358.

J. Liu, A. G. Rinzler, H. Dai, J. H. Hafner, R. K. Bradley, P. J. Boul, A. Lu, T. Iverson, K. Shelimov, C. B. Huffman, F. Rodriguez-Macias, Y. Shon, T. R. Lee, D. T. Colbert and R. E. Smalley (1998). "Fullerene Pipes." Science, Vol.280, 1253-1256.

S. K. Doorn, M. J. O'Connell, L. Zheng, Y. T. Zhu, S. Huang, J. Liu (2005). "Raman spectral imaging of a carbon nanotube intramolecular junction." Phys. Rev. Lett., Vol.94(1), 016802/1-016802/4.

Gennett, T.; Dillon, A. C.; Alleman, J. L.; Jones, K. M.; Hasoon, F. S.; Heben, M. J. Formation of Single-Wall Carbon Nanotube Superbundles. Chemistry of Materials (2000), 12(3), 599-601.

Sano, Masahito; Kamino, Ayumi; Okamura, Junko; Shinkai, Seiji. Noncovalent self-assembly of carbon nanotubes for construction of "cages". Nano Letters (2002), 2(5), 531-533.

H. Kataura, Y. Maniwa, S. Masubuchi, S. Kazama, X. Zhao, Y. Ando, Y. Ohtsuka, S. Suzuki, Y. Achiba and R. Saito (2000). "Bundle effects of single-wall carbon nanotubes." AIP Conf. Proc.Vol.544, 262-265.

R. Zacharia, H. Ulbricht and T. Hertel (2004). "Interlayer cohesive energy of graphite from thermal desorption of polyaromatic hydrocarbons." Phys. Rev. B, Vol.69(15), 155406/1-155406/7.

S. Iijima and T. Ichihashi (1993). "Single-shell carbon nanotubes of 1-nm diameter." Nature, Vol.363, 603-605.

N. Hamada, S. Sawada and A. Oshiyama (1992). "New one-dimensional conductors: Graphitic microtubules." Phys. Rev. Lett., Vol.68, 1579–1581.

M. S. Dresselhaus, G. Fresselhaus and R. Saito (1995). "Physics of Carbon Nanotubes." Carbon, Vol.33, 883–891.

M. Ouyang, J. Huang and C. Lieber (2002). "Fundamental Electronic Properties and Applications of Single-Walled Carbon Nanotubes." Acc. Chem. Res., Vol.35(12), 1018-1025.

J. W. Mintmire and C. T. White (1998). "Universal Density of States for Carbon Nanotubes." Phys. Rev. Lett., Vol.81, 2506–209.

S. M. Bachilo, M. S. Strano, C. Kittrell, R. H. Hauge, R. E. Smalley and R. B. Weisman (2002). "Structure-Assigned Optical Spectra of Single-Walled Carbon Nanotubes." Science, Vol.298(5602), 2361-2366.

D. Ferry and S. Goodnick (1997). "Transport in Nanostructures." Cambridge Universtiy Press, New York.

Z. Yao, C. Dekker and P. Avouris (2001). "Topics in Applied Physics." Springer-Verlag, Berlin.

E. Dujardin, T. W. Ebbesen, A. Krishnan, P. N. Yianilos AND M. M. J. Treacy (1998). "Young's Modulus of Single-Walled Nanotubes." Phys. Rev. B, Vol.58(20), 14013-14019.

C. Niu, E. K. Sickel, R. Hoch, D. Moy, and H. Tennent (1997). "High power electrochemical capacitors based on carbon nanotube electrodes." Appl. Phys. Lett., Vol.70, 1480-1482.

N. S. Lee, D.S. Chung, I.T. Hana, J.H. Kang, Y.S. Choi, H.Y. Kim, S.H. Park, Y.W. Jin, W.K. Yi, M.J. Yun, J.E. Jung, C.J. Lee, J.H, You, S.H. Jo, C.G. Lee and J.M. Kim (2001). "Application of carbon nanotubes to field emission displays." Diamond Relat. Mater., Vol.10, 265-270.

C. Klumpp, K. Kostarelos, M. Prato and A. Bianco (2006). "Functionalized carbon

nanotubes as emerging nanovectors for the delivery of therapeutics." Biochimica

Et Biophysica Acta-Biomembranes, Vol.1758, 404-412.

S.J. Tans, R.M. Verschueren and C. Dekker (1998). "Room-temperature transistor based on a single carbon nanotube." Nature, Vol.393, 49-52.

J. Kong, N. R. Franklin, C. Zhou, M. G. Chapline, S. Peng, K. Cho and H. Dai (2000). "Nanotube Molecular Wires as Chemical Sensors." Science, Vol.287, 622-625.

T. Ramanathan, F. T. Fisher, R. S. Ruoff and L. C. Brinson (2005). "Functionalized SWNT/polymer nanocomposites for dramatic property improvement." J. Poly. Sci. B, Vol.43, 2269-2279.

Y. Yan, M. B. Chan-Park and Q. Zhang (2007). "Advances in carbon-nanotube assembly." Small, Vol.3, 24-42.

Y. G. Zhang, A. Chang, J. Cao, Q. Wang, W. Kim, Y. M. Li, N. Morris, E. Yenilmez, J. Kong and H. J. Dai (2001). "Electric-field-directed growth of aligned single-walled carbon nanotubes." Appl. Phys. Lett., Vol.79, 3155-3157.

E. Joselevich and C. M. Lieber (2002). "Vectorial Growth of Metallic and Semiconducting Single-Wall Carbon Nanotubes." Nano. Lett., Vol.2, 1137–1141.

L. H. Chen, J. F. AuBuchon, A. Gapin, C. Daraio, P. Bandaru, S. Jin, D. W. Kim, I. K. Yoo and C. M. Wang (2004). "Control of carbon nanotube morphology by change of applied bias field during growth." Appl. Phys. Lett., Vol.85(22), 5373-5375.

A. Nojeh, A. Ural, R. F. Pease and H. J. Dai (2004). "Electric-field-directed growth of carbon nanotubes in two dimensions." J. Vac. Sci. Technol. B, Vol.22, 3421-3425.

A. M. Cassell, N. R. Franklin, T.W. Tombler, E. M. Chan, J. Han and H. J. Dai (1999). "Directed Growth of Free-StandingSingle-Walled Carbon Nanotubes." J. Am. Chem. Soc., Vol.121, 7975-7976.

N. R. Franklin and H. J. Dai (2000). "An Enhanced CVD Approach to Extensive Nanotube Networks with Directionality." Adv. Mater., Vol.12, 890-894.

X. Nan, Z. Gu and Z. Liu (2002). "Immobilizing Shortened Single-Walled Carbon Nanotubes (SWNTs) on Gold Using a Surface Condensation Method.", J. Colloid Interface Sci., Vol.245, 311-318.

H. Garmestani, M. Al-haik, K. Dahmen, R. Tannenbaum, D. Li, S. S. Sablin and M. Hussaini (2003). "Polymer-mediated alignment of carbon nanotubes under high magnetic fields." Adv. Mater., Vol.15(22), 1918-1921.

L. Jin, C. Bower and O. Zhou (1998). "Alignment of carbon nanotubes in a polymer matrix by mechanical stretching." Appl. Phys. Lett., Vol.173, 1197-1199.

S. Nemat-Nasser and J. Y. Li (2000). "Electromechanical Response of Ionic Polymer-Metal Composites."J. Appl. Phys., Vol.87(7), 3321-3331.

S. Nemat-Nasser and C. Thomas (2001). "Ionomeric Polymer-metal Composites, , Electroactive Polymer (EAP) Actuators as Artificial Muscles - Reality, Potential and Challenges", Bar-Cohen (Eds), SPIE, Chp. 6, 139-191.

S. Nemat-Nasser (2002). "Micromechanics of Actuation of Ionic Polymer-Metal Composites." J. Appl. Phys., Vol.92(5), 2899-2915.

Chapter 2

Analytical Evaluation of CNTs Self-assembly Through Ionic Clustering

2.1. Introduction

The self-assembly process for single-walled carbon nanotubes (SWCNTs) in aqueous electrolyte solution consists of two important states: a bundled state and an interconnected state. The bundled state describes parallel nanotubes that are positioned very close to one another, where Van der Waals force is the primary driving force. The interconnected state represents nanotubes that are adjoined with each other through end clustering, where ionic interaction is the main driving force. A stable state of end-clustered SWCNTs is the key to forming interconnected network structures.

Carbon nanotube states in aqueous solution can be affected by various factors: length, diameter, chirality, number of walls, capped or uncapped ends, surface functionalization conditions, solvent properties, etc. Some factors can dominate over others in certain situations. For example, in aqueous solutions, raw carbon nanotubes will more likely form bundle precipitates instead of uniform dispersions. Dispersed carbon nanotubes, on the other hand, were observed by covalent (Saini *et al*., 1999,

Riggs *et al*., 2000), ionic (Chen *et al*., 2001; Vigolo *et al*., 2000) and shortening (Ziegler *et al*., 2005) modifications. The ionic force between nanotubes and solvent is regarded as a dominating force over the Van der Waals (VDW) force between bundled nanotubes to achieve the dispersion (Zhou *et al*., 2003; Matarredona *et al*., 2003; Li et *al*., 2003; Sano *et al*., 2001; Xu *et al*., 2005). Self-assembled structures by multiple nanotubes in water were also fabricated. Kubat *et al*. (2009) reported self-assembled sulfonic acid-functionalized SWCNTs in water in the presence of porphyrin moieties; however, the micro-level structures of the self-assembly were quite randomly orientated.

The relationship between nanotube behavior and associated physical parameters, such as nanotube length and solvent properties, is not well understood. Nemat-Nasser (2002) developed an ionic clustering model for ionic polymer metal composite (IPMC) materials wherein the author successfully related IPMC electrical-chemical-mechanical behavior to the ionic clustering between anion attached polymer chains and free counter cations. This chapter adopts the ionic clustering idea to study the nanotube behavior in aqueous solutions, attempting to provide insight to the fabrication of SWCNTs self-assembly. A better understanding of the mechanism of SWCNTs dispersion and self-assembly behaviors can also assist in their applications.

Chapter 2 is constructed as follows: First, VDW forces and ionic forces are addressed as the major competing counterparts. Then, single-walled carbon nanotubes in aqueous solution are discussed, and essential parameters are identified. A simple

model based on key parameters is introduced to study the phase change behavior of SWCNTs from bundle to cluster in aqueous electrolyte solution. The model is applied to a situation of interest for SWCNTs, and the results are outlined. Guidance from this simple model successfully led to the actual self-assembly of SWCNTs as observed with microscopes in Chapter 3. The length of self-assembled SWCNTs remarkably coincided with the range predicted by the model.

2.2. Overcoming Van der Vaals (VDW) attraction by ionic force

In network structures, carbon nanotubes interconnect with one another. The network characteristic requires that adjacent linear nanotubes have angular relationships with each other. However, a parallel bundled state is more favorable for raw carbon nanotubes. Carbon nanotubes have large surface area (Zuettel and Orimo, 2002). Furthermore, based upon their linear geometry, closely placed parallel CNTs can develop a high interstitial VDW attraction potential, given a large overlapping length. The VDW attraction is the main cause of the bundling of long CNTs (Tiano *et al.*, 2001). Raw SWCNTs are usually long and exist in bundled form. In order to prevent CNTs from bundling together, either a reduction of the VDW attraction or the provision of a competing force (or both) is required.

Ionic force has been indicated as an effective driving force against VDW force. Chen *et al*. (1998) reported covalently bound SWCNTs with octadecylamine and dispersed SWCNTs in carbon disulfide and dichrolobenzene. Hamon *et al*. (1999)

later described that SWCNT–COOH and octadecylamine (C_{18}–NH_2) form a soluble polyionic complex (SWCNTs–COO^- $H_3N^+C_{18}$). After this initial study, polyethylene glycol (Huang *et al.*, 2003), crown ethers (Kahn *et al*., 2002), and glucosamine (Pompeo *et al.*, 2002) were also covalently bound to SWCNTs for their dispersion in aqueous electrolytes.

2.3. Key physical factors affecting CNTs behavior in aqueous electrolyte solution

After many experimental studies of nanotube behavior in water, it is natural to extract essential physical factors from experimental observations that affect nanotube topological configuration in aqueous electrolyte solution.

2.3.1 Essential physical parameters

Nanotube length. Nanotube length is a crucial factor as its reduction leads to a decrease of maximum VDW attraction between nanotubes.

To achieve shorter lengths, raw long carbon nanotubes must be shortened. Single-walled carbon nanotubes are easier to cut with acid oxidation (Ziegler *et al*., 2005) as compared to multi-walled carbon nanotubes (MWCNTs). This work employs SWCNTs for the self-assembly.

Nanotube diameter. The present work sought to covalently attach ions to the ends of carbon nanotubes. Given an uncapped nanotube, each carbon atom at the end edge of the sidewall has a chance to be covalently functionalized. Hence, the number

of the possible functionalization sites at the nanotube end is defined by the diameter and chirality. To simplify the calculation, it is assumed that all the nanotubes are armchair.

Solvent dielectric constant. In this study, ionic force is considered to be the major driving force in SWCNTs self-assembly. The dielectric constant of the solvent has a significant effect because it represents the effectiveness of a solvent (water) to reduce the attraction between oppositely charged molecules by surrounding each charged species with a layer of molecules, allowing the charged species to coexist in solution (Bohinsky, 1987). Different ion concentrations lead to different dielectric constants. The properties of the ion pair are also important to the ionic interactions.

2.3.2 A simple model to study CNTs self-assembly

A simple model is introduced to understand the different states of SWCNTs in water. Consider carbon nanotubes in aqueous electrolyte solution. Each nanotube is end-functionalized with terminal anionic chain functionalities. Counter cations exist in the solution to balance the total charge. Consider the simple cases illustrated in Figure 2.1 wherein nanotubes have two possible states when placed close to each other. Two nanotubes can be parallel to one another in a bundle (Figure 2.1 (A)). The nanotubes can also join by the ends to form a radial pattern or cluster (Figure 2.1 (B); radial pattern partially drawn). The anionic termini of the nanotubes can interact with counter cations in the solution. In cluster configuration, counter ions and organic termini join together and form a cluster. Assume the cluster joint area is spherical.

Denote r_c as the radius of the cluster. The zigzag line represents the functional group linking the nanotube end to the terminal charge. This model studies multiple-nanotube configurational change between parallel bundles and end-to-end joint clusters. To separate a nanotube from the bundle, the VDW potential must be overcome. To pull one nanotube from a cluster, the electrostatic ionic potential appears to be the major influence to overcome. The comparison of these disassociation potentials facilitates the understanding of which state is more stable in water. A stable cluster state is the premise for nanotubes to form the inter-connected network.

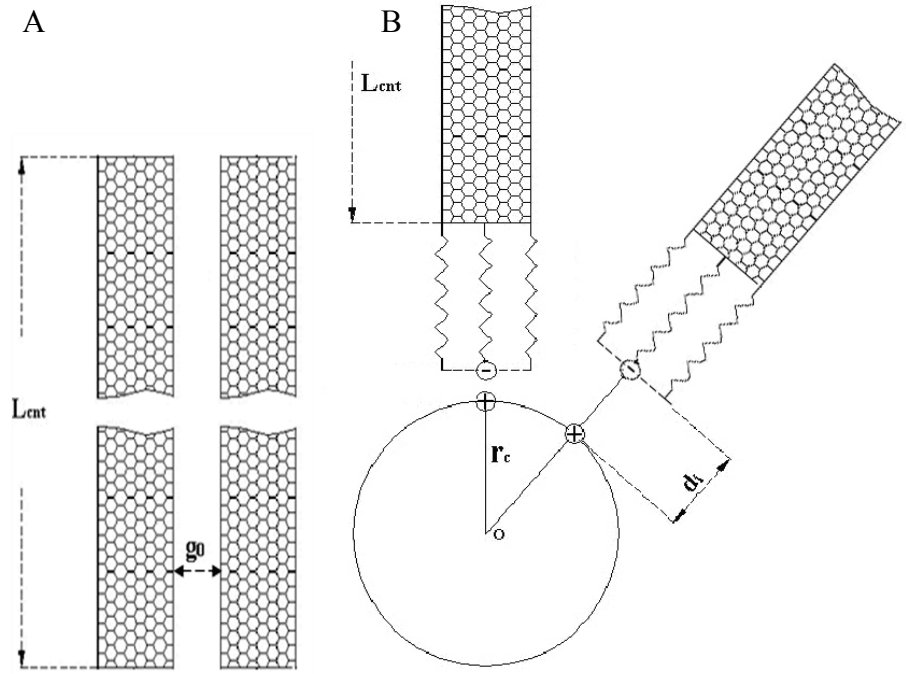

Figure 2.1. Illustration of two states of two adjacent nanotubes: (A) Parallel bundle and (B) radial cluster (left black CNT and right black CNT; Radial pattern partially drawn). The nanotubes are not drawn to scale.

When CNTs are closely bundled, the equilibrium gap between the walls of adjacent single walled carbon nanotubes is approximately 0.3 nm (Sun *et al*., 2005). Water molecules and ions with a water shell cannot enter the gap between the nanotubes. Therefore, the VDW potential between the two tubes is considered equivalent to that in vacuum. Consider two parallel nanotubes at their equilibrium gap distance (g_0), Sun *et al*. (2005) calculated the vacuum VDW potential per unit length (ϕ_0) between adjacent SWCNTs of various diameters. Denote L_{CNT} as nanotube length, the VDW potential is

$$U_{VDW} = \phi_0 L_{CNT} \tag{1}$$

To debundle the two nanotubes, the VDW potential in equation (1) must be overcome.

In the cluster case, functionalized nanotubes join ends and form a radial shape. The gap distance increases between the tubes, and the Lennard-Jones (LJ) type VDW potential decreases quickly ($O(r^{-6})$). Water molecules enter the gap, making the VDW attraction even weaker. The VDW force is negligible in comparison to the ionic force in this case. To pull one nanotube from the radial cluster, one needs to overcome the ionic interaction between the terminal anions at nanotube ends and the counter cations in the cluster. Assume that a nanotube end has q_{end} terminal anionic charges. The corresponding cations provide $q_{counter}$ effective charges. Coulomb's law gives the effective ionic potential.

$$U_{ion} = \frac{q_{counter} q_{end}}{4\pi\kappa_e \varepsilon_0 d_i} \tag{2}$$

Here $\varepsilon_0 = 8.85\times10^{-12}$ F/m is the vacuum dielectric constant, κ_e is the effective dielectric constant of the cluster, and d_i is the effective distance between the ion pair.

To estimate κ_e, note that water molecules are polar. As part of the hydration shell of an ion, water has a dielectric constant of 4, however as free molecules, it has a dielectric constant of 78.4 at 298 K. The static hydration shell of Na^+, for example, is approximately 6, equivalent to the corresponding hydration number (Van Geet, 1972). The effective dielectric constant can be expressed as (Nemat-Nasser *et al*., 2000)

$$\kappa_e = \frac{2\kappa_1 + \kappa_2 - f(\kappa_1 - \kappa_2)}{2\kappa_1 + \kappa_2 + f(\kappa_1 - \kappa_2)}\kappa_1; \text{ where } \qquad f = \frac{m_{counter}}{m_{water}} \tag{3}$$

Here κ_1 and κ_2 are the dielectric constants for water and counter ions, respectively; $m_{counter}$ and m_{water} are the moles of counter ions and water in the cluster, respectively.

To calculate f, assume zero total charge in the cluster. Thus the total number of counter ions equals the total number of end ions attached to the nanotubes, e.g., $q_{counter} = q_{end}$. Assume that nanotube terminal anions are uniformly distributed over the surface of the cluster sphere, so the ion areal density is

$$\rho_{END} = \frac{N_{END}}{\left(\pi \frac{D_{CNT}^2}{4}\right)} \tag{4}$$

Here N_{END} is the number of terminal anions per nanotube end, and D_{CNT} is nanotube diameter. The total number of end ions in the cluster can then be calculated from the areal density as

$$N_{CNT\_TOT} = \frac{N_{END}}{\left(\pi \frac{D_{CNT}^2}{4}\right)} \times 4\pi r_c^2 \tag{5}$$

Note that total charges are balanced. The molar ratio of counter ions over solvent in the cluster is then calculated as

$$f = \frac{m_{counter}}{m_{water}} = \frac{N_{CNT\_TOT}}{M_{water} \Big/ \left(MW_{H_2O} N_A\right)} = \frac{N_{END} \Big/ \left(\pi \frac{D_{CNT}^2}{4}\right) \times 4\pi r_c^2}{\frac{4}{3}\pi r_c^3 \rho_{H_2O} \Big/ \left(MW_{H_2O} N_A\right)} = \frac{3 N_{end} MW_{H_2O}}{4\pi r_c D_{CNT}^2 N_A \rho_{H_2O}} \tag{6}$$

Here M_{water} is the water mass, ρ_{H_2O} = 1×10^3 kg/m^3 (the mass density of water), N_A = 6.0221415 $\times10^{23}$ mol^{-1} (Avogadro constant), and MW_{H_2O} = 18.0153×10^{-3} kg/mol (the molecular weight of water).

Effective ionic distance d_i is taken as the equilibrium distance between the ion pair.

The effective ionic potential in equation (3) is then expressed as a function of cluster radius.

$$U_{ion} = \frac{q_{counter} q_{end}}{4\pi \frac{2\kappa_1 + \kappa_2 - f(\kappa_1 - \kappa_2)}{2\kappa_1 + \kappa_2 + f(\kappa_1 - \kappa_2)} \kappa_1 \varepsilon_0 d_i} \tag{7}$$

Note that the expression for f is provided in equation (6).

The comparison of the effective VDW potential and ionic potential gives insight to the SWCNTs self-assembly behavior. When the effective ionic potential is larger than the VDW potential, more effort is needed to break clustered nanotubes. Thus the cluster state is considered stable in comparison to the bundled state. On the contrary, when the VDW potential is larger, the bundled state is more favorable. It is evident from equation (2) that the decrease of nanotube length will directly lead to the decrease of the VDW potential. Hence, short SWCNTs are less likely to maintain a bundled status. This agrees with the fact that nanotube dispersions are easier to achieve for short tubes. Strong ionic interactions, on the contrary, keep the constantly vibrating nanotubes together in network structures. The maximum number of SWCNT termini ions is constant for a nanotube with a given diameter, so the ion pair potential has an upper limit at the equilibrium distance. The VDW potential can increase, however, well beyond that limit of the ionic potential since the length of nanotubes can increase to micro-meters. In this situation, the nanotubes must be short enough to lower the VDW attraction potential so that the ionic potential can overcome it.

2.4. Analysis for Single-walled carbon nanotubes (SWCNTs) self-assembly through ionic clustering

For a given cluster size, the nanotubes need to be shorter than a certain length so that the VDW potential is smaller than the ionic potential, thus maintaining the clustered status.

In this study, consider that 1.4 nm diameter SWCNTs are functionalized with polymer chains and terminal anions. Assume that all possible end sites of the nanotubes are functionalized, and are attached with carboxylate anions, common functionalities for carbon nanotubes in the literature (Tasis *et al*., 2006). Sodium serves as the counter cation. The functionalized SWCNTs are placed in water. The parameters are listed in Table 2.1. The calculation shows that the single-walled carbon nanotubes must be shorter than approximately 100 nm to have a stable 10 nm radius cluster.

Table 2.1. Parameters for functionalized single-walled carbon nanotubes in electrolyte.

SWNT geometry		VDW parameters (Sun et al., 2005)		Dielectric constants (Van Geet, 1972)		Ion pair equilibrium distance (Carrell et al., 1988)
D_{CNT} (nm)	N_{END}	g_0 (nm)	ϕ_0 (kJ/nm/mol)	κ_1	κ_2	d_i (nm)
1.4	46	0.3164	125.9	78.4	6	0.245 (COO^- Na^+)

2.5. Concluding remarks

This chapter introduces a simple model to compare the stabilities of the bundled state and the interconnected state of SWCNTs in aqueous electrolyte solution. The interconnected state is promoted via ionic clustering at nanotube ends. VDW attraction is the major driving force of the bundled state, while ionic interaction is the dominating factor in the clustered state. The analysis shows that short nanotube length, end-concentrated functionalizations with terminal ions, and a polar solvent with

counter ions are key factors to effect SWCNTs self-assembly. The results indicate that when a nanotube is short enough, the cluster state is more favorable than the bundled state. Specifically, for 1.4 nm SWCNTs having carboxylate terminal anions in water with sodium ions present, the nanotubes must be shorter than ~100 nm to have stable 10 nm size clusters. The results provide an important guide to the fabrication of the self-assembly.

2.6. Acknowledgement

This chapter is prepared for publication by S. Nemat-Nasser, Y. Gao and Y. Tor. The dissertation author was the primary investigator and author of this paper. This work has been conducted at the Center of Excellence for Advanced Materials, CEAM, Department of Mechanical and Aerospace Engineering, University of California, San Diego, and has been supported by the Air Force Office of Scientific Research Grant Number N0001404M0164.

2.7. References

R. K. Saini, I. W. Chiang, H. Peng, R. E. Smalley, W. E. Billups, R. H. Hauge and J. L. Margrave (1999). "Covalent Sidewall Functionalization of Single Wall Carbon Nanotubes." Adv. Mater., 1999, Vol.11, 834-838.

J. E. Riggs, Z. Guo, D. L. Carroll and Y. Sun (2000). "Strong Luminescence of Solubilized Carbon Nanotubes." J. Am. Chem. Soc., Vol.122, 5879-5880.

J. Chen, A. M. Rao, S. Lyuksyutov, M. E. Itkis, M. A. Hamon, H. Hu, R. W. Cohn, P.C. Eklund, D. T. Colbert, R. E. Smalley and R. C. Haddon (2001). "Dissolution of Full-Length Single-Walled Carbon Nanotubes." J. Phys. Chem., Vol.105, 2525-2528.

B. Vigolo, A. Pénicaud, C. Coulon, C. Sauder, R. Pailler, C. Journet, P. Bernier and P. Poulin1 (2000). "Macroscopic Fibers and Ribbons of Oriented Carbon Nanotubes" Science, Vol.290, 1331-1334.

J. K. Ziegler, Z.N. Gu, H.Q. Peng, E.L. Flor, R.H. Hauge and R.E. Samlley (2005). "Controlled Oxidative Cutting of Single-Walled Carbon Nanotubes" J. Am. Chem. Soc., Vol.127, 1541-1547.

B. Zhou, Y. Lin, H. Li, W. Huang, J. W. Connell, L. F. Allard and Y. Sun (2003). "Absorptivity of functionalized single-walled carbon nanotubes in solution." J. Phys. Chem. B, Vol.107, 13588–13592.

O. Matarredona, H. Rhoads, Z. Li and J. H. Harwell (2003). "Dispersion of single-walled carbon nanotubes in aqueous solutions of the anionic surfactant NaDDBS." J. Phys. Chem. B, Vol.107, 13357–13367.

M. Sano, J. Okamura and S. Shinkai (2001). "Colloidal nature of single-walled carbon nanotubes in electrolyte solution: The Schulze-Hardy rule." Langmuir, Vol.17, 7172–7173.

J. Xu, S. Chatterjee, K. W. Koelling, Y. Wang and S. E. Bechtel (2005). "Shear and extensional Rheology of carbon nanofiber suspensions." Rheol. Acta, Vol.44, 537–562 .

P. Kubat, K. Lang, P. Janda, O. Frank, I. Matulkova, J. Sykora, S. Civis, M. Hof and L. Kavan (2009). "Self-Assemblies of Cationic Porphyrins with FunctionalizedW ater-Soluble Single-WalledCarbon Nanotubes." J. Nanosci. Nanotechnol., Vol.9(10), 5795-5802.

S. Nemat-Nasser (2002). "Micromechanics of Actuation of Ionic Polymer-Metal Composites." J. Appl. Physics, Vol.92(5), 2899-2915.

A. Zuettel and S. I. Orimo (2002). "Hydrogen in nanostructured, carbon-related, and metallic materials." MRS Bulletin, Vol.27(9), 705-711.

T. Tiano, M. Roylance and K. Smith (2001). "Surface modifications of single-wall carbon nanotubes." Proceedings of the American Society for Composites, 16th, 307-316.

J. Chen, M. A. Hamon, H. Hu, Y. Chen, A. M. Rao, P. C. Eklund and R. C. Haddon (1998). "Solution Properties of Single-Walled Carbon Nanotubes." Science, Vol.282, 95-98.

M. A. Hamon, J. Chen, H. Hu, Y. Chen, M. E. Itkis, A. M. Rao, P. C. Eklund and R. C. Haddon (1999). "Dissolution of Single Walled Carbon Nanotubes." Adv. Mater., Vol.11, 834-840.

W. Huang, S. Fernando, L. F. Allard and Y. P. Sun (2003). "Solubilization of Single-Walled Carbon Nanotubes with Diamine-Terminated Oligomeric Poly(ethylene Glycol) in Different Functionalization Reactions." Nano Lett., Vol.3, 565-568.

M. G. C. Kahn, S. Banerjee and S. S. Wong (2002). "Solubilization of Oxidized Single-Walled Carbon Nanotubes in Organic and Aqueous Solvents through Organic Derivatization." Nano Lett., Vol.2, 1215-1218.

F. Pompeo and D. E. Resasco (2002). "Water Solubilization of Single-Walled Carbon Nanotubes by Functionalization with Glucosamine." Nano Lett., Vol.2, 369-373.

R. C. Bohinsky (1987). "Modern Concepts in Biochemistry." Allyn and Bacon, Inc., Boston, MA.

C. Sun, L. Yin, F. Li, G. Lu and H. Cheng (2005). "Van der Waals interactions between two parallel infinitely long single-walled nanotubes." Chem. Phys. Lett., Vol.403, 343-346.

D. Tasis, N. Tagmatarchis, A. Bianco and M. Prato (2006). "Chemistry of Carbon Nanotubes." Chem. Review., Vol.106 (3), 1105-1136.

A. L. Van Geet (1972). "Hydration number of sodium ions determined by sodium magnetic resonance." J. Am. Chem. Soc., Vol.94 (16), 5583-5587.

C. J. Carrell, H. X. Carrell, J. Eriebacher and J. P. Glusker (1988). "Structural aspects of metal ion carboxylate interactions." J. Am. Chem. Soc., Vol.110(7), 8651 .

S. Nemat-Nasser and J. Y. Li (2000). "Electrochemical response of ionic polymer-metal composites." J. Appl. Physics, Vol.87(7), 3321-3331.

Chapter 3

Material Fabrication for SWCNTs Self-assembly

3.1. Guidance from theoretical analysis

Carbon nanotubes (CNTs) behavior in aqueous solvent is influenced by many factors: nanotube geometry, number of walls, end-capped or -uncapped, surface functionalization conditions, solvent properties, and other co-existing chemicals, etc. Due to the difficulty associated with manipulating CNTs and their aforementioned complexity, it is reasonable to narrow the focus to several critical aspects affecting assembly. A simple model and brief analysis in Chapter 2 provided significant guidance to the material fabrication of the nanotubes self-assembly. Carbon nanotubes need to be de-bundled prior to the self-assembly in solvent. It is simpler to form individual dispersions from short nanotubes, based on existing literature and the analysis in Chapter 2. As pointed out in section 3.2.2, single-walled carbon nanotubes (SWCNTs) are easier to shorten in comparison to multi-walled carbon nanotubes (MWCNTs). This work seeks to use ionic force to realize the self-assembly. Aqueous electrolyte solution can provide an excellent ionic environment. Radial clustered

nanotubes, as pointed out in Chapter 2, are the key towards interconnected network structures. Ionic-terminated end functionalizations of nanotubes will provide superior anisotropy for the purpose of clustering. Note that nanotubes are hydrophobic and ionic functionalities can be hydrophilic. The following fabrications were guided by these understandings.

3.2. Introduction to CNTs functionalization and defect site chemistry

3.2.1 General introduction

Raw carbon nanotubes are highly hydrophobic, tend to bundle together, and do not dissolve in most solvents. They can be dispersed in some solvents via ultrasound, but will precipitate once sonication ceases. The CNTs hydrophobicity significantly limits their manipulation and applications. Introducing chemical groups to CNTs could improve their solubility for integration into inorganic and organic systems. Tasis *et al*. (2006) grouped the main modification approaches into three categories:

(a) The endohedral filling of their inner empty cavity

(b) The non-covalent adsorption or wrapping of various functional molecules

(c) The covalent attachment of chemical groups through reactions onto the π-conjugated skeleton of CNTs.

In the endohedral filling approach, open capped nanotubes can encapsulate either inorganic species or organic molecules into their inner cavities. Dujardin *et al*. (1994) predicted that any liquid with a surface tension below ~180 mN/m should be

able to wet the inner cavity of nanotubes through an open end at atmospheric pressure. Intensive studies have been implemented to fill nanotubes with different elements. For example, Toth *et al*. (2008) enhanced the thermal stability of atomic nitrogen inside C60 (N@C60) when encapsulating the N@C60 with single-walled carbon nanotubes. Cao *et al*. (2007) predicted that the discharging gravimetric storage capacity of hydrogen in a diamond-shaped bundle of SWCNTs with optimized parameters reaches 2.5 wt% at 300 K and 12.1 MPa. Encapsulation modifies the inner gap of nanotubes. It is useful for energy storage applications such as hydrogen absorption. This approach, however, is unlikely to assist nanotube de-bundling and dispersion in aqueous environment.

Non-covalent wrapping of the tubular surface by various species helps exfoliate the nanotube bundles and prepares individual CNTs for dissovation or stable dispersion in solvents. The following are a few representative examples. Blanch *et al*. (2010) optimized the surfactant concentrations for the aqueous dispersion of SWCNTs for sodium deoxycholate (1.6 wt%), sodium dodecylbenzene sulfonate (0.5 wt%), Triton X-405 (3 wt%), Brij S-100 (2 wt%), Pluronic F-127 (5 wt%) and polyvinylpyrrolidone-55 (3 wt%). Kang *et al*. (2009) wrapped single-walled carbon nanotubes by water soluble poly(p-phenyleneethynylene), and thereby effected highly individualized nanotube dispersion. Hrapovic *et al*. (2008) trapped an enzyme by κ-carrageenan wrapped CNTs (both MWCNTs and SWCNTs) in aqueous solutions. The non-covalent interaction between the wrapping agent and nanotubes is based on VDW forces or π- π stacking.

The covalent attachment of chemical groups can be effected by two types of approaches. The target functional group can be covalently bonded to carbon nanotubes directly via a one-step reaction. Covalent functionalization can also be effected by first introducing defect sites onto nanotube surface, and then attaching the target molecules at these sites.

Many studies have been implemented for the one-step covalent functionalization of carbon nanotubes using strong oxidants, including (Tasis et al., 2006) sidewall halogenations, cycloaddition, electrophilic addition, plasma activation, etc. Recently, Yoon et al. (2008) described an interesting phenomenon when oxidizing single-walled carbon nanotubes using chloro oxoanion with cholrine atoms at various oxidation states. At a low oxidant concentration with species of a high oxidation state, selective oxidation was observed on the metallic carbon nanotubes with a minimal effect on the semiconducting nanotubes, where the charges are extracted mainly from the metallic nanotubes to the adsorbates. Alvaro et al. (2004) modified nanotubes by thermal 1, 3-dipolar cycloaddition of nitrile imines. The reaction under microwave conditions afforded functionalized SWCNTs or MWCNTs in 15 min. Direct functionalization provides a rapid method of introducing simple functionality to the surface of nanotubes. The one-step treatment generally distributes the chemical groups across the nanotube surface, while this study seeks to develop a method to achieve concentrated functional molecules at nanotube ends.

3.2.2 Defect site chemistry

Defect site functionalization originated from the purification of raw carbon nanotubes with acid oxidants (Ivanov *et al*., 1995). As-synthesized carbon nanotubes contain impurities such as catalyst particles and amorphous carbon. Acid oxidation removes the tube caps and also introduces holes into the sidewalls. The purified nanotubes usually develop oxygenated groups at their ends and sidewalls. People use IR spectroscopy, thermogravimetry, and other techniques to study the chemical nature of these moieties at the defect sites. Liu *et al*. (1998) used a mixture of concentrated sulfuric acid and 12 M nitric acid (3:1) to oxidize single-walled carbon nanotubes. It was demonstrated that the groups attached to the acid-cut nanotubes were carboxylates. The carboxylate groups can easily couple with amines through acylation and amidation reactions. Chen *et al*. (1998) reacted acid oxidized nanotubes with octadecylamine (ODA) via acylation and acquired the first-reported functionalized single-walled carbon nanotubes soluble in organic solvents. Subsequent research was carried out with various amine bearing molecules. The amidation approach has become popular for attachment of large moieties to nanotubes. Wang *et al*. (2004) described DNA biosensors based on multi-walled carbon nanotubes. The probe DNA oligonucleotides were immobilized by forming covalent amide bonds between carboxyl groups of the nanotubes and amino groups at the ends of the DNA oligonucleotides. Hybridization between the probe and target DNA oligonucleotides was confirmed by changes in the voltammetric peak of the indicator of methylene blue. Kumar *et al*. (2009) attached gold nanoparticles to multi-walled carbon nanotubes

utilizing acid oxidation and amidation reactions. The hybrid nanostructures of metal nanoparticles (NPs) and carbon nanotubes could provide a novel strategy for the preparation of promising nanomaterials for highly efficient sensors and imaging science applications.

Regarding this dissertation, the functionalization of single-walled carbon nanotubes pursues short SWCNTs with chain molecules attached at the ends. The other termini of the chain molecules are expected to bear ionic charges such as carboxylate anions.

Based upon the brief review of functionalization methods for carbon nanotubes, covalent functionalization is an appropriate approach for this study. The defect site chemistry of carbon nanotubes provides the following systematic approach for attachment of chain molecules:

(a) Carboxylation through acid oxidation

(b) Acylation for acid chloride

(c) Coupling with target chain molecule via amidation.

After conjugating one terminus of the chain molecule to the nanotube end, the other termini can be modified to bear ionic charge.

3.2.3 Shortening of SWCNTs

To promote successful self-assembly, the nanotubes must be short and the chain-molecule functional groups must concentrate at nanotube ends. Based on the above description for carbon nanotube functionalization, acid oxidation has the ability

to shorten carbon nanotubes. However, the mentioned conventional acid oxidation approach boils SWCNTs in a mixture of concentrated sulfuric acid and 12 M nitric acid (3:1). The resultant shortened SWCNTs will likely have end and sidewall defect sites. If this is the case, coupling with chain molecules will result in undesirable general functionalization across the nanotube surfaces.

Ziegler *et al*. (2005) described an intriguing method to shorten single-walled carbon nanotubes with minimal introduction of new defect sites to the nanotube surface via piranha solutions (concentrated sulfuric acid and 30% hydrogen peroxide, 4:1). The article viewed the cutting process as a two-step process:

(a) Introduction of sidewall damage

(b) Consumption or cutting of damaged sites.

In the cutting process, piranha solutions are capable of attacking existing damage sites in the nanotube sidewall, resulting in the shortening of SWCNTs. However, the mild reactions are incapable of introducing new damage sites into the side wall (Ziegler et al., 2005).

3.2.4 Polyethylene glycol chain molecules

Long chain polyethylene glycols (PEG) are very hydrophilic and have been used to functionalize carbon nanotubes in various studies. Chattopadhyay *et al*. (2006) attached PEG chains (H_2N-mPEG-OMe, MW = 5000 g/mol) to single-walled carbon nanotubes, forming stable dispersion in water over ten days. The author first introduced carboxylic acid groups to SWCNTs and then coupled the nanotubes with

amine-terminated polyethylene glycol chains. Recently, Yang *et al*. (2009) reported a biodefunctionalization study of PEG-functionalized single-walled carbon nanotubes in mice. Using Raman and photoluminescence measurements, the author detected meaningful defunctionalization of the PEG-SWCNT conjugate in the liver over time, yet not in the spleen under similar conditions.

Besides superior hydrophilicity of the long chain PEG, this work seeks a heterobifunctional molecular chain wherein one terminus bonds to the single-walled carbon nanotubes, while the other terminus bears the ionic charge. The high molecular weight polyethylene glycol is usually a mixture of chain molecules with a varying number of monomers. These chain molecules have different chemical structures and molecular weights, thereby rendering modification of PEG towards heterobifunctional chain very difficult. Note that polyethylene glycol has the same terminus at both ends. Modification of one end of the PEG chain must be effected first, followed by modification the other end. The uncertain composition of PEG renders this impossible due to the inability of characterization of both the final heterobifunctional PEG chain and intermediate products using current techniques such as nuclear magnetic resonance (NMR) spectroscopy and mass spectroscopy. Thus polyethylene glycol with uniform structure is necessary for this study.

Hexaethylene glycol (HEG) is selected for this study because of superior hydrophilicity, uniform chemical structure, relatively long (2.7 nm in relaxed state) chain size, and amenability toward chemical modification.

3.3. Materials

Single-walled carbon nanotubes were obtained from Apex Nanomaterials (San Diego, CA). The diameter of the individual tubes is 1.4 nm. The length of the as-synthesized nanotubes varies from 100 nm to 10 μm. The SWCNTs were synthesized via chemical vapor deposition (CVD) and underwent no treatment after synthesis.

Nitric acid (HNO_3) and sulfuric acid (H_2SO_4) were purchased from Sigma-Aldrich (Milwaukee, WI) at 12 M and 98% concentration, respectively. Hexaethylene glycol (97%) was purchased from Sigma-Aldrich. Hydrogen peroxide (30%) aqueous solution was obtained from UCSD storehouse (La Jolla, CA). Argon gas (95% purity, UCSD storehouse) was obtained for the creation of inert, moisture-free atmospheres. FT-IR grade potassium bromide (KBr) was purchased from Sigma-Aldrich with ≥ 99% purity.

Durcupan ACM resin components were purchased from Electron Microscopy Science Inc. (Hatfield, PA). Various types of copper grids, aluminum plate holders, and other microscope supplies were purchased from Tedpella, Inc. (Redding, CA).

Other various chemicals were obtained from Sigma-Aldrich.

3.4. Preparation of short SWCNTs with carboxylic acid groups

This section describes the preparation of the carboxylic acid functionalized short single-walled carbon nanotubes for conjugation with the chain molecules. As briefly shown in Scheme 3.1, raw SWCNTs were first purified with mild acid oxidant

to remove metal catalysts and amorphous carbon. Defect sites were also introduced during the purification step. The purified SWCNTs were treated with concentrated acid mixture to introduce additional defect sites. Piranha solution was then used to cut long nanotubes at the defect sites. Short SWCNTs were collected and subjected to final acid oxidation to introduce carboxylic acid groups for conjugation to amines via acylation and amidation reactions.

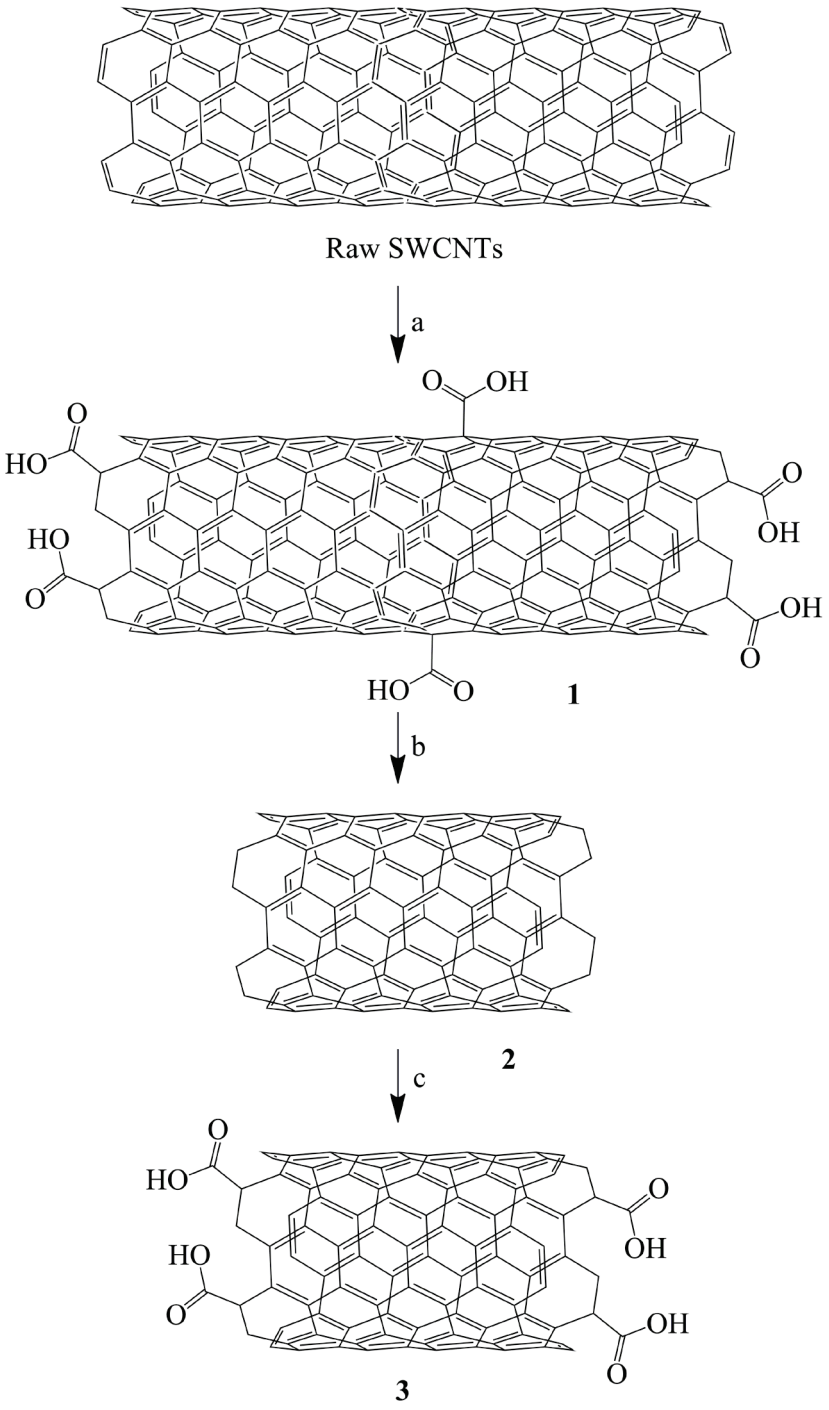

Scheme 3.1. Preparation of carboxylate acid functionalized short SWCNTs (**3**). Reagents and conditions. (a) i. 2.6 M HNO_3, 120 ºC, 24 h; ii. H_2SO_4/HNO_3 (3:1), rt, 4 h; (b) H_2SO_4/H_2O_2 (4:1), 70 ºC, 5 h; and (c) H_2SO_4/HNO_3 (3:1), 120 ºC, 45 min. Note that the nanotubes are not drawn to scale.

3.4.1 SWCNTs purification

As-synthesized SWCNTs were purified first with 2.6 M nitric acid based upon existing literature (Liu *et al*., 1998). In a typical procedure, 0.61 g raw SWCNTs were sonicated in 2.6 M HNO_3 (200 mL) for 4 h. The mixture was then refluxed for 24 h at 120 ºC. Upon cooling, the mixture was centrifuged in a vial at 9000 rpm for 15 min. The supernatant acid was decanted off. Fresh deionized water was added to the vial, followed by vigorous shaking to re-suspend the solid. The vial of the mixture was submitted to a second centrifugation-decantation cycle. The black solid was re-suspended in deionized water. The nanotube suspension was then filtered over 0.45 μm filter paper, yielding a black oxidized nanotube film. Drying in an oven at 110 ºC for 2 h afforded 0.354 g of a black solid (58 wt% yield).

3.4.2 Introducing defect sites into SWCNT sidewalls

The purified nanotubes were subject to sonication in acid mixture to introduce defect sites into the sidewalls (Wang *et al*., 2006). The nanotubes were re-suspended in 50 mL isopropanol in a round bottom flask via 4 h sonication at room temperature. The solvent was then removed by reduced pressure, leaving a black coating at the bottom of the flask. A mixture of concentrated H_2SO_4 and 12 M HNO_3 (50 mL, 3:1) was added to the flask. The contents were sonicated for 4 h at room temperature, followed by two wash cycles of centrifugation-decantation and re-suspension in fresh deionized water. The resulting suspension in deionized water was filtered through a

cellulose ester membrane (0.22 μm pore). The black solid (**1**) was dried over P_2O_5 in a dessicator.

3.4.3 Cutting SWCNTs at defect sites

Shortening of the SWCNTs was achieved via treatment with piranha solution (4:1 mixture of concentrated H_2SO_4 and 30% aqueous H_2O_2) based on the work of Ziegler *et al*. (2005). In a typical procedure, purified nanotubes (14.1 mg) were suspended in isopropanol via 4 h sonication at room temperature. The solvent was then removed by rotary evaporation. This step provided a fine layer of SWCNTs coating at the bottom of the flask. Piranha solution (20 mL) was prepared and immediately added to the black solid. The resulting suspension was briefly sonicated and then refluxed with magnetic stirring at 70 ºC for 5 h. The suspension was cooled to 0 ºC in an ice bath, washed with deionized water, and subjected to two cycles of centrifugation-decantation and re-suspension.

Size separation of nanotubes was performed via membrane filtration. The final suspension, maintained via frequent sonication, was filtered through a 0.22 μm pore size membrane. The filtrate suspension was then filtered through a 0.05 μm pore size membrane to yield 4.0 mg nanotubes (28 wt% yield) after drying in an oven at 110 ºC for 2 h. The length of the shortened nanotubes (**2**) was considered to be in the range of 50–220 nm. The rate of filtration became sluggish when the carbon nanotubes started to accumulate on the filter membrane. A similar phenomenon was described in work by Liu et al. (1998).

3.4.4 Oxidizing short SWCNTs

Carboxylic acid groups were attached in accordance with the well-known procedure (Liu *et al*., 1998). Typically, shortened SWCNTs (4.0 mg) ranging in length of 50–200 nm were suspended in a mixture of concentrated H_2SO_4 and 12 M HNO_3 (12 mL, 3:1). The contents were refluxed at 120 ºC for 45 min, followed by immediate cooling to 0 ºC in an ice bath. The mixture was slowly diluted with three volumes of deionized water at 0 ºC. The diluted suspension was then filtered through a 0.1 μm pore size membrane with frequent sonication. The filtrate suspension was then filtered through a 0.05 μm pore size membrane and dried. The resulting short SWCNTs with carboxylic acid groups (**3**) were considered to be in 50–100 nm range in length. 1.4 mg product (35 wt% yield) was obtained after drying over P_2O_5 in a dessicator overnight.

3.5. Preparation of heterobifunctional hexaethylene glycol (HEG) linker

The objective for the heterobifunctional linker is that one end of the HEG chain couples to the carbon nanotubes, while the other end bears ionic charge. Upon conjugation, the long chain HEG linker assists in SWCNT interaction with other nanotubes.

To compare the effect of the terminal ions, two types of heterobifunctional hexaethylene glycol linkers were synthesized (Scheme 3.2). Both linkers have an amine terminus for conjugation with single-walled carbon nanotubes. One linker (**6**)

had a remaining ethanol terminus (–OH), which does not provide ionic charge in water. The other linker (**8**) had a remaining ethyl ester group (–COOEt), which can be converted into a carboxylic acid group (–COOH) or carboxylate anion ($–COO^-$). The detailed HEG modification procedures, based upon existing methods for triethylene glycol (Shirude *et al*., 2005) and tetraethylene glycol (Dhawan *et al*., 2000), are described in the following sub-sections.

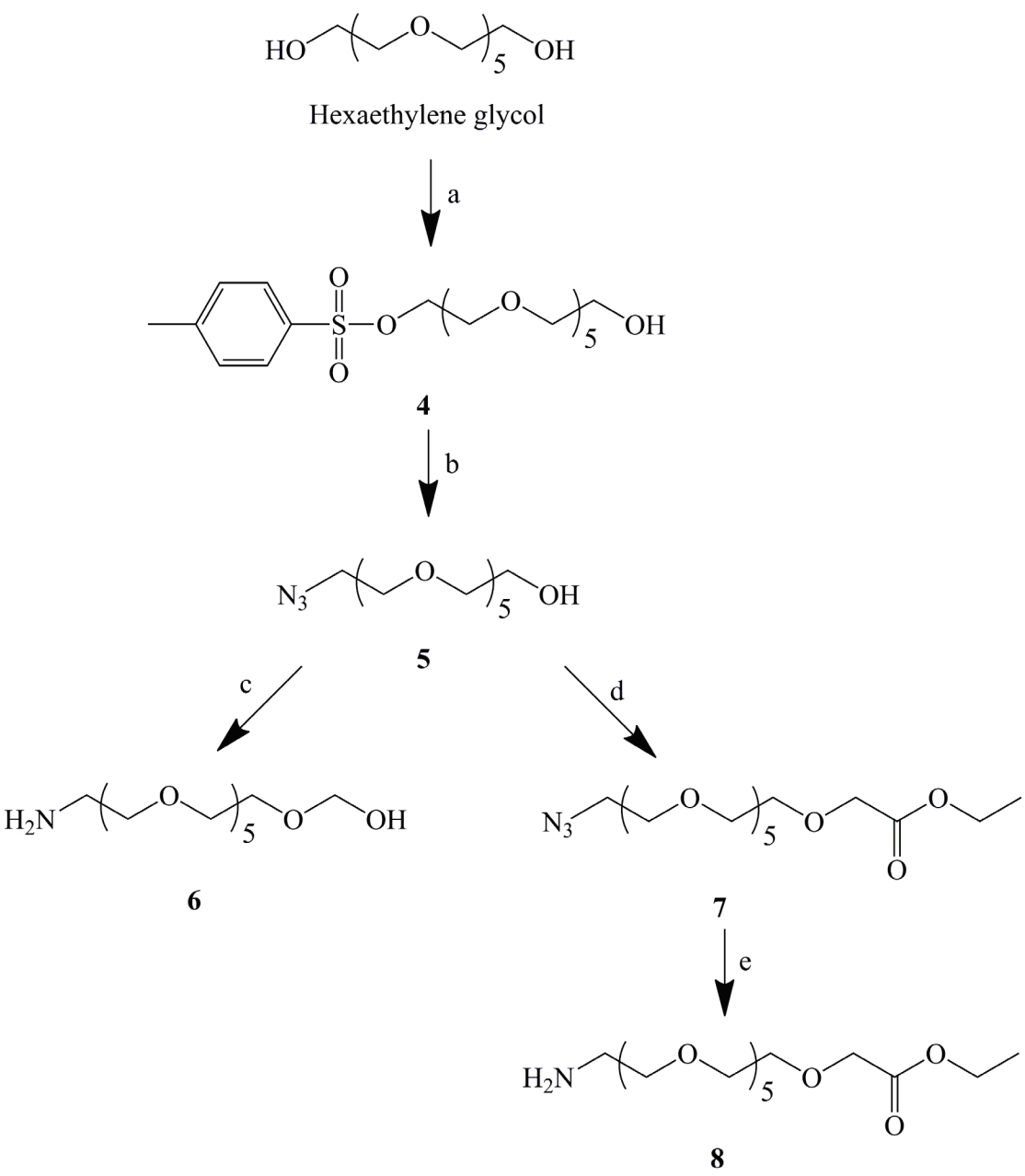

Scheme 3.2. Modifications of heterobifunctional hexaethylene glycol linkers. Reagents and conditions. (a) TsCl/TEA (1:1 mol. ratio), DCM, rt, 12 h; (b) NaN_3, DMF, 100 ºC, 3 h; (c) PPh_3, THF, H_2O, rt, 12 h; (d) NaH, $BrCH_2COOEt$, DMF, 45 ºC, 12 h; and (e) Pd/C, H_2 (45 psi), EtOH/EtOAc (1:1), rt, 2 h. Abbreviations. TsCl=4-toluenesulfonyl chloride; DCM=dichloromethane; DMF=N,N-dimethylformamide; Pd/C=Palladium on carbon catalyst; PPh_3=triphenylphosphine; THF=tetrahydrofuran; EtOH=ethanol; EtOAc=ethyl acetate.

3.5.1 17-Hydroxy-3,6,9,12,15-pentaoxaheptadecyl-4-methylbenzenesulfonate(**4**)

In a typical procedure, triethylamine (5.0 mL, 35.9 mmol) was added to a solution of hexaethylene glycol (5.95 g, 21 mmol) in dry dichloromethane (DCM, 40 mL) at 0 ºC. Separately, 4-toluenesulfonyl chloride (4.47 g, 23 mmol) was dissolved in anhydrous DCM (40 mL) and the solution was added dropwise to the HEG solution while vigorously stirring over 45 min. The reaction solution was stirred for 12 h at room temperature (rt) under argon. The resultant mixture was washed with deionized water (2×40 mL), saturated sodium bicarbonate (2×40 mL), and 2 M hydrochloric acid (2×40 mL). The organic phase was dried ($MgSO_4$), filtered and evaporated under reduced pressure. Submission of the crude material to chromatography (SiO_2, gradient elution with 0–5% MeOH–DCM) afforded mono-tosylated HEG derivative **4** (3.34 g, 7.67 mmol, 36% yield). ESI-MS: $[M+NH_4]^+$ calculated for $C_{19}H_{36}NO_9S$, 454.21; found, 454.07. Full spectrum can be found in Appendices section 3.11.1.

3.5.2 1-Azido-17-hydroxy-3,6,9,12,15 pentaoxaheptadecane (**5**)

In a typical procedure, **4** (3.34 g, 7.7 mmol) was dissolved in dry dimethylformamide (DMF, 20 mL). Excess sodium azide (1.5 g, 23 mmol) was added to the DMF solution, forming a suspension. The reaction mixture was stirred for 3 h at 100 ºC under argon. All volatiles were removed *in vacuo*. The residual material was dissolved in DCM (40 mL), and washed with deionized water (2×40 mL). The organic phase was dried ($MgSO_4$), filtered and evaporated under reduced pressure. Submission of the crude material to chromatography (SiO_2, elution with 5% MeOH–DCM)

afforded **5** (0.16 g, 5.21 mmol, 91% yield). ^{1}H NMR (400 MHz, $CDCl_3$): δ 2.979 (s, 1H); 3.381 (t, 2H); 3.601 (t, 2H); 3.620–3.681 (m, 18H); 3.719 (t, 2H). ESI-MS: $[M+NH_4]^+$ calculated for $C_{12}H_{25}N_3O_6$, 325.17; found, 325.00. Full spectra can be found in Appendices section 3.11.2.

3.5.3 1-Amino-17-hydroxy-3,6,9,12,15 pentaoxahectadecane (**6**)

In a typical procedure, **4** (5.05 g, 12.6 mmol) was dissolved in THF, followed by the addition of triphenylphosphine (4.0 g, 15.2 mmol). Water (~2mL) was added dropwise, and the mixture was stirred at room temperature (rt) overnight. Rotary evaporation was followed by submission of the crude material to chromatography (SiO_2, elution with 5% MeOH–DCM), affording **6** (2.9 g, 10.3 mmol, 82% yield). ^{1}H NMR (400 MHz, DMSO-d_6): δ 2.863 (t, 2H); 3.398 (t, 4H); 3.44–3.50 (m, 16H); 3.52 (t, 4H). ESI-MS: $[M+H]^+$ calculated for $C_{12}H_{27}NO_6$, 282.36; found, 282.24. Full spectra can be found in Appendices section 3.11.3.

3.5.4 Ethyl 20-azido-3,6,9,12,15,18-hexaoxaicosan-1-oate (**7**)

After one terminus of the hexaethylene glycol chain (**5**) was protected with an azide group, the other hydroxy-end was subject to *O*-alkylation. To a mixture of **5** (0.95 g, 3.1 mmol) and sodium hydride (0.16 g, 6.6 mmol) was added dry DMF (10 mL). The mixture was stirred for 5 min, and was added dropwise neat ethyl bromoacetate (0.45 mL, 4.1 mmol) while stirring over 15 min. The reaction solution was stirred for 12 h at 45 ºC under argon. All volatiles were removed *in vacuo*.

Submission of the crude material to chromatography (SiO_2, elution with 5% MeOH–DCM) afforded **7** (0.134 g, 0.34 mmol, 11% yield). ^{1}H NMR (400 MHz, $CDCl_3$): δ 1.283 (t, 3H); 3.398 (t, 2H); 3.655–3.696 (m, 26H); 4.147 (s, 2H); 4.210 (q, 2H). ESI-MS: $[M+NH_4]^+$ calculated for $C_{16}H_{31}N_3O_8$, 411.47; found, 411.19. Full spectra can be found in Appendices section 3.11.4.

3.5.5 Ethyl 20-amino-3,6,9,12,15,18-hexaoxaicosan-1-oate (**8**)

To a solution of **7** (0.134 g, 0.34 mmol) in 1:1 EtOH/EtOAc (2.0 mL) was slowly added palladium on carbon (Pd/C) catalyst (5.0 mg). The reaction mixture was shaken under pressurized (45 psi) hydrogen for 2 h at rt. The catalyst was filtered and washed with methanol/ethyl acetate mixture. The filtrate was concentrated under vacuum to give the crude material, which was submitted to chromatography (SiO_2, gradient elution with 0–5% MeOH–DCM) and afforded **8** (0.10 g, 0.28 mmol, 82% yield). ^{1}H NMR (400 MHz, DMSO-d_6): δ 1.231 (t, 2H); 3.11 (t, 2H); 3.345–3.539 (m, 20H); 3.850 (t, 2H); 4.125 (q, 2H); 4.415 (s, 2H); 6.791 (s, 2H). ESI-MS: $[M+H]^+$ calculated for $C_{16}H_{33}NO_8$, 368.44; found, 368.28. Full spectra can be found in Appendices section 3.11.5.

3.6. Synthesis of HEG-functionalized short SWCNTs and their self-assembly

The conjugation of heterobifunctional hexaethylene glycol and short carbon nanotubes (**3**) was through the acyl chloride-activated amidation of the carboxylic acid

groups on the nanotubes and the amine terminus of the HEG molecules, based on an existing method (Zhao et al., 2004). The procedure of bonding HEG linker (**8**) and carboxylic acid functionalized short SWCNTs (**3**) is shown in Scheme 3.3.

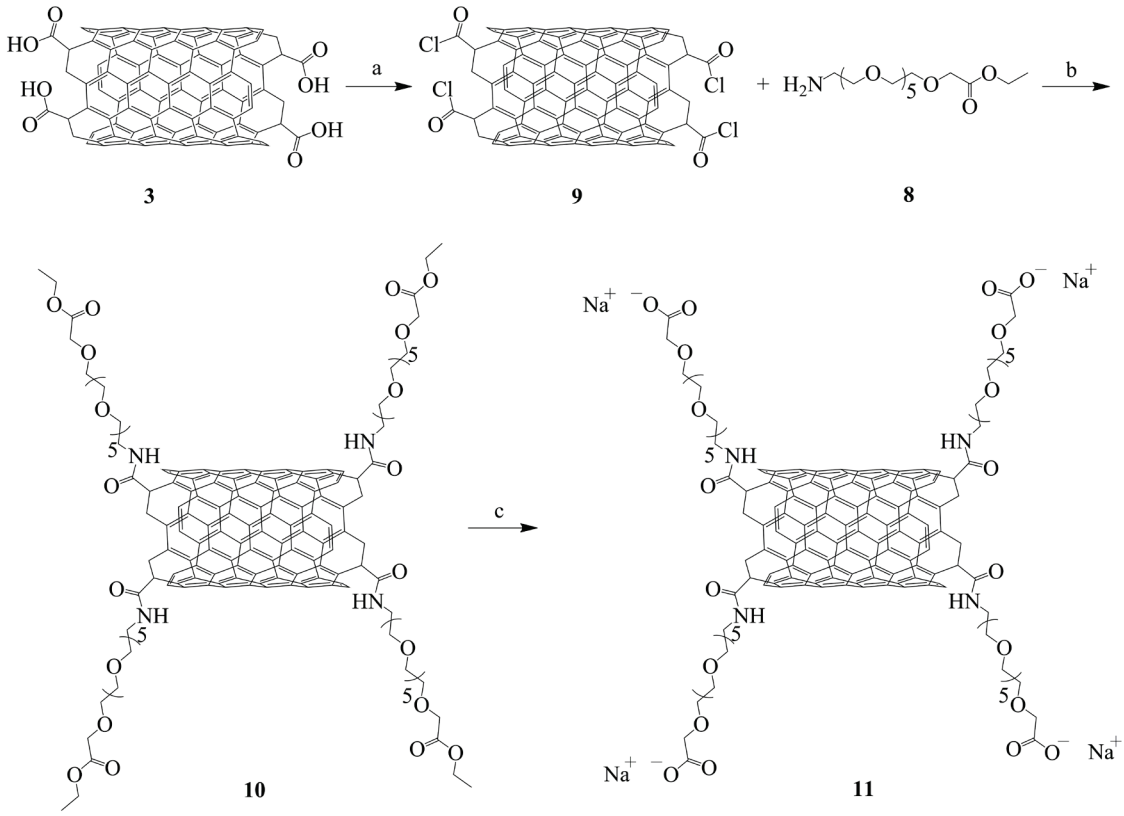

Scheme 3.3. Synthesis of HEG-functionalized short SWCNTs. Reagents and conditions. (a) Oxalyl chloride, DMF (cat.), 70 ºC, 24 h; (b) Pyridine, DMF, DMAP, rt, 2 h; and (c) 1 M NaOH/ethanol (1:1), rt, 2 h. Abbreviations. DMF=dimethylformamide; DMAP=4-dimethylaminopyridine. The nanotubes were not drawn to scale.

3.6.1 Conjugating HEG linker to SWCNTs

In a typical procedure, carboxylic acid functionalized short SWCNTs **3** (1.4 mg) were suspended in dry oxalyl chloride (5 mL) with brief sonication. The reaction mixture was stirred for 24 h at 70 ºC under argon, whereupon the volatiles were removed *in vacuo* to yield **5**. The acyl chloride activated short SWCNTs **9** were immediately resuspended in dry DMF (2 mL). Separately, to a solution of pyridine (1 mL, 0.013 mmol) and 4-dimethylaminopyridine (2 mg, 0.016 mmol) in dry DMF (2 mL) was added **8** (2 mg, 0.005 mmol). The heterobifunctional HEG solution was cannula transferred to the SWCNTs suspension. The reaction mixture was stirred for 2 h at rt under argon, followed by centrifugation at 10000 rpm for 5 min. The supernatant liquid was decanted and the precipitated black solid was resuspended in deionized water via sonication, followed by another centrifugation to precipitate **10**.

3.6.2 Introducing ions to functionalized SWCNTs in water

Upon attaching the amine terminus of the HEG chain to the nanotubes, the remaining ester terminus was reduced to carboxylate anion. SWCNT-HEG conjugate (**10**) from the previous step was readily resuspended in a solution of ethanol and 1M sodium hydroxide (2 mL, 1:1) by high-power tip sonication (Biosonik IV; 540 W, 50%, 50 kHz) for 30 s. The mixture was shaken for 2 h at rt, followed by two centrifugation-decantation washing cycles. The resultant solid was resuspended in water and the pH was adjusted to slightly above 7 by dilution with water. The

nanotube suspension of **11** (0.7 mg/mL) was subject to electron microscopy (EM) characterization.

3.7. Results and discussions

Based on the discussion in Chapter 2, short nanotube length, end-functionalization characteristics, and ionic environment are key factors in the SWCNTs self-assembly process. Scanning electron microscopy (SEM) was used to monitor nanotube length and topological characteristics, Fourier transform infrared (FT-IR) spectroscopy was applied to monitor the functionalization procedure, and Raman spectrum spectroscopy facilitated the understanding of nanotube structural changes.

Material characterization methods and procedures are described separately in Chapter 4. The associated results are outlined and discussed here.

Figure 3.1 shows the SEM images of the single-walled carbon nanotubes before and after functionalization. Raw SWCNTs contain various impurities such as catalyst particles and amorphous carbon (Figure 3.1 (A)). The purified SWCNTs (Figure 3.1 (B)) were very long and were bundled together. After the acid treatments, the oxidized nanotubes between 50–100 nm long were isolated via filtration. Visually apparent from Figure 3.1 (C) is a preponderant nanotube length of approximately 100 nm. Prior to the shortening procedure, the long nanotubes were oxidized under mild conditions: either boiling dilute acid or concentrated acids at rt. These mild oxidation treatments slowly damaged the graphite structure and introduced a large number of

defect sites into the ends and sidewalls of the single-walled carbon nanotubes. In the following shortening treatment, piranha solution was reported (Ziegler *et al*., 2005) to cut single-walled carbon nanotubes via existing defect sites with minimum introduction of new defect sites to the nanotube sidewall surfaces. The resulting short nanotubes had defect sites concentrated at their two ends. The subsequent HEG functionalization occurred predominately at the tube ends, satisfying the requirement of the theoretical investigation in Chapter 2.

After the short nanotubes were functionalized with one end of the HEG linker, the other terminal ethyl ester of the HEG linker was converted to the carboxylate anion. The short SWCNT-HEG-COO^- conjugates were placed in water in the presence of sodium ion. The ether components of the HEG linker assist dispersion of the short SWCNTs in water (Lin *et al*., 2009). The HEG linkers, at one nanotube end, provide approximately 50 end anions for 1.4 nm diameter SWCNTs (based on Chapter 2). The SWCNT end HEG linkers, and their terminal anions, develop a highly hydrophilic domain in comparison to the hydrophobic sidewall of the SWCNTs. The hydrophile-hydrophobe-hydrophile structure and terminal anions of individual short SWCNTs promote nanotube floatation in aqueous electrolyte solutions and induce the clustering with each other at nanotube ends.

Clusters formed at short SWCNTs ends join multiple nanotubes into interconnected network structures, as remarkably observed with the SEM (Figure 3.1 (D)) after drying a drop of SWCNTs suspension **11** (0.7 mg/mL) on a carbon film. Similar two-dimensional (2D) network structures were obtained from transmission

electron microscopy (Figure 3.6 (D)). In comparison, longer nanotubes (>100 nm) were collected and submitted to the same functionalization procedure. It was observed that the relatively long nanotubes clustered into islands instead of an interconnected network (Figure 3.1 (E)). The drastic topological change indicates that the VDW attraction outweighs the ionic influence when the nanotube length is >100 nm.

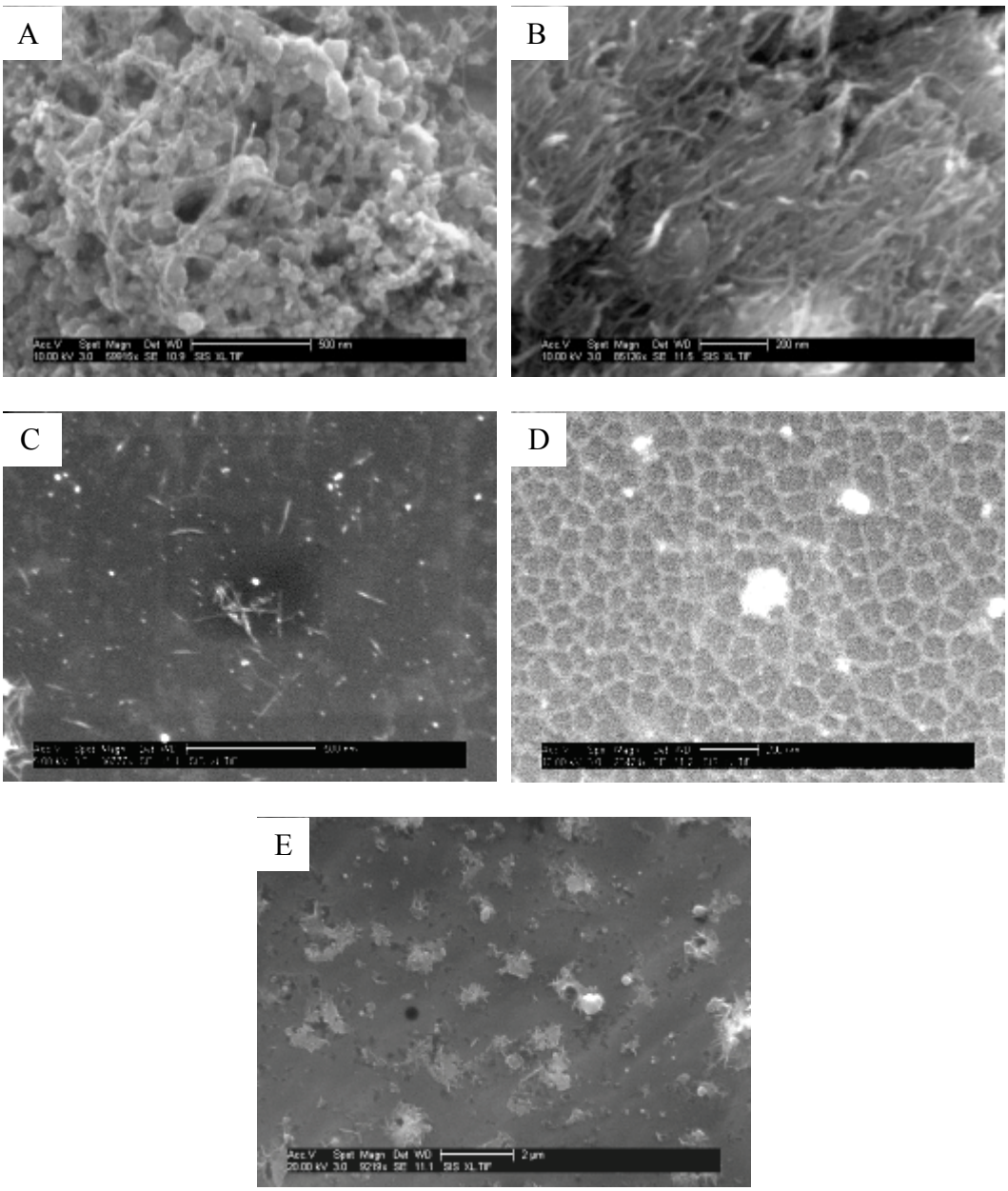

Figure 3.1. Scanning electron microscope (SEM) images of the single-walled carbon nanotubes. (A) Raw SWCNTs (bar length is 500 nm); (B) Purified SWCNTs (bar length is 200 nm); (C) Short SWCNTs (50–100 nm, bar length is 500 nm); (D) Interconnected network formed by drying a drop of aqueous dispersion of SWCNT-HEG-COO^- (50–100 nm) with the presence of Na^+ (bar length is 200 nm); and (E) Isolated cluster islands formed by drying a drop of aqueous dispersion of long (>100 nm) SWCNT-HEG-COO^- with the presence of Na^+ (bar length is 2μm).

The lengths of SWCNTs in the network structures were measured from the microscope images. Figure 3.2 shows the length distribution chart of 742 nanotubes. 80% of the nanotubes are in the range of 50–100 nm, which is expected from the size separation process. 16% of the nanotubes are smaller than 50 nm. This may be a result of filter membrane pore blockage during the filtration through 0.05 μm pore membrane. The average length was 67.2 nm.

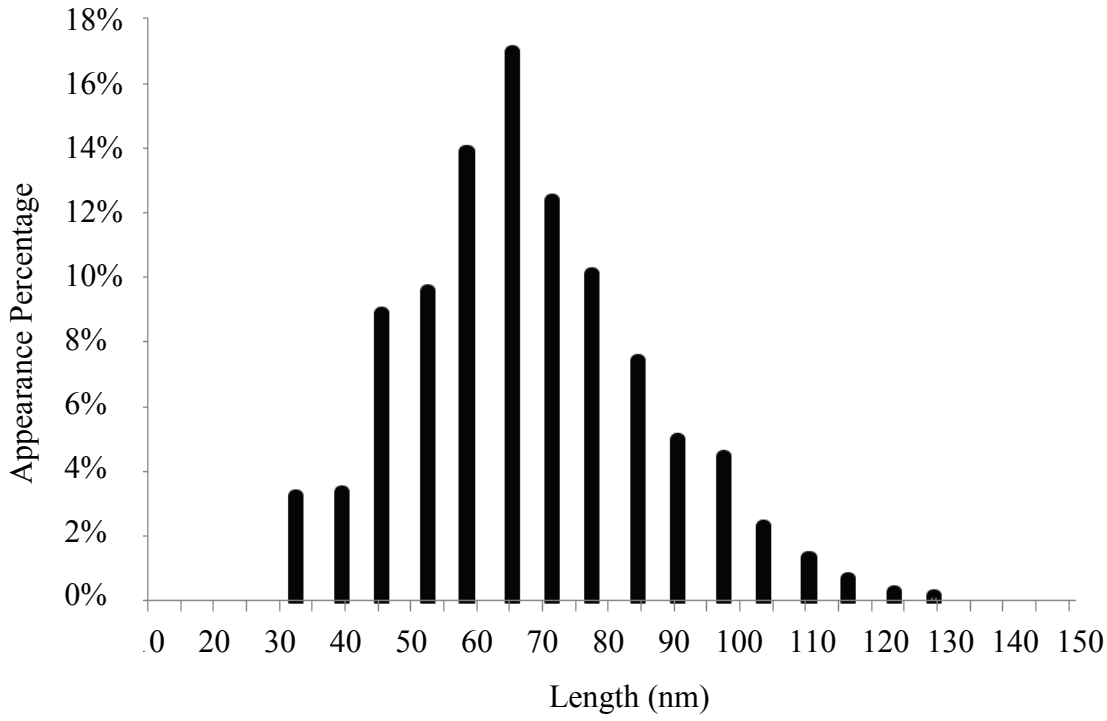

Figure 3.2. Length distribution of SWCNTs in self-assembled the network structure.

When a drop of SWCNTs aqueous suspension was dried on a carbon substrate, the 3D network structure collapsed into the 2D structure, as observed with SEM. A

representative sample of SWCNTs joints (273) was analyzed for the 2D structure using SEM images (Figure 3.3). Of these, 72% of the joints were formed by three nanotubes, 25% by four nanotubes, and a few percent by five nanotubes. The result indicates that the three-nanotube joints are much more favorable than other types of joints. This provides understanding of SWCNTs 3D structure in water.

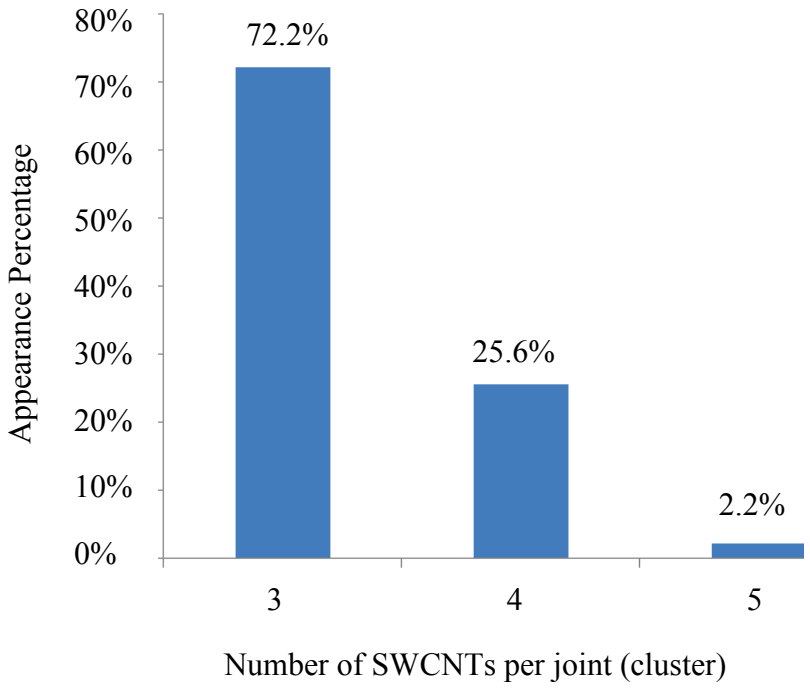

Figure 3.3. Joint/cluster formation by different nanotube number.

To maximize filtration yield of the short SWCNTs, a parametric study was implemented to optimize the shortening treatment with piranha solution. Experiments at different temperatures and time lengths were conducted, and the yields were compared. The parameters and corresponding yields are indicated in Table 3.1. At room temperature, a one-hour treatment resulted in high overall yield, however, it did

not afford measurable short SWCNTs between 50–100 nm. Neither increased reaction time nor increased temperature significantly affected the yield of short SWCNTs. Treatment at 70 °C for 5 hours, although providing a low overall yield (31.9 %), resulted in the formation of more (28.4%) short nanotubes (50–100 nm) when compared to other conditions.

Table 3.1. Parametric study for higher yield of short SWCNTs.

SWCNTs (mg)	Treatment with piranha solution	Total yield	Yield composition	
			>100 nm	100-50 nm
31.4	1 Hour, 25°C	74.0%	74%	0%
30.4	5 Hour, 25°C	74.5%	71.9%	2.6%
61.8	1 Hour, 70°C	55.4%	51.5%	3.9%
26.8	5 Hour, 70°C	31.9%	3.5%	28.4%

Fourier transform infrared (FT-IR) spectroscopy monitored certain bonding information of the intermediate products of the SWCNTs. Figure 3.4 (A) shows the FT-IR spectrum of raw SWCNTs. The broad peak around 3500 cm^{-1} is usually accredited to the O–H bond of the water molecules in the air. A study by Kim *et al*. (2005) assigned the broad peak around 1100 cm^{-1} to C–O stretching modes of ether or alcohol groups attached to the amorphous carbon or other carbonaceous fragments. After acid treatment, a new peak appeared at 1721 cm^{-1} (Figure 3.4 (B)) due to the C=O stretching mode of COOH groups (Chen *et al*., 1998). Upon further reaction of the SWCNTs with the HEG linker followed by careful washing, a peak appeared at 1094 cm^{-1} (Figure 3.4 (C)). This peak represents the C–O stretching mode of the ether group (Riggs *et al*., 2000), which is characteristic for HEG derivatives (Figure 3.4 (D)). Peaks at 1654 cm^{-1} and 1560 cm^{-1} also appeared, representing the C=O

stretching and amide-II bending modes in the (C=O)NH group (Kim *et al*., 2005). Lin *et al*. (2009) has shown that polyethylene glycol, if physically absorbed onto SWCNTs, can be completely removed from the acid-treated SWCNTs by aqueous washing. Thus the existence of the amide group indicates that the HEG linker is chemically bonded to SWCNTs through the (C=O)NH groups.

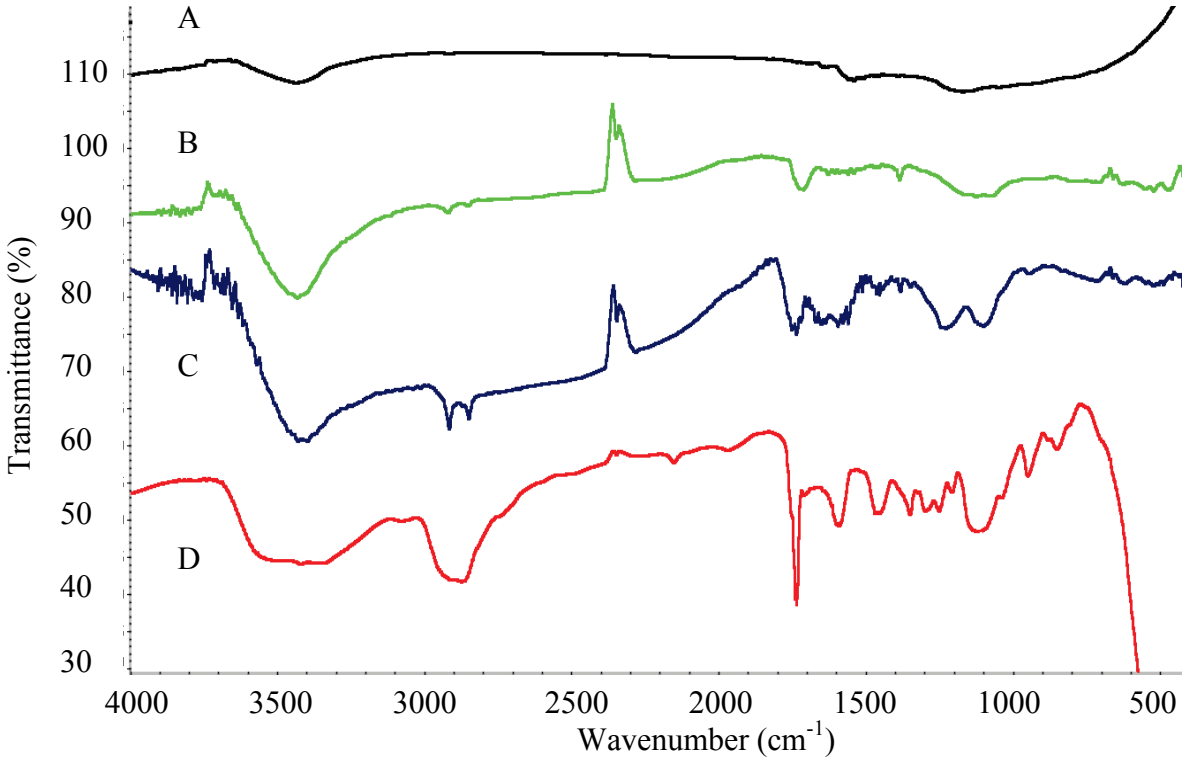

Figure 3.4. Fourier transform infrared (FT-IR) spectra of SWCNTs and HEG linker. (A) Raw SWCNTs; (B) SWCNTs after acid treatment (**3**); (C) SWCNT-HEG-COOEt (**10**) conjugate; and (D) Heterobifunctional HEG linker (**8**).

The structural change of the SWCNTs during the functionalization was studied via Raman spectroscopy. Figure 3.5 displays the Raman spectra for raw SWCNTs,

carboxylic acid functionalized short SWCNTs (**3**), and HEG functionalized short SWCNTs (**10**). The D-band at ~1350 cm^{-1} is defect activated and a measure for defect densities (Dresselhaus *et al*., 2005). The G-band, also known as the tangential-displacement mode (TDM), corresponds to Raman-active optical phonons at the Γ-point. Two modes (G^+ ~1590 cm^{-1} and G^- at energy slightly below) are usually visible (Jorio *et al*., 2002). To have a realistic comparison, all the Raman spectra were normalized with respect to the G band. Raw SWCNTs (Figure 3.5 (C)) have a narrow G band due to their low distortion of the tubular structure and a low level of defects (Wang *et al*., 2004). The G band broadened for the functionalized short SWCNTs in Figure 3.5 (A) and (B). The G band broadening in HEG functionalized SWCNTs (**10**) is greater than that in the acid treated SWCNTs (**3**), indicating that the HEG functionalization causes more structural distortion to the nanotube than the carboxylic acid functionalization. The defect-activated D band represents the in-plane substitutional heteroatoms, vacancies, grain boundaries or other defects, all of which lower the translational symmetry and violate the momentum conservation principle (Ferrari and Robertson, 2001). In the present study, the appearance of the D band for the functionalized short SWCNTs is accredited to the introduction of defect sites and functional groups. The increase in D band intensity indicates the increased level of defect influence from acid treated SWCNTs (Figure 3.4 (B)) to HEG functionalized SWCNTs (Figure 3.5 (A)). Note that the number of defect sites did not change when attaching HEG linkers to the carboxylic acid terminated SWCNTs. This indicates that attaching larger moiety leads to a stronger D band. The intensity ratio of deconvolved

D and G bands (I_D/I_G) is typically used to quantify the degree of total disorder (Antunes *et al*., 2007). In this study, the ratio increases from 0 (pristine SWCNTs) to ~1 (HEG functionalized SWCNTs), indicating a large increase of the structural disorder during the nanotube functionalization.

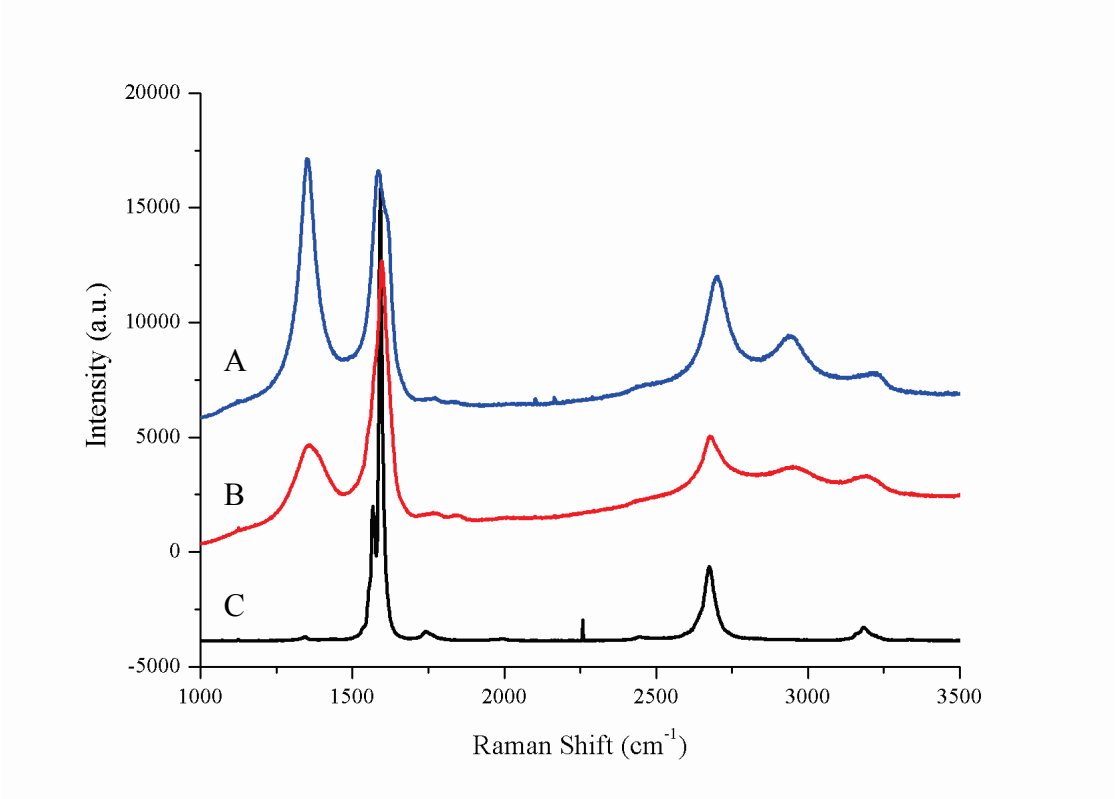

Figure 3.5. Raman spectra of SWCNTs. (A) HEG functionalized SWCNTs (**10**); (B) Carboxylic acid functionalized Short SWCNTs (**3**); and (C) Raw SWCNTs.

Novel application of electron tomography was utilized to investigate the three dimensional (3D) topology of post-synthetic single-walled carbon nanotubes and their self-assembled network structures in aqueous solution. The SWCNTs suspension in aqueous sodium electrolyte was subjected to an immobilization procedure. The

suspension content was first pre-immobilized with agarose gel, and then the water was gradually replaced with ethanol. Durcupan resin was then gradually infiltrated to replace the ethanol, followed by curing at 60 °C for two days. The fully solidified specimen was then sectioned, followed by negative staining with aqueous 2% uranyl acetate and Reynolds lead citrate. The detailed procedures are described in Chapter 4.

In single-axis-tilt tomography (Frank, 1992), an image series was taken when tilting the sample section from –60° to +60° from its untilted position, with 2° increments. Figure 3.6 illustrates the concept of single-axis-tilt tomography. The detailed procedures are described in Chapter 4.

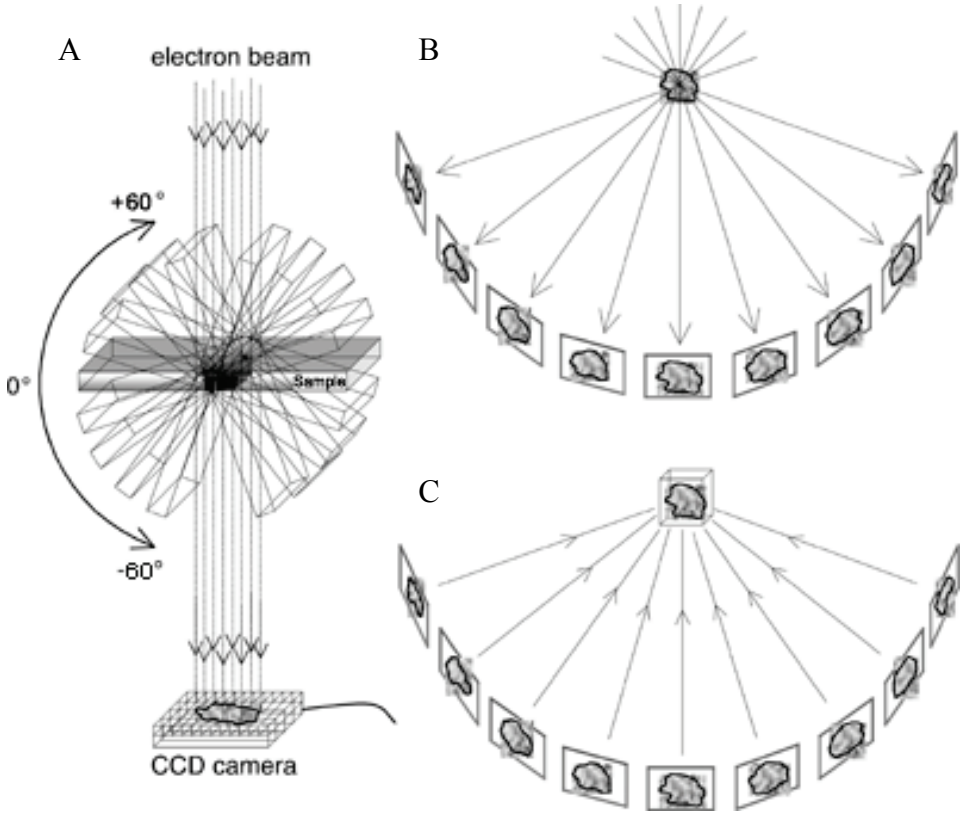

Figure 3.6. Illustration of single-axis-tilt electron tomography. Two-dimensional transmission electron micrographs (projection images) are recorded at different tilt angles for the individual 3D object. (A) The specimen holder is tilted incrementally around an axis perpendicular to the electron beam, and projection images of the same specimen area (field of view) are recorded on a CCD camera at each position. A more schematic diagram (B) illustrates the images projected by a specimen at successive tilt angles. After translationally and rotationally aligning all of these projection images, the imaged object is (C) reconstructed into a 3D density map (often called the tomogram) by a weighted-backprojection procedure (Radermacher, 1992). Adapted from Steven and Belnap (Steven and Belnap, 2005), courtesy of Steven and Belnap.

Figure 3.7 (A) and (B) illustrate two examples of untilted section and its +16° tilt projection. The gold beads (black dots in the images) served as references during the imaging and post-processing. It is evident that the SWCNTs network structures deforms due to the tilted projection, while the general characteristics of the structure

and the tube-tube relationships remain unaffected. The image series was subject to fiducial alignment, back projection, and surface rendering to re-construct the three dimensional profile of the interconnected carbon nanotubes. Figure 3.7 (C) shows a snapshot of the re-constructed model in which the interconnection characteristics were established. In comparison, a drop of SWCNTs suspension in water was placed on a carbon film, and a 2D image (Figure 3.7 (D)) was taken by TEM. Topological differences are evident from the 2D and 3D structures. The 2D structures have a uniform network where three to five nanotube linkers form a joint and several nanotube linkers form the boundary of a polygon cell. All cells have similar dimensions of ~100 nm. The immobilized 3D counterpart, although having interconnected characteristics and uniform nanotube distribution, exhibits a relatively random assembly. The nanotube linker length in the 3D structures is also longer than that in 2D.

The drastic topological change could be due to the different solvent system used during sample preparation, and may also attributed to the different sample preparation methods. In the 2D situation, sodium ions and water provide a very polar environment, which is desired for the nanotubes to form clusters and assemblies based upon the analytical model discussed in this work. The addition of agarose gel, although necessary to pre-immobilize the structures, decreases environment polarity. Thus end functionalized and charged short nanotubes may receive less ionic influence, hence the VDW attraction could dominate. In this scenario, short nanotubes may form bundles first and then, when more end charges are obtained, the thicker and longer

bundles can form cluster joints to interconnect, forming a network. The invasive sample preparation for the 3D characterization may distort the SWCNTs network structures. The electron tomography is popular in tissue sample preparation. However the cell and tissue structures are usually constructed by a stronger bonding force in comparison to the ionic force that assembles the nanotubes. Both agarose and Durcupan resin are more viscous than water, and will introduce a strong surface adhesion force to drag the nanotubes away from their original positions. A non-invasive pre-immobilization treatment could reduce the conformational distortion in the electron tomography of the SWCNTs related structures.

Low electron contrast was also an issue when embedding nano-sized carbon-based tubes into carbon/oxygen based resin. The negative stain notably improved the visibility of the SWCNTs in the resin matrix. However the nanotube-resin interface still had very poor contrast due to SWCNT's minute diameter. The nanotube boundaries were difficult to locate, resulting in a coarse reconstructed 3D model. An alternate immobilization matrix with heavier atomic composition and/or a better stain solution could help the 3D model reconstruction of the SWCNTs related structures.

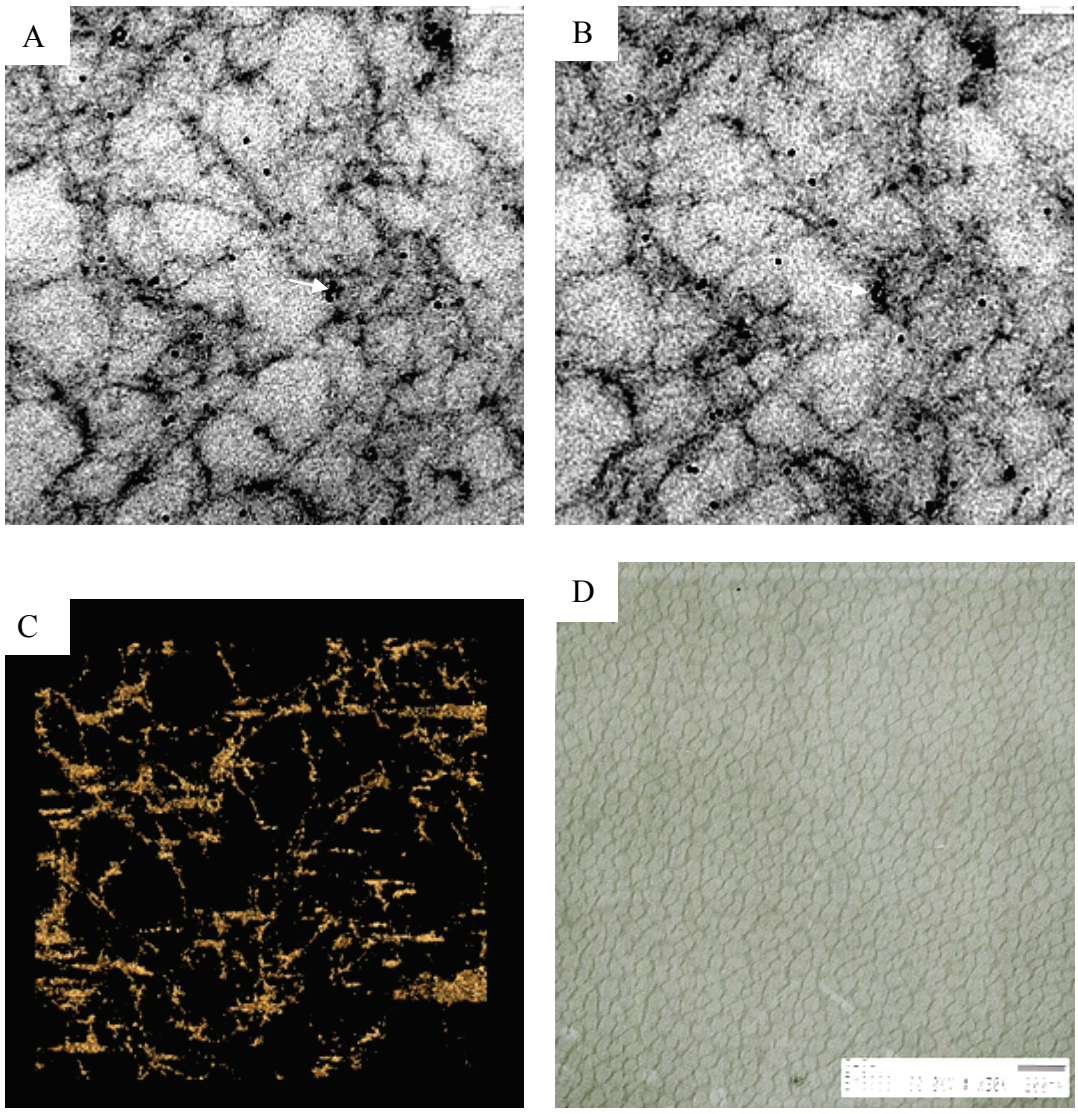

Figure 3.7. Transmission electron microscope (TEM) images for SWCNTs and snap-shot of the reconstructed three-dimensional (3D) model. (A) and (B) Example section images of immobilized HEG-SWCNT conjugate in Durcupan resin, 0° and +16° tilt, respectively (White arrows point to reference gold bead (10 nm). Up-right bar length is 100 nm); (C) Re-constructed 3D model from the tilt image series; and (D) Interconnected network structures after drying a drop of aqueous dispersion of HEG-SWCNT-COO^- with the presence of Na^+ (Bar length is 200 nm).

3.8. Concluding remarks

The present work established the existence of SWCNTs self-assembly into orderly network structures. The network structure is directly identified by electron microscopes. The 2D structures, formed by drying a drop of the sample onto carbon film, are more orderly than the 3D structures observed through electron tomography.

This work also served as a proof of concept to the theoretical investigation in Chapter 2. It is believed that small nanotube length, charged end-functionalization, and aqueous ionic environment are key factors in the formation of self-assembled structures from carbon nanotubes.

This chapter describes a simple protocol to develop the SWCNTs with lengths between 50–100 nm. The concentrated functionalization was indicated by the interconnected network structures that connect through the nanotube ends. A hexaethylene glycol linker serving as chain connection between nanotubes and their end charges, was covalently attached to the nanotubes as indicated by IR spectra. Raman spectra confirmed the increase of nanotube structural disorder during the functionalization.

In a novel manner, electron tomography was adopted to study SWCNTs network structures in aqueous electrolyte solution. A 3D model was reconstructed. The major characteristics of the network were obtained. The difference between the 2D structure and the 3D profile is discussed and possible reasons are addressed.

3.9. Acknowledgement

This chapter is prepared for publication by S. Nemat-Nasser, Y. Gao and Y. Tor. The dissertation author was the primary investigator and author of this paper. This work has been conducted at the Center of Excellence for Advanced Materials, CEAM, Department of Mechanical and Aerospace Engineering, University of California, San Diego, and has been supported by the Air Force Office of Scientific Research Grant Number N0001404M0164. I would like to thank Dr. Tam Victor and Dr. S. G. Srivatsan for many helpful discussions regarding the chemical synthesis. I would also like to thank Mason Mackey for many helpful discussions regarding the electron tomography procedure. The author also acknowledges the TEM usage in the National Center for Microscopy and Imaging Research (NCMIR). The author also acknowledges the SEM usage in Nano3 Clean Room and Analytical Labs in UCSD. The author also acknowledges the IR spectrometer usage in Professor David Hendrickson's lab in Department of Chemistry and Biochemistry in UCSD. The author also acknowledges the Raman spectrometer usage in the Center for Magnetic Recording Research (CMRR) in UCSD. The author also acknowledges the Mass spectrometer usage and NMR usage in the Department of Chemistry and Biochemistry in UCSD.

3.10. References

D. Tasis, N. Tagmatarchis, A. Bianco and M. Prato (2006). "Chemistry of Carbon Nanotubes." Chem. Rev., Vol.106(3), 1105–1136.

E. Dujardin, T. W. Ebbesen, H. Hiura and K. Tanigaki (1994). "Capillarity and Wetting of Carbon Nanotubes ." Science, Vol.265, 1850-1852.

Q. Chen, J. L. Herberg, G. Mogilevsky, H. Wang, M. Stadermann, J. Holt and Y. Wu (2008). "Identification of Endohedral Water in Single-Walled Carbon Nanotubes by 1H NMR." Nano Lett., Vol.8(7), 1902-1905.

S. Toth, D. Quintavalle, B. Nafradi, L. Korecz, L. Forro and F. Simon (2008). "Enhanced thermal stability and spin-lattice relaxation rate of N@C60 inside carbon nanotubes." Phys. Rev. B, Vol.77, 214409.

D. Cao and W. Wang (2007). "Storage of hydrogen in single-walled carbon nanotube bundles with optimized parameters: Effect of external surfaces." J. Hydro. Ener., Vol.32(12), 1939-1942.

A. J. Blanch, C. E. Lenehan and J. S. Quinton (2010). "Optimizing Surfactant Concentrations for Dispersion of Single-Walled Carbon Nanotubes in Aqueous Solution." Phys. Chem. B, Vol.114(30), 9805-9811.

K. Kang, O. Lee, P. Deria, S. H. Kim, T. Park, D. A. Bonnell, J. G. Saven and M. J. Therien (2009). "Helical Wrapping of Single-Walled Carbon Nanotubes by Water Soluble Poly(p-phenyleneethynylene)." Nano Lett., Vol.9(4), 1414-1418.

S. Hrapovic, K. B. Male, Y. Liu and J. H. T. Luong (2008). "Preparation of Polymer-Carbon Nanotube Composite Materials and Their Applications for Enzyme Entrapment." Analy. Lett., Vol.41(2), 278-288.

S. Yoon, S. J. Kim, H. Shin, A. Benayad, C. Anass, J. Seong K. K. Kim, S. M. Kim, Y. J. Park, G. Kim, J. Choi and Y. H. Lee (2008). "Selective Oxidation on Metallic Carbon Nanotubes by Halogen Oxoanions." J. Am. Chem. Soc., Vol.130(8), 2610-2616.

M. Alvaro, P. Atienzar, P. de la Cruz, J. L. Delgado, H. Garcia and F. J. Langa (2004). Phys. Chem. B, Vol.108, 12691-12697.

V. Ivanov, A. Fonseca, J. B. Nagy, A. Lucas, P. Lambin, D. Bernaerts and X. Zhang (1995). "Catalytic production and purification of nanotubules having fullerene-scale diameters" Carbon, Vol.33, 1727-1738.

J. Liu, A. G. Rinzler, H. Dai, J. H. Hafner, R. K. Bradley, P. J. Boul, A. Lu, T. Iverson, K. Shelimov, C. B. Huffman, F. Rodriguez-Macias, Y. Shon, T. R. Lee, D. T. Colbert and R. E. Smalley (1998). "Fullerene Pipes." Science, Vol.280, 1253-1256.

J. Chen, M. A. Hamon, H. Hu, Y. Chen, A. M. Rao, P. C. Eklund and R. C. Haddon (1998). "Solution Properties of Single-Walled Carbon Nanotubes." Science, Vol.282, 95-98.

S. G. Wang, R. Wang, P. J. Sellin and Q. Zhang (2004). "DNA biosensors based on self-assembled carbon nanotubes." Biochem. Biophys. Res. Commun., Vol.325(4), 1433-1437.

N. A. Kumar, S. H. Kim, J. S. Kim, J. T. Kim and Y. T. Jeong (2009). "Functionalization of multi-walled carbon nanotubes with cysteamine for the construction of CNT/gold nanoparticle hybrid nanostructures." Surf. Rev. Lett., Vol.16(3), 487-492.

J.K. Ziegler, Z.N. Gu, H.Q. Peng, E.L. Flor, R.H. Hauge and R.E. Samlley (2005). "Controlled Oxidative Cutting of Single-Walled Carbon Nanotubes" J. Am. Chem. Soc., Vol.127, 1541-1547.

Y. Wang, L. Gao, J. Sun, Y. Liu, S. Zheng, H. Kajiura, Y. Li and K. Noda (2006). "An integrated route for purification, cutting and dispersion of single-walled carbon nanotubes." Chem. Phys. Lett., Vol.432, 205-208.

J. Chattopadhyay, F. de Cortez, S. Chakraborty, N. K. H. Slater and W. E. Billups (2006). "Synthesis of Water-Soluble PEGylated Single-Walled Carbon Nanotubes." Chem. Mater., Vol.18(25), 5864-5868.

P. S. Shirude, V. A. Kumar and K. N. Ganesh (2005). "BisPNA Targeting to DNA: Effectof Neutral Loop on DNA Duplex Strand Invasion by aepPNA-N7G/aepPNA-C Substituted Peptide Nucleic Acids." Eur. J. Org. Chem., Vol.24, 5207-5215.

R. Dhawan, M. G. A. Kadijk, T. J. Joikinen, M. Feng and S. M. Ansell (2000). "Synthesis of Polyamide Oligomers Based on 14-Amino-3,6,9,12-tetraoxatetradecanoic Acid." Bioconjugate Chem., Vol.11, 14-21.

B. Zhao, H. Hu and R. C. Haddon (2004). "Synthesis and Properties of a Water-Soluble Single-Walled Carbon Nanotube–Poly(m-aminobenzene sulfonic acid) Graft Copolymer." Adv. Funct. Mater., Vol.14(14), 71-76.

T. Lin, C. G. Salzmann, L. Shao, C. Yu, M. L. H. Green and S. Tsang (2009). "Polyethylene glycol grafting and attachment of encapsulated magnetic iron oxide silica nanoparticles onto chlorosilanized single-wall carbon nanotubes." Carbon, Vol.47, 1415-1420.

U. J. Kim, C. A. Furtado, X. Liu, G. Chen and P. C. Eklund (2005). "Raman and IR Spectroscopy of Chemically Processed Single-Walled Carbon Nanotubes." J. Am. Chem. Soc., Vol.127(44),15437-15445.

J. E. Riggs, Z. Guo, D. L. Carroll and Y. P. Sun (2000). "Strong Luminescence of Solubilized Carbon Nanotubes." J. Am. Chem. Soc., Vol.122(24), 5879-5880.

M. S. Dresselhaus, G. Dresselhaus, R. Saito, and A. Jorio (2005). "Raman spectroscopy of carbon nanotubes." Phys. Rep., Vol.409, 47-99.

A. Jorio, A. G. Souza Filho, G. Dresselhaus, M. S. Dresselhaus, A. K. Swan, M. S. U Unlu, B. B. Goldberg, M. A. Pimenta, J. H. Hafner, C. M. Lieber and R. Saito (2002). "G-band resonant Raman study of 62 isolated single-wall carbon nanotubes." Phys. Rev. B, Vol.65, 155412.

Y. Y. Wang, S Gupta and R. J. Nemanich (2004). "Role of thin Fe catalyst in the synthesis of double- and single-wall carbon nanotubes via microwave chemical vapor deposition" Appl. Phys. Lett., Vol.85(13), 2601-2603.

A.C. Ferrari and J. Robertson (2001). "Interpretation of Raman spectra of disordered and amorphous carbon." Phys. Rev. B, Vol.61, 14095.

E. F. Antunes, A. O. Lobo, E. J. Corat and V. J. Trava-Airoldi (2007). "Influence of Diameter in the Raman Spectra of Aligned Multi-walled Carbon Nanotubes." Carbon, Vol.45, 913–921.

J. Frank (1992). "Electron Tomography: Three-dimensional Imaging with the Transmission Electron Microscope", Plenum Press, New York.

A. Steven1 and D. Belnap (2005). "Electron Microscopy and Image Processing: An Essential Tool for Structural Analysis of Macromolecules." Curr. Protoc. Prot. Sci., 17.2.1–17.2.39.

3.11. Appendices

3.11.1 Mass spectrum of 17-hydroxy-3,6,9,12,15-pentaoxaheptadecyl 4-methylbenzenesulfonate (**4**)

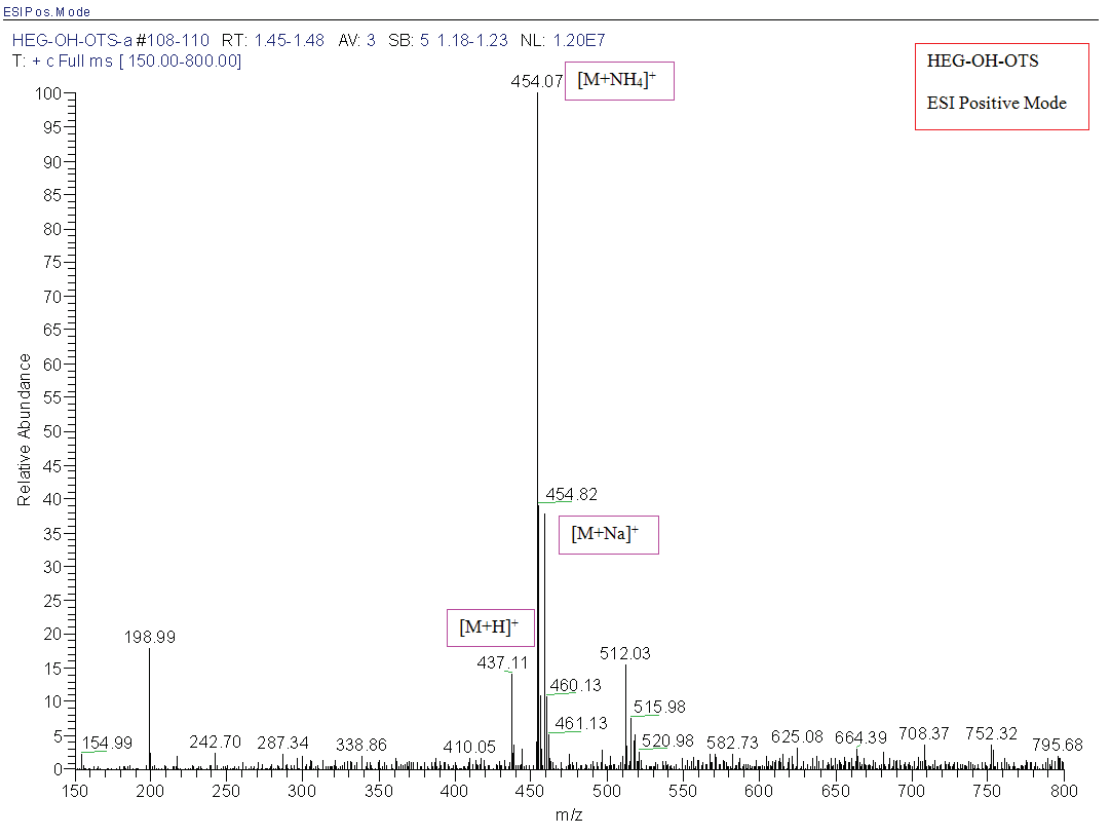

Figure 3.8. Mass spectrum of 17-hydroxy-3,6,9,12,15-pentaoxaheptadecyl 4-methylbenzenesulfonate (**4**).

3.11.2 Proton NMR and mass spectra of 1-azido-17-hydroxy-3,6,9,12,15 pentaoxaheptadecane (**5**)

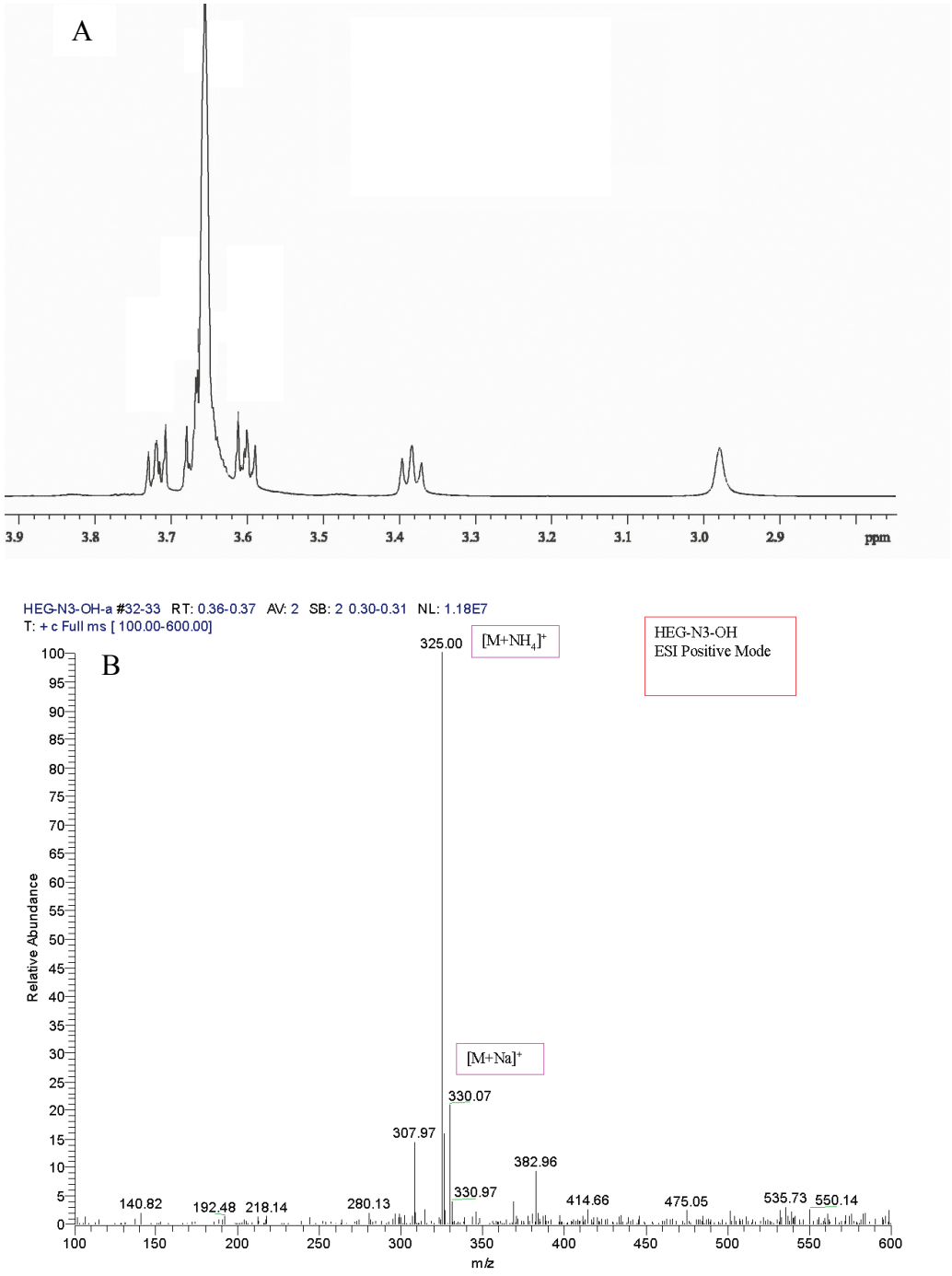

Figure 3.9. Proton NMR (A) and mass spectra (B) of 1-azido-17-hydroxy-3,6,9,12,15 pentaoxaheptadecane **(5)**.

3.11.3 Proton NMR and mass spectra of 1-amino-17-hydroxy-3,6,9,12,15 pentaoxahectadecane (**6**)

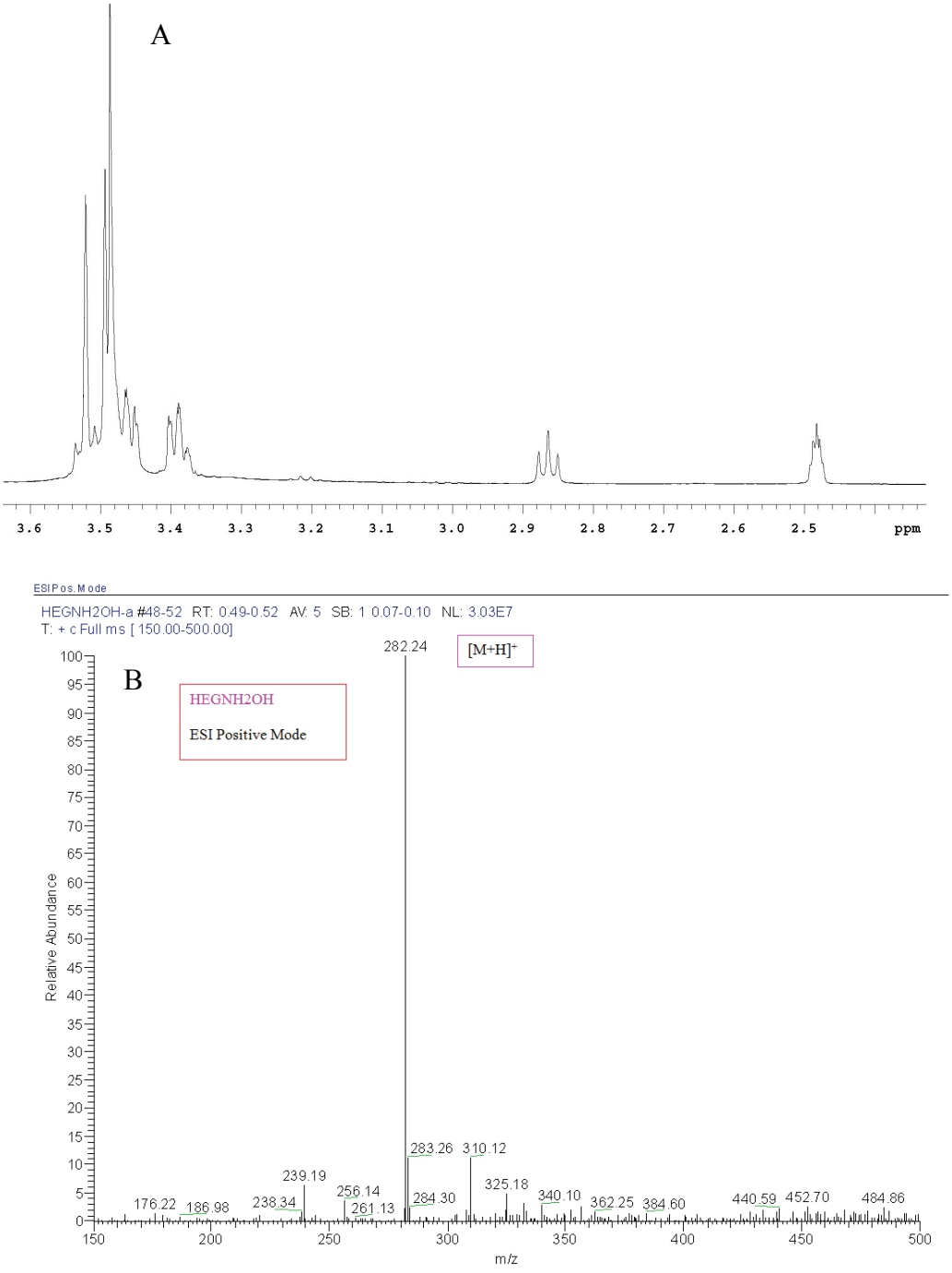

Figure 3.10. Proton NMR (A) and mass spectra (B) of 1-amino-17-hydroxy-3,6,9,12,15 pentaoxahectadecane (**6**).

3.11.4 Proton NMR and mass spectra of Ethyl 20-azido-3,6,9,12,15,18-hexaoxaicosan-1-oate (**7**)

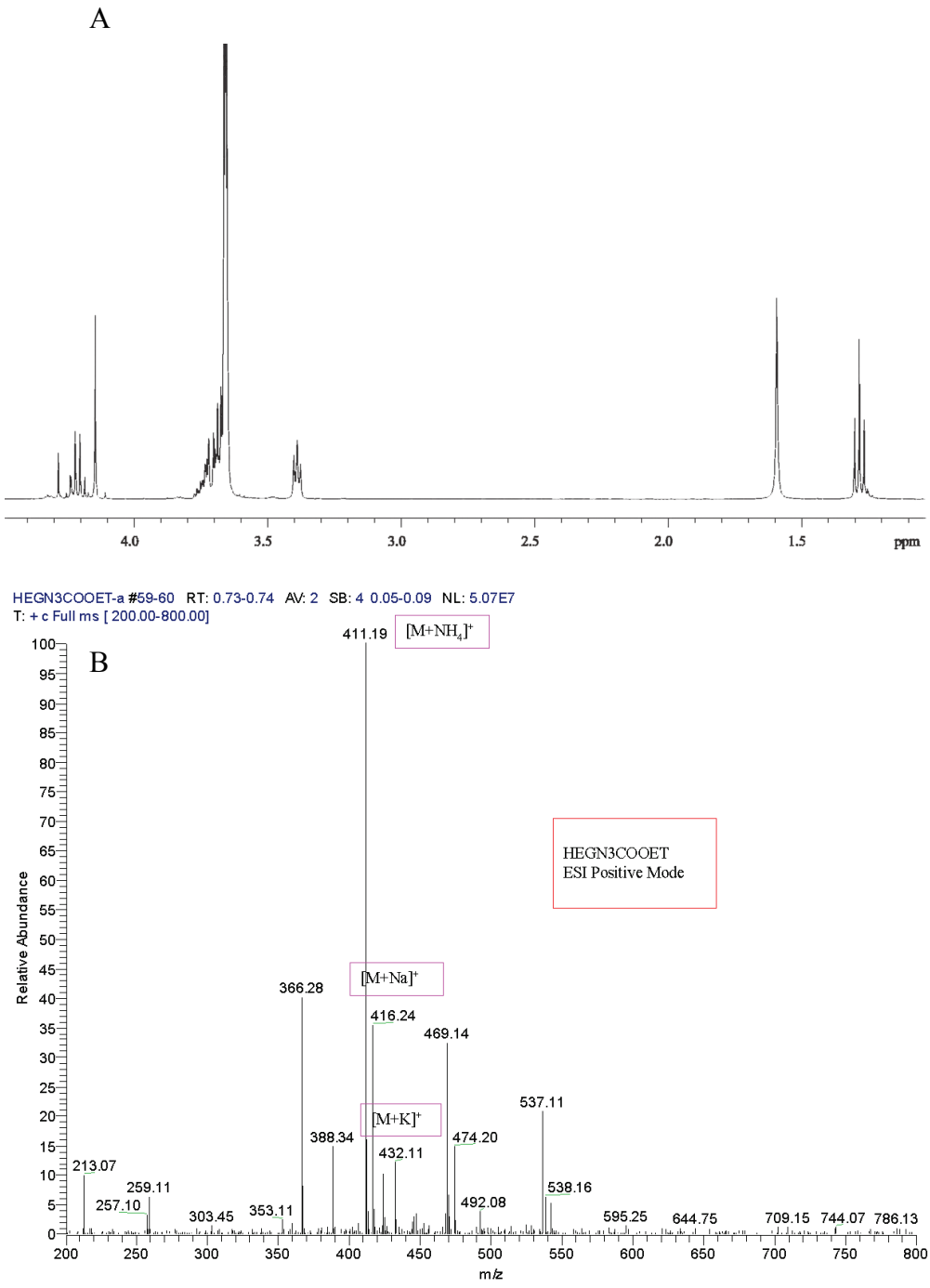

Figure 3.11. Proton NMR (A) and mass spectra (B) of Ethyl 20-azido-3,6,9,12,15,18-hexaoxaicosan-1-oate (**7**).

3.11.5 Proton NMR and mass spectra of Ethyl 20-amino-3,6,9,12,15,18-hexaoxaicosan-1-oate (**8**)

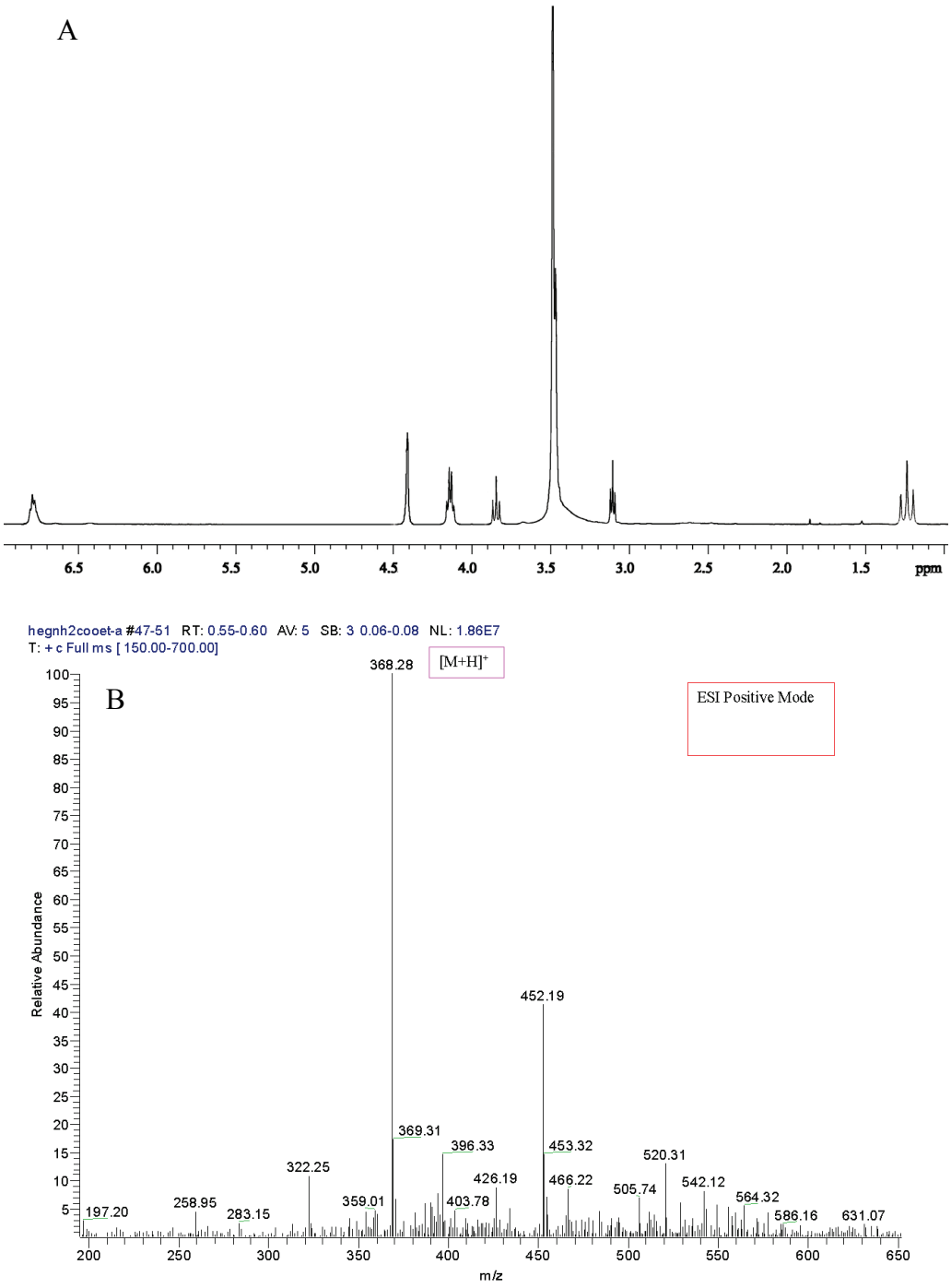

Figure 3.12. Proton NMR (A) and mass spectra (B) of Ethyl 20-amino-3,6,9,12,15,18-hexaoxaicosan-1-oate (**8**).

Chapter 4

Material Characterization Methods

Various material characterization methods used in the fabrication in Chapter 3 are described in this chapter.

4.1. General microscopic characterization methods

4.1.1 Scanning electron microscopy

Scanning electron microscope (SEM) images were obtained with a Phillips XL30 (0.5–30kV) environmental scanning electron microscope (FEI Corp., Hillsboro, OR). In a typical procedure, one drop of dilute SWCNTs aqueous suspension was placed on a carbon film coated copper grid. The drop was dried over P_2O_5 in a dessicator. The residue was submitted to SEM with 5–30 kV working voltage. Raw SWCNTs powder was placed on double-sided carbon tape before the SEM study.

4.1.2 Transmission electron microscopy

General transmission electron microscopy (TEM) studies were conducted on a JEOL-2000EX (200 kV) CryoElectron Microscope (JEOL Inc., Peabody, MA). The images were captured by a Tietz 4Kx4K digital camera. To study the two-dimensional

(2D) characteristics, one drop of dilute SWCNTs aqueous suspension was placed on a carbon film coated copper grip and dried in a dessicator. The specimen was viewed with 200 kV working voltage.

The electron tomography procedure for three-dimensional (3D) study of SWCNTs self-assembled network structures is described in section 4.2.

4.2. Electron tomographic reconstruction

To study the three-dimensional characteristics of the self-assembled HEG-SWCNTs in aqueous electrolyte solution, the method of electron tomography (Frank, 1992) was applied.

Electron tomography is a popular means to obtain 3D electron microscope datasets in biology (Frank, 1992). A soft tissue sample is fixed in resin and sectioned into thin specimen. A 3D sample model can be mathematically reconstructed using object projections obtained by tilting the sample through multiple angles. Schematic diagrams of single-axis-tilt electron tomography can be found in Figure 3.5.

Prepared as indicated in Chapter 3, carboxylate-anion-terminated hexaethylene glycol (HEG) functionalized SWCNTs (SWCNT-HEG-COO^-) may dynamically form and breakup interconnected structures in aqueous sodium electrolyte solution. However, the sub-micron level structures in a liquid cannot be directly observed with a microscope. The method of electron tomography provides the possibility to characterize the structures in a liquid. The present method was based on the standard

electron tomography procedure wherein the structure was frozen, imaged at various angles, and finally a model was re-constructed with tomographic characteristics.

4.2.1 Frozen SWCNTs network structures in gel

After confirming the 2D network structures via electron microscopy, the corresponding SWCNTs aqueous suspension was submitted to a 3D reconstruction procedure.

In this procedure, SWCNTs aqueous suspension (1.0 mL, 0.7 mg/mL) was placed in a vial and diluted with 2% agarose water solution (1.0 mL). The resulting mixture was placed in an ice bath for 15 min, allowing the agarose gel to form. The soft gel was gently removed from the vial, and cut into small pieces (~2mm size cubes). At 0°C, the SWCNTs containing gel pieces were immersed into 20%, 50%, 70% and then 90% (v/v) ethanol-water solutions, successively, for 5 min each. Finally, the gel pieces were placed in high purity ethanol (>99.5%) for 5 min. The final step was repeated twice to quantitatively remove water.

4.2.2 Solidified network structure in resin

Further resin infiltration and hardening were conducted over five days by immersing the gel samples in Durcupan ACM resin prepolymer. The gel pieces from last step were immersed first in 50% (v/v) Durcupan in ethanol overnight. Upon the following day, the specimens were immersed in 100% Durcupan prepolymer for overnight infiltration. On the third day, the specimens were immersed in fresh 100%

Durcupan overnight to remove residual ethanol. The samples were then polymerized at 60°C in a vacuum oven over a two day period.

4.2.3 Thin-sample sectioning, staining and reference coating

Typically, the solidified SWCNTs/resin sample was mounted on a cylinder platform, and then sectioned with a diamond knife on a Richert-Jung Ultracut E ultramicrotome (Capovani Brothers Inc., Scotia, NY). Both thin (80~100 nm) and thick (~200 nm) sections were obtained, and mounted on uncoated copper grids (200 beehive-shaped).

Heavy metal staining, popular for improving electron contrast of the embedded bio-materials in TEM imaging (Ellisman, 2006), was applied to the SWCNTs/resin specimen. Uranyl acetate (2%) and Reynold's lead citrate aqueous solutions were prepared prior to the negative staining (Venable and Coggeshall, 1965). The sectioned sample was stained first in 2% aqueous uranyl acetate for 30 minutes, and then in aqueous Reynold's lead citrate for 2 min. Upon drying, the specimen was observed with the TEM at 200kV to confirm the existence of the network structures before proceeding to the reference coating.

The 200 nm thick sectioned specimen was sputter-coated on both sides, each side with a very thin layer of carbon film. Gold beads (10 nm) were then sparsely sputter-coated on both sides of the section specimen as references.

The photos of the specimen created during the preparation are shown in Figure 4.1.

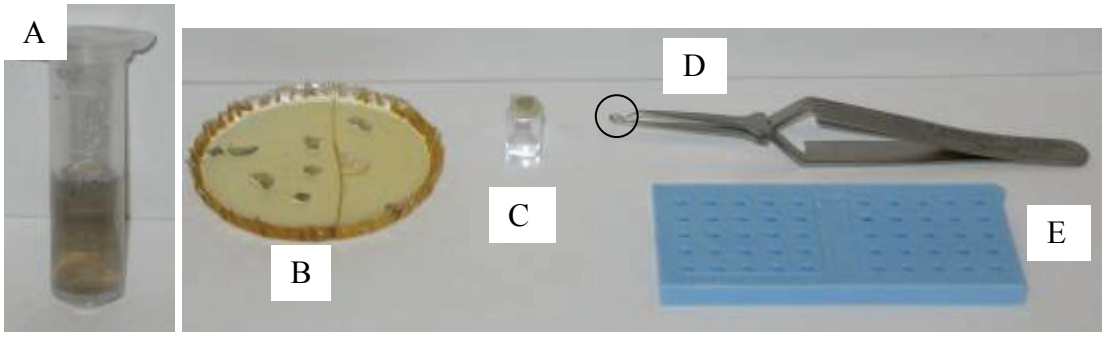

Figure 4.1. Photos of (A) Carboxylate anion terminated HEG functionalized SWCNTs in water electrolyte (Na^+), 0.7 mg/mL; (B) SWCNTs/resin pieces (dark) embedded in a resin pan; (C) SWCNTs/resin piece mounted on top of a cylinder platform; (D) SWCNTs/resin section on top of a copper grid (circled), which is held by a tweezers; and (E) Container with copper grids inside.

4.2.4 Single-axis-tilt electron microscopic imaging and tomographic reconstruction

A series of electron images was acquired under 200kV working voltage following standard procedure (Ellisman, 2006) for single-axis-tilt tomographic reconstruction.

Tilt series were recorded at 50,000× magnification with Tietz 4Kx4K digital camera at 55033332 dpi producing images of size 2084 × 2084 pixels. The pixel size of the raw images was 0.46 nm. The specimen was tilted with an angular increment of 2° from –60° to +60° about an axis perpendicular to the optical axis of the microscope. A computer-controlled goniometer was used to accurately increase the angular steps. During the tilt, gold beads were used as reference for the sake of the following alignment. Sample images are shown in Figure 4.2.

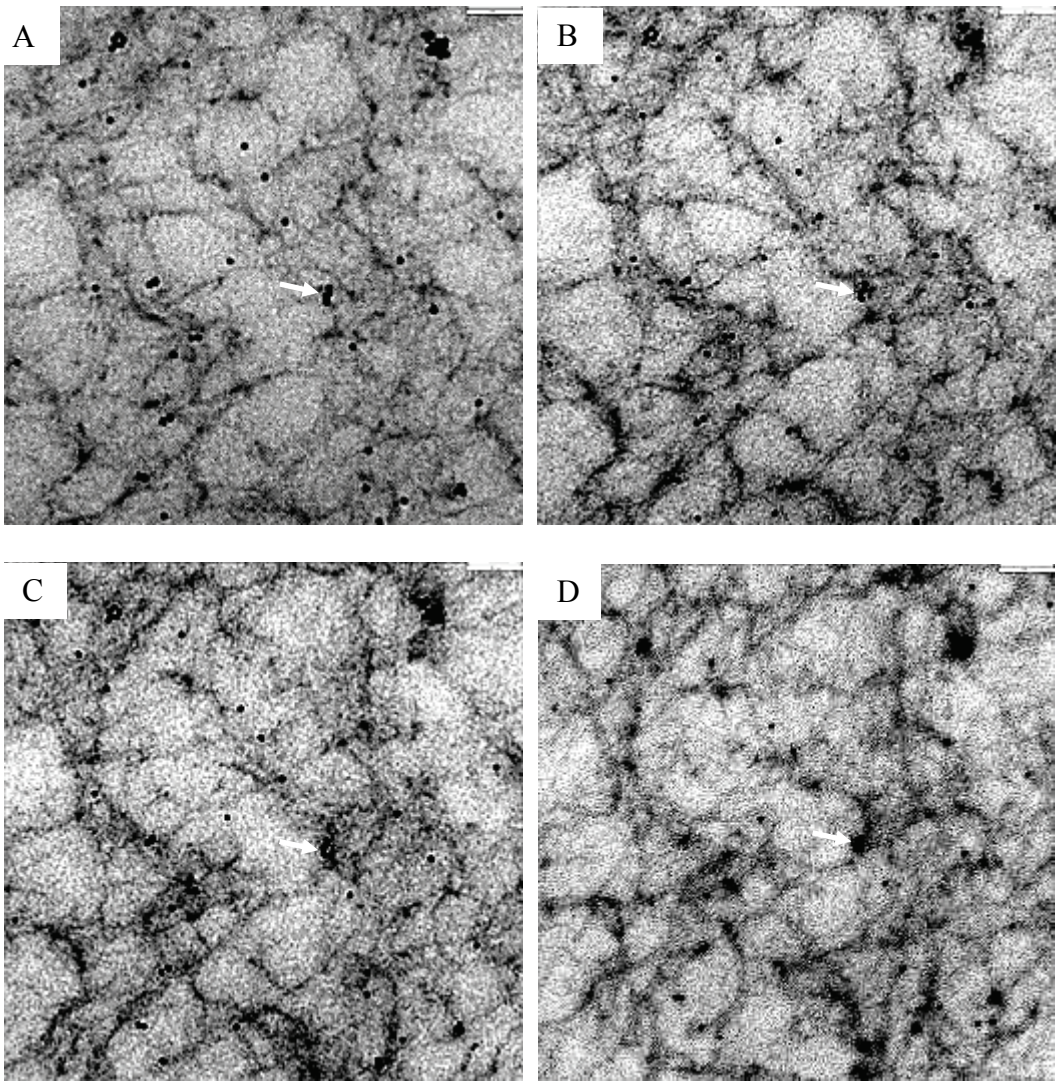

Figure 4.2. Transmission electron microscope (TEM) images for SWCNTs at –16° tilt (A), 0° tilt (B), +16° tilt (C) and 34° tilt (D). The tilt of the shown images is around horizontal direction. White arrows point to one set of reference gold bead (10 nm). Up-right bar is 100 nm.

The image series was analyzed and aligned with the IMOD program package (Boulder Laboratory for 3-Dimensional Electron Microscopy of Cells, University of Colorado) for fiducial alignment and data manipulation prior to the back projection, which was conducted using the TxBr package (Ellisman, 2006).

In the alignment of SWCNTs network structures, gold beads were numbered and were marked for the images at every tilting angle. Altogether, 22 gold beads were used in the alignment. Figure 4.3 (A) and (B) show the 0° tilt image and its counterpart with gold beads marked, respectively.

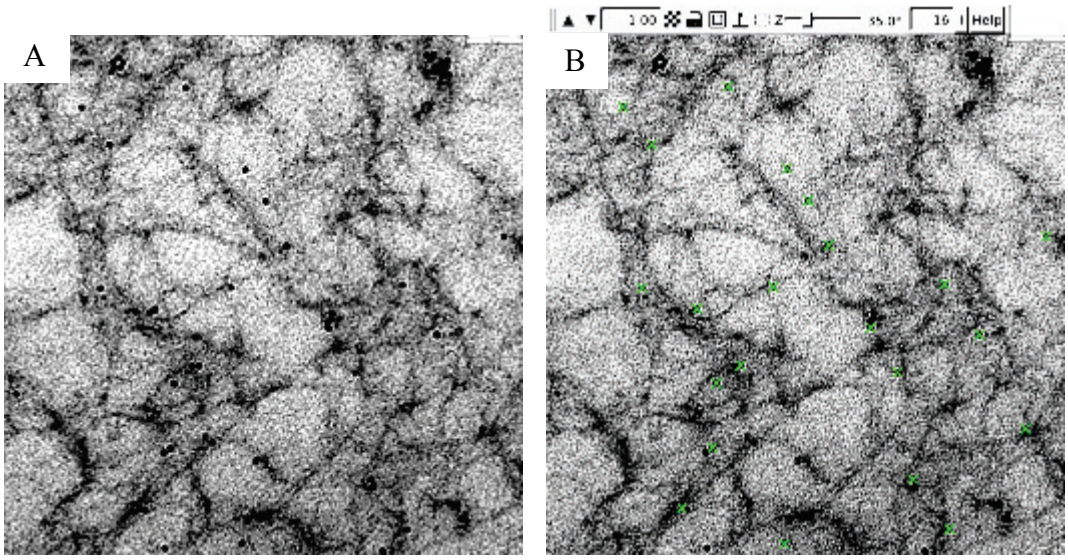

Figure 4.3. Illustration of image alignment. 0° tilt image with gold beads unmarked (A) and marked (B). Up-right bar is 100 nm.

After alignment of the gold beads, the surrounding SWCNTs structures were aligned accordingly based on the geometric relationships. Figure 4.4 shows example pairs of images before and after the alignment. A movie was produced from the aligned image series to illustrate the SWCNTs appearance during the tilting. The aligned image series provide continuous 3D information for the SWCNTs in the resin matrix.

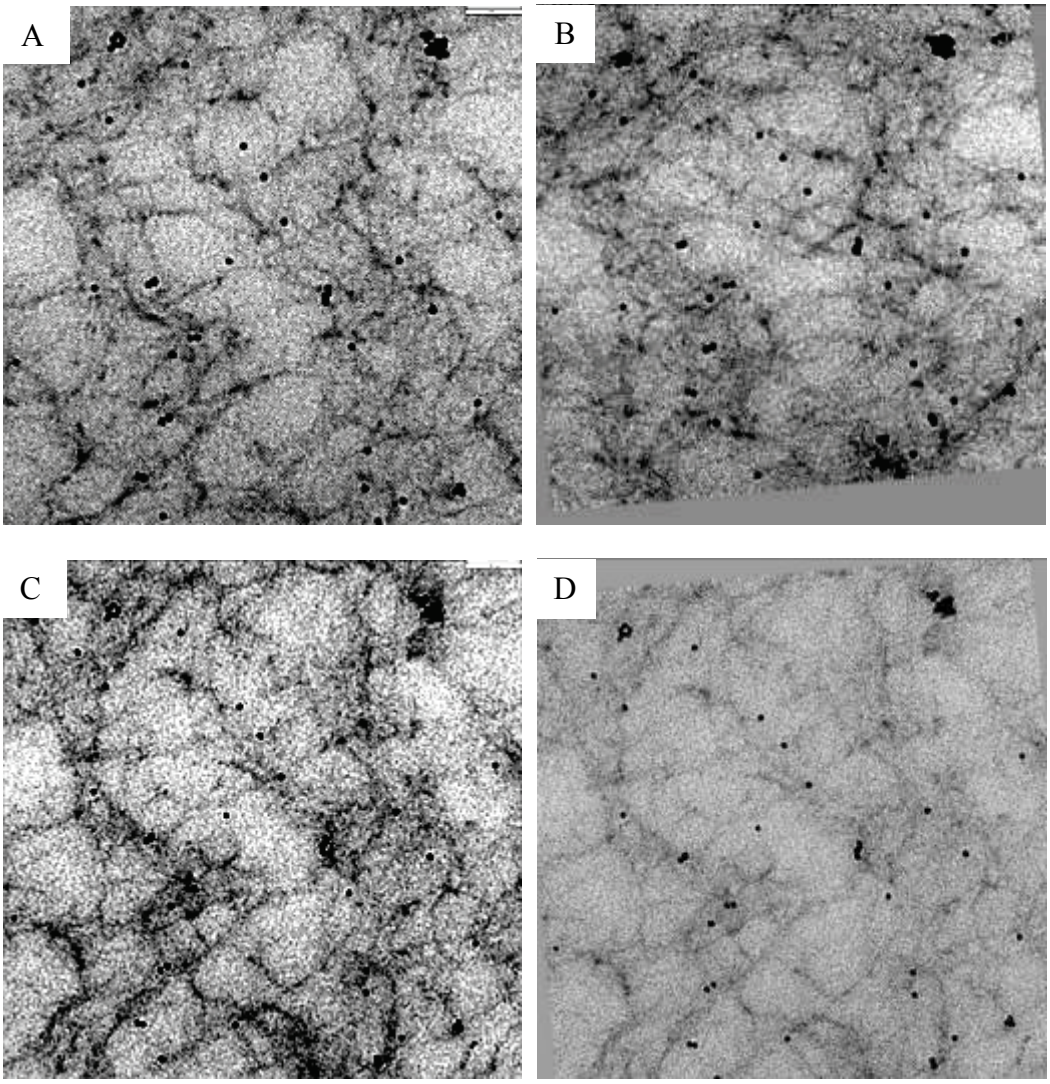

Figure 4.4. Example projection images before and after alignment. (A) and (B) for –16° tilt before and after alignment, respectively. (C) and (D) for +16° tilt before and after alignment, respectively. Up-right bar in (A) and (C) is 100 nm.

IMOD extracted three-dimensional information from the aligned image series, and a model was reconstructed for the SWCNTs network structures in the resin (Figure 4.5) based on the electron contrast. Heavier elements, such as gold or uranium, have better electron contrast in comparison to lighter elements such as carbon or oxygen. The gold beads, which were necessary for alignment of the image series,

introduced a significant artifact to the model reconstruction due to the high electron contrast. The electron contrast of the single carbon shell and the surrounded cylindrical gap was comparatively low. Heavy metal staining with uranyl acetate and Reynold's lead citrate provided additional electron contrast of the SWCNTs. The electron contrast of the stained SWCNTs, based on model reconstruction, was still low.

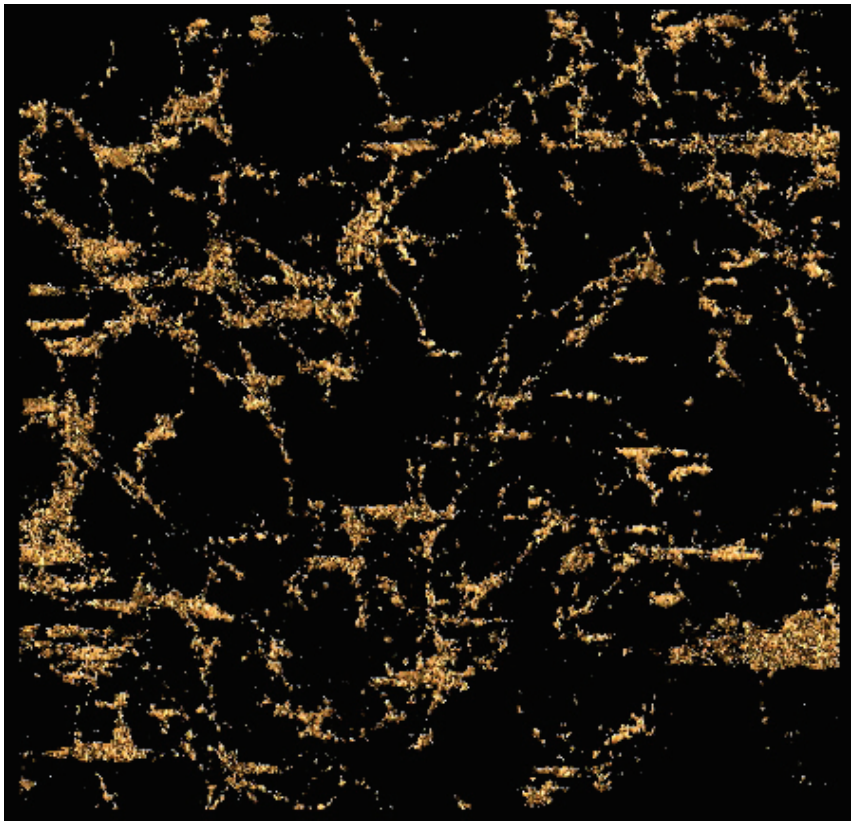

Figure 4.5. Reconstructed 3D model of the SWCNTs in resin.

4.3. Spectroscopic characterization methods

4.3.1 Infrared spectroscopy

Fourier Transform Infrared (FT-IR) spectra were recorded in transmission mode on a Nicolet 510P FT-IR Spectrometer (Thermo Fisher Scientific Inc., Waltham, MA) over a wavenumber range of 400 to 4000 cm^{-1}. Typically, a small amount of CNT powder was mixed with FT-IR grade potassium bromide (KBr), and the mixture was pressed into a transparent thin disc. The spectrum was taken at 4 cm^{-1} resolution averaging 128 scans. The liquid samples were prepared differently. Typically, one drop of the liquid was placed in between two transparent KBr discs for the FT-IR experiment.

4.3.2 Raman spectroscopy

Raman spectra were taken on a Renishaw Ramascope Raman Spectrometer (Renishaw plc., Hoffman Estates, IL) using a green laser (Argon laser, 514 nm wavelength) at 25 mW laser power. The Raman analysis covers a wavenumber range of 200 to 4000 cm^{-1}.

4.3.3 Nuclear magnetic resonance spectroscopy

Nuclear magnetic resonance (NMR) spectroscopy studies were conducted on a Mercury Plus 400 Actively Shielded NMR System (Varian Inc., Santa Clara, CA). Typically, one drop of hexaethylene glycol species containing amine groups was dissolved in DMSO-d_6 (2 mL) in a NMR tube before the experiment. Other

hexaethylene glycol species and non-amine containing specimen were dissolved in $CDCl_3$ for the NMR experiment.

4.3.4 Mass spectroscopy

Mass spectroscopy studies were conducted on a quadrupole-time-of-flight (QTOF) mass spectrometer (Agilent Technologies Inc., Santa Clara, CA). Typically, one drop of the liquid chemical was diluted in 5 mL acetone and before submission to the Mass spectroscopy experiment.

4.4. Acknowledgement

This chapter is prepared for publication by S. Nemat-Nasser, Y. Gao and Y. Tor. The dissertation author was the primary investigator and author of this paper. This work has been conducted at the Center of Excellence for Advanced Materials, CEAM, Department of Mechanical and Aerospace Engineering, University of California, San Diego, and has been supported by the Air Force Office of Scientific Research Grant Number N0001404M0164. I would also like to thank Mason Mackey for many helpful discussions regarding the electron tomography procedure. The author also acknowledges the TEM usage in the National Center for Microscopy and Imaging Research (NCMIR). The author also acknowledges the SEM usage in Nano3 Clean Room and Analytical Labs in UCSD. The author also acknowledges the IR spectrometer usage in Professor David Hendrickson's lab in Department of Chemistry

and Biochemistry in UCSD. The author also acknowledges the Raman spectrometer usage in the Center for Magnetic Recording CMRR) in UCSD.

4.5. References

J. Frank (1992). "Electron Tomography: Three-dimensional Imaging with the Transmission Electron Microscope", Plenum Press, New York.

A. Steven1 and D. Belnap (2005). "Electron Microscopy and Image Processing: An Essential Tool for Structural Analysis of Macromolecules." Curr. Protoc. Prot. Sci., 17.2.1–17.2.39.

J. H. Venable and R. Coggeshall (1965). "A simplified lead citrate stain for use in electron microscopy." J. Cell Biol., Vol.25, 407-408.

A. Lawrence, J. C. Bouwer, G. Perkins and M. H. Ellisman. "Electron Tomographic Analysis of Cytoskeletal Cross-Bridges in the Paranodal Region of the Node of Ranvier in Peripheral Nerves." J. Struct. Biol 154, 144 (2006).

Chapter 5

Numerical Modeling and Free Energy Analysis of SWCNTs Network Structure

Free energy analysis was conducted to further understand the self-assembly behavior of functionalized single-walled carbon nanotubes (SWCNTs). Energetic and entropic components of the Gibbs free energy are discussed for the SWCNTs network. The results from experimental observations (Chapter 3) were adopted in this chapter. Numerical modeling methods are used to assist the analysis.

This Chapter first introduces the concept of calculating the Gibbs free energy for the SWCNTs network. The associated experiment results are reviewed. Related numerical methods are introduced in section 5.1. Section 5.2 describes the atomistic modeling and numerical simulations of SWCNTs in small domains, such as the cluster domain, to evaluate their contribution to Gibbs free energy. Section 5.3 calculates the configurational entropy that affects the Gibbs free energy, which is then calculated and the results discussed. Finally, coarse-graining of SWCNTs is described, and preliminary Monte Carlo simulations are presented.

5.1. Introduction

5.1.1 Gibbs free energy of SWCNTs network structure

Consider SWCNTs network structure in a unit volume (V) of water electrolyte. The Gibbs free energy change ($\Delta G_{network}$) of the SWCNTs' network structure in comparison to their random state can be divided into energetic and entropic contributions.

$$\Delta G_{network} = \Delta U_{network} - T\Delta S_{configuration} \quad (1)$$

Here $\Delta U_{network}$ represents the internal energy change of the SWCNTs' network structure in comparison to their random state. $\Delta S_{configuration}$ is the configurational entropy difference when SWCNTs form orderly network from the random state. T is the absolute temperature. The temperature (T), pressure (P) and volume (V) of the SWCNTs water suspension are considered constants in the calculation of Gibbs free energy.

The change in system internal energy ($\Delta U_{network}$) is primarily affected by the inter-nanotube potentials among SWCNTs. In a dilute suspension, when SWCNTs are randomly distributed in water, the distance between any two nanotubes is large, and hence the interaction potential is negligible. On the other hand, when SWCNTs interconnect with each other and form a network structure, the inter-nanotube potential at the end joint, e.g. the cluster domain, provides the driving force that binds nanotubes together. In this scenario, the system's Gibbs free energy is evaluated as follows:

$$\Delta G_{network} = \sum_{n_p} \Delta U_{cluster} - T\Delta S_{configuration} \quad (2)$$

Here $\sum_{n_p} \Delta U_{cluster}$ is the summation of interaction potentials for the small cluster domains in the network structure. n_p is the number of clusters. $\Delta U_{cluster}$, total energy of the small but complex cluster domain, can be evaluated based upon molecular simulations. $\Delta S_{configuration}$ can be calculated based on the probability of SWCNTs forming the network structure from random distributions. Associated parameters are extracted from experiments.

5.1.2 Input from experimental results

In the experimental work, 1.4 nm diameter single-walled carbon nanotubes were shortened and end-functionalized with heterobifunctional hexaethylene glycol (HEG) derivatives. The free termini of the HEG chains were modified to bear carboxylate anions. The functionalized SWCNTs were placed in aqueous electrolyte containing sodium cations. The pH was adjusted to approximately 7. Remarkably, interconnected network structures were observed with electron microscopes in both two-dimensional (2D) or three-dimensional (3D) settings. Based on the length distribution (Figure 3.2), 96% of the SWCNTs in the 2D network structure were smaller than 100 nm. The average length was 65.2 nm.

5.1.3 Atomistic modeling, coarse-graining, and Monte Carlo simulation

Computer simulations are convenient tools to study the molecular-level behavior of functionalized SWCNTs in water. The computer simulations permit investigations of the thermodynamics of the behavior of SWCNTs, for example, in the nanometer-scale cluster domain. The molecular models for the computer simulations can be divided into two principle categories by the modeling methods: atomistic models and coarse-grained models.

Atomistic models describe individual atoms as simulation particles in the simulation systems. Due to the small size of atoms, atomistic models are generally used for molecular systems up to tens of nanometers in size. An atomistic model includes not only the molecular structure, but also the chemical bonding, electrostatic, and VDW interactions (Jue, 2010). Due to the small interaction scale, atomistic simulations implement a time step that can be as short as a tenth of the period of the fastest mode in the system (Mackerel, 2004), e.g., a covalent bond stretch. The simulations usually consist of up to tens of nanoseconds of data. The force-field approach is a popular method to define the intra- and inter-atomic interactions. The force field method uses a set of empirical formulas to mimic the interactions in an average fashion (Burkert and Allinger 1989). Atomistic models, together with the force field method, are widely used to investigate the behavior of one single-walled carbon nanotube in various situations. Nativ *et al*. (2007) applied atomistic models in dynamic simulations to study adsorption and aggregation of amphiphilic molecules on a single wall carbon nanotube. Wallace *et al*. (2007) used atomistic dynamic

simulations to investigate the dependence of adsorbed structures on the bulk concentration, and calculated the average orientation of the surfactant molecules with respect to the CNT-axis to characterize the structures. Song *et al*. (2005) studied the self-assembly mechanism of cytosine and guanine functionalized single-walled carbon nanotubes utilizing *ab initio* calculations combined with empirical molecular dynamics simulations at atomistic scale.

In the present study, SWCNTs self-assembled via ionic clustering. A cluster domain formed by the ends of several SWCNTs involving attached chain molecules, terminal anions and counter ions in aqueous environment. The size of a cluster domain may be up to tens of nanometers. Thus, the atomistic model with a force field method is a suitable tool to investigate the potentials within the small cluster domain.

Atomistic modeling is computationally expensive, although it may provide the details necessary to understand molecular structure and localized interactions. The size and time scales of the atomistic models are usually limited. For events such as self-assembly of many SWCNTs, where individual nanotube length is ~65 nm, the system size is well beyond atomistic capabilities. In this scenario, coarse-grained (CG) or mesoscale models are required. Reducing the degrees of freedom by combining multiple atoms into one effective particle and eliminating short-range dynamics are two techniques used in CG models that speed up simulations and permit analysis of mesoscale phenomena (Nielsen *et al*., 2004). Although the CG models lack atomistic details, they can preserve many significant aspects of the structural and chemical information. Typically, an atomistic structure formed by multiple atoms is mapped

into a CG particle. The interaction between two CG particles is mapped from the interaction between two sets of corresponding atomistic structures. This mapping can overcome the size limits of atomistic models.

The coarse-grained models are often linked to Monte Carlo (MC) simulations in molecular studies (Van Voorst Tot Voorst, 2008). Monte Carlo methods are used to generate Boltzmann-probability-distributed configurations of the coarse-grained particles whose intra- and inter-particle interactions are treated via a coarse-grained force field (Arya, 2009). MC simulations with CG modeling have been applied to study SWCNTs. Duren and Keil (2007) used Monte Carlo simulations with coarse-grained models to study the adsorption of methane inside SWCNTs. Gurevitcha and Srebnik (2008) used the Monte Carlo method to investigate the wrapping of polymers around SWCNTs.

5.2. Atomistic modeling of SWCNTs, attached chain linkers and ions in water

Atomistic modeling provides detailed descriptions for the interactions between different types of atoms, making it an excellent candidate to study the complex structure of the SWCNTs cluster domain. The cluster domain involves the interactions between many different chemical components such as nanotube ends, attached polymer chain linkers, terminal anions and counterions, and water. The system size for atomistic scale modeling, however, is limited due to the expensive computation cost.

5.2.1 Atomistic models with force fields

To model the 1.4 nm diameter SWCNTs used in the fabrication, this dissertation assumes that chirality was not a major factor in SWCNTs self-assembly. A (10,10) single-walled carbon nanotube was adopted with a calculated diameter of 1.357 nm. The nanotube segment was open on both sides. The nanotube atomistic structure with connection information was generated by TubeGen 3.3 package (Frey and Doren, 2005). A geometrical model of the nanotube body segment is shown in Figure 5.1 (A). The length of the SWCNT segment was 1.357 nm. When the nanotube segment represents the end of a functionalized SWCNT, one end of the SWCNT segment was bonded with carboxylate anion terminated HEG linkers (20-amino-3,6,9,12,15,18-hexaoxaicosan-1-oate) via an amide bond. The HEG linker was drawn with ChemBio3D Ultra 11.0, and the geometrical information was extracted. The linker was then connected to a carbon atom at the end of the nanotube segment. Figure 5.2(B) shows an example model of the nanotube end segment with one HEG linker attached to the end.

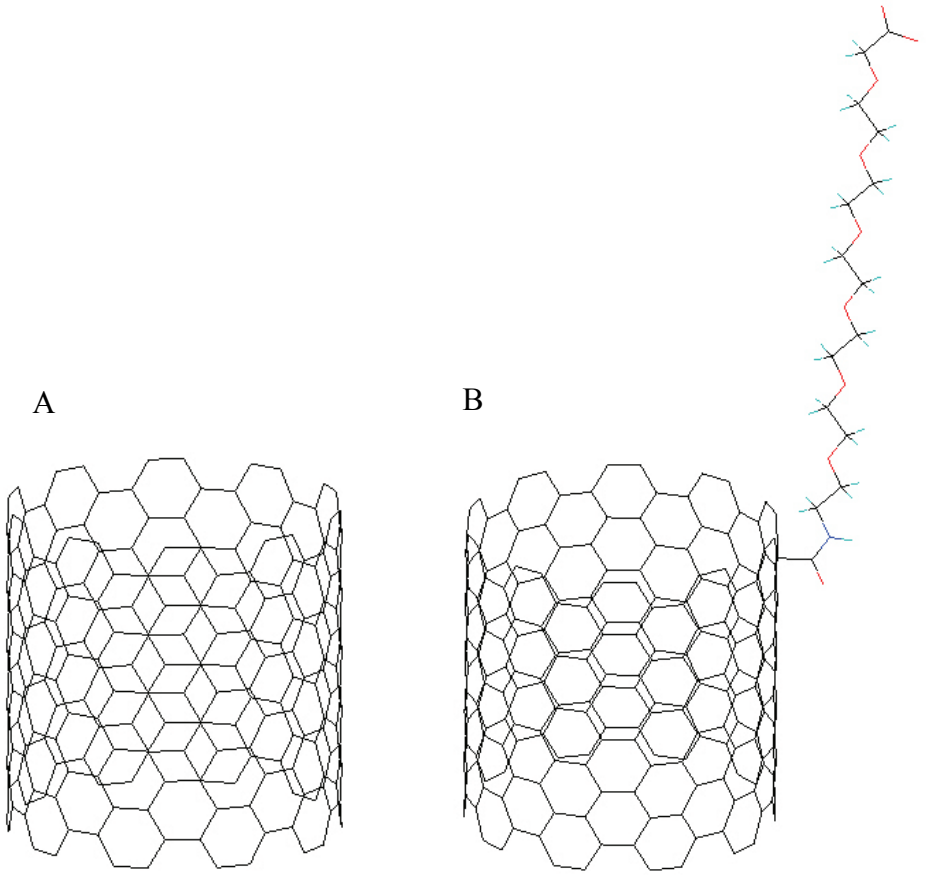

Figure 5.1. Example atomistic structures of (A) SWCNT segment and (B) SWCNT segment with one end attached with one hexaethylene glycol linker. The carbon atoms are shown in black, the oxygen atoms are shown in red, the nitrogen atom is shown in blue, the hydrogen atoms are shown in cyan. Each atom is represented as a bead.

The force field was applied to describe the interactions (i.e. bond and angle) among atoms. SWCNT segments, sodium cations and water molecules were modeled with GROMACS OPLS (Optimized Potentials for Liquid Simulations) all atom force field (Jorgensen and Tirado-Rives, 1988; Jorgensen *et al.*, 1996), which has been widely used for molecular simulations. The force field for the hexaethylene glycol (HEG) linker was applied following the works of Borodin *et al*. (2003), which is compatible with the OPLS force field, and concomitantly provides better descriptions

for the interactions involving a polyethylene glycol chain. The bonding between the SWCNT and attached HEG linker was modeled with the OPLS all atom force field.

5.2.2 Cluster formed at functionalized nanotube ends

To study the cluster formed by functionalized SWCNTs at the ends, explicit-solvent molecular dynamic simulations of small functionalized SWCNT segments were conducted using GROMACS 3.2 with aforementioned models and force fields.

In a typical simulation procedure, two nanotube end segments were oriented co-axially, with the HEG functionalized ends facing each other so that they could form a cluster. Forty HEG linkers were attached to the nanotube end. The distance between the segment mass centers is 3.8 nm. The nanotube portion was constrained throughout the simulations using 40 strong harmonic springs, each having a spring constant of 2000 kJ/mol/Å^2. A simulation box of dimensions 6.5 × 6.5 × 6.5 nm^3 was employed with periodic boundary conditions.

A short 2000-step steepest descent energy minimization was conducted with the "mdrun" command to remove steric clashes resulting from addition of the HEG linkers to the SWCNT ends. The structures were then solvated with TIP3P water molecules using the "genbox" command. Sodium cations were added to maintain electroneutrality using the "genion" command. The resulting configuration was energy minimized using 2000 steps of steepest descent. A snapshot of the system during the final energy minimization is displayed in Figure 5.2.

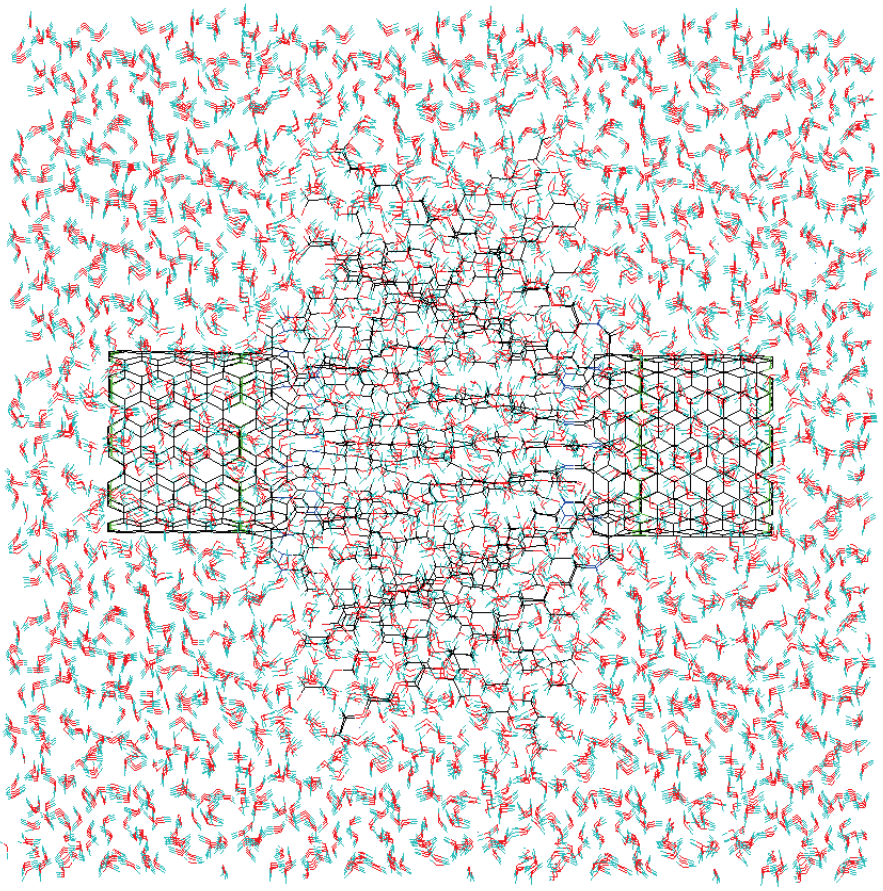

Figure 5.2. Example cluster domain during the energy minimization atomistic structures of two HEG functionalized SWCNT end segments. The carbon atoms are shown in black, the oxygen atoms are shown in red, the nitrogen atom is shown in blue, the hydrogen atoms are shown in cyan. The constraining atom is shown in green. Each atom is represented as a simulation bead.

In a canonical ensemble (*NVT*), the number of particles (*N*), the volume (*V*) and the system temperature (*T*) are constants. *NVT* conditions were achieved by coupling the systems to the Nose-Hoover thermostat (Nose, 1984; Hoover, 1985) with a coupling time constant of 0.5 ps. The particle mesh Ewald (PME) algorithm (Tom *et al*., 1993) was applied to model electrostatic interactions with a space cutoff of 1.0 nm, the same as for the cutoff of van der Waals interactions. The pair list was updated

during every step, and Lincs constraints (Hess *et al*., 1997) were applied to all bonds involving hydrogen atoms, permitting a time step of 0.5 fs.

The system was first permitted to equilibrate for 200 ps in the NVT ensemble. After equilibration, an 800 ps long production run was conducted under NVT conditions at 300 K. The SWCNT portion was constrained during the equilibration and production runs.

5.2.3 Potential of mean force (PMF) calculations

To determine the "effective" interaction between two HEG functionalized SWCNT ends, the PMF was calculated as a function of the separation distance d, defined as the distance between two segment centers. The PMF is essentially a free energy of the system where the two SWCNT segments are constrained within a specific distance apart. The segments are still free to sample their remaining degrees of freedom, such as HEG chain configurations. Hence, the PMF is an accurate indicator of the effective interaction between SWCNT segments, as it contains contributions from both the energy and entropy. In this dissertation, the PMF was computed by first calculating the average force ($\langle F(d) \rangle$) experienced by two SWCNT segments in the direction along the segment centers due to the remaining degrees of freedom. $\langle F(d) \rangle$ was evaluated from Hooke's law as the inverse of the average force posed by the constraints in the direction along the segment centers.

$$\langle F(d) \rangle = -\left\langle \sum_{N_{constr}} k_{constr} \Delta \boldsymbol{x} \right\rangle \tag{3}$$

The force was defined in the direction parallel to the vector connecting two SWCNT segment centers. The average is over the production run.

The PMF, $\Delta U_{cluster}(d)$, is computed by integrating the calculated force as follows:

$$\Delta U_{cluster}(d) = -\int_{\infty}^{d} \langle F(d') \rangle d' \tag{4}$$

Note that the PMF is essentially the total energy for the cluster domain.

The computed PMF for the cluster is plotted in Figure 5.3. The PMF has the most negative potential (–150 kJ/mol), indicating maximal attraction at a distance of 2.76 nm. When two functionalized nanotube ends approach each other, the HEG linkers initiate contact at a distance of ~5 nm, indicating a long range interaction. When two nanotube ends are closer, the HEG linkers interact with each other and gradually form a cluster. At ~2.76 nm distance, the tangled HEG linkers saturate the space domain in between the two nanotube ends. The attraction potential reaches the maximum indicating a more stable cluster. When two nanotube segments are placed closer, the already saturated cluster domain is rendered unable to accommodate the additional HEG linkers, resulting in strong repulsion.

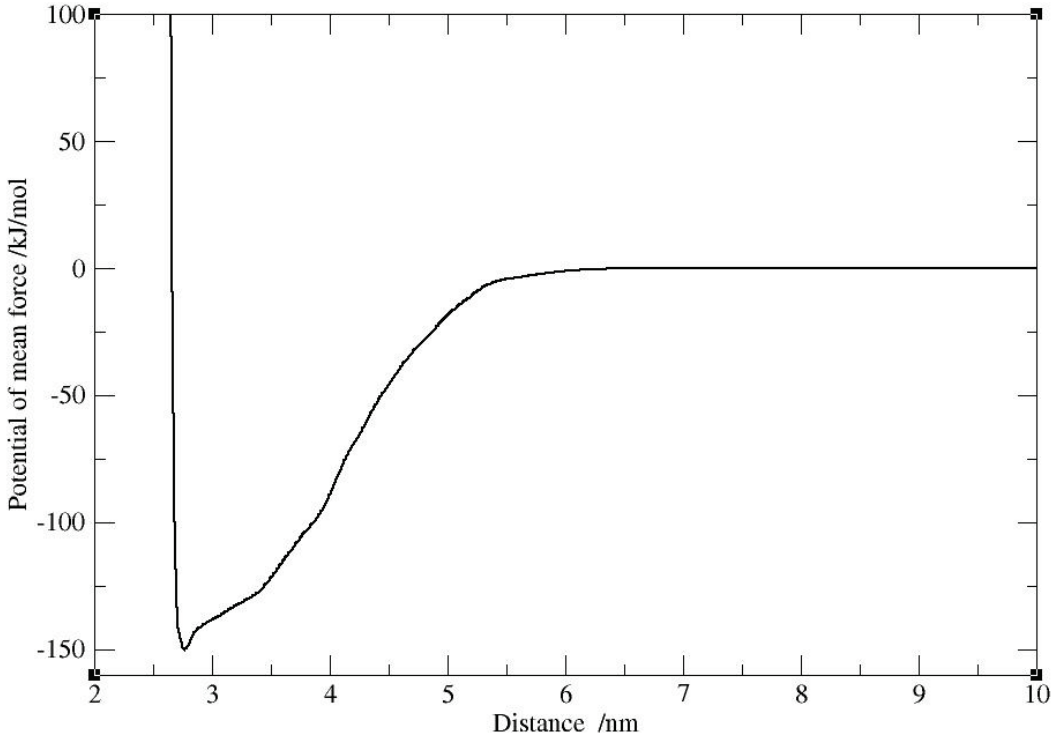

Figure 5.3. Potential of mean force for the cluster formed by two SWCNTs.

5.2.4 PMF of other simple configurations of two SWCNT ends

End-concentrated HEG functionalized SWCNTs possess amphiphilic characteristics. The functionalized end presents hydrophilic properties while the un-functionalized or less functionalized nanotube sidewall keeps its hydrophobic characteristics. Hence, a short SWCNT in this study can be divided into two types of regions: hydrophilic end region (HER) and hydrophobic sidewall region (HSR). There are three types of interactions between the two different regions: HER-HER, HSR-HSR and HER-HSR interactions. A cluster formed by nanotube ends results primarily from the HER-HER type of interactions, which exhibit strong and long term attraction. The other two types of interactions are also modeled atomistically for comparison

following the procedure described in section 5.2.2. HSR-HSR interaction was modeled by constraining two nanotube sidewall segments parallel to each other and at a given distance between the segment centers (Figure 5.4). HSR-HER interaction was modeled by constraining one nanotube sidewall segment and one functionalized nanotube end segment at a given distance between the segment centers. Yet, in this case, the two nanotube axes are perpendicular to each other in the same plane (Figure 5.5). PMF was calculated from the mean force following the procedures described in section 5.2.3.

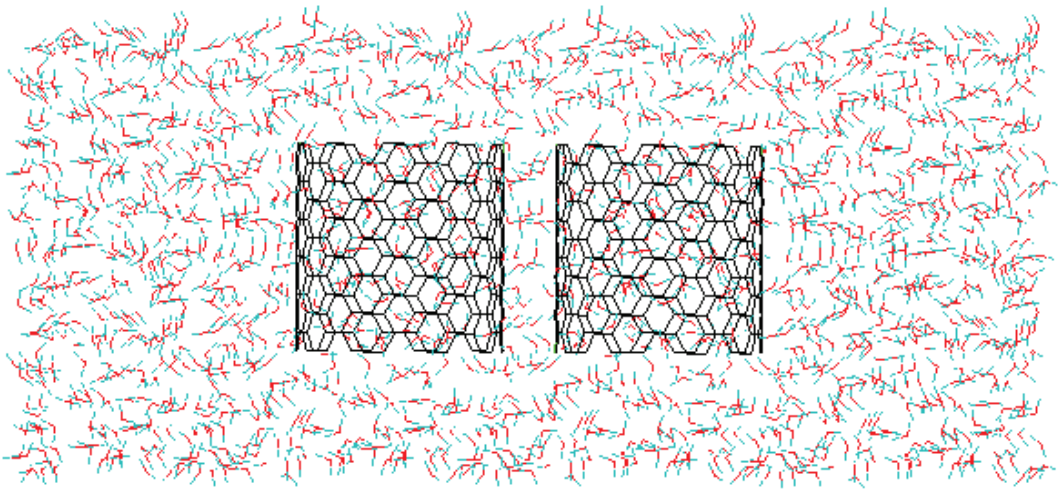

Figure 5.4. Example system containing two nanotube body segments in water. The distance between two nanotube segment centers is 1.7 nm. The carbon atoms are shown in black, the oxygen atoms are shown in red, the hydrogen atoms are shown in cyan. Each atom is represented as a bead.

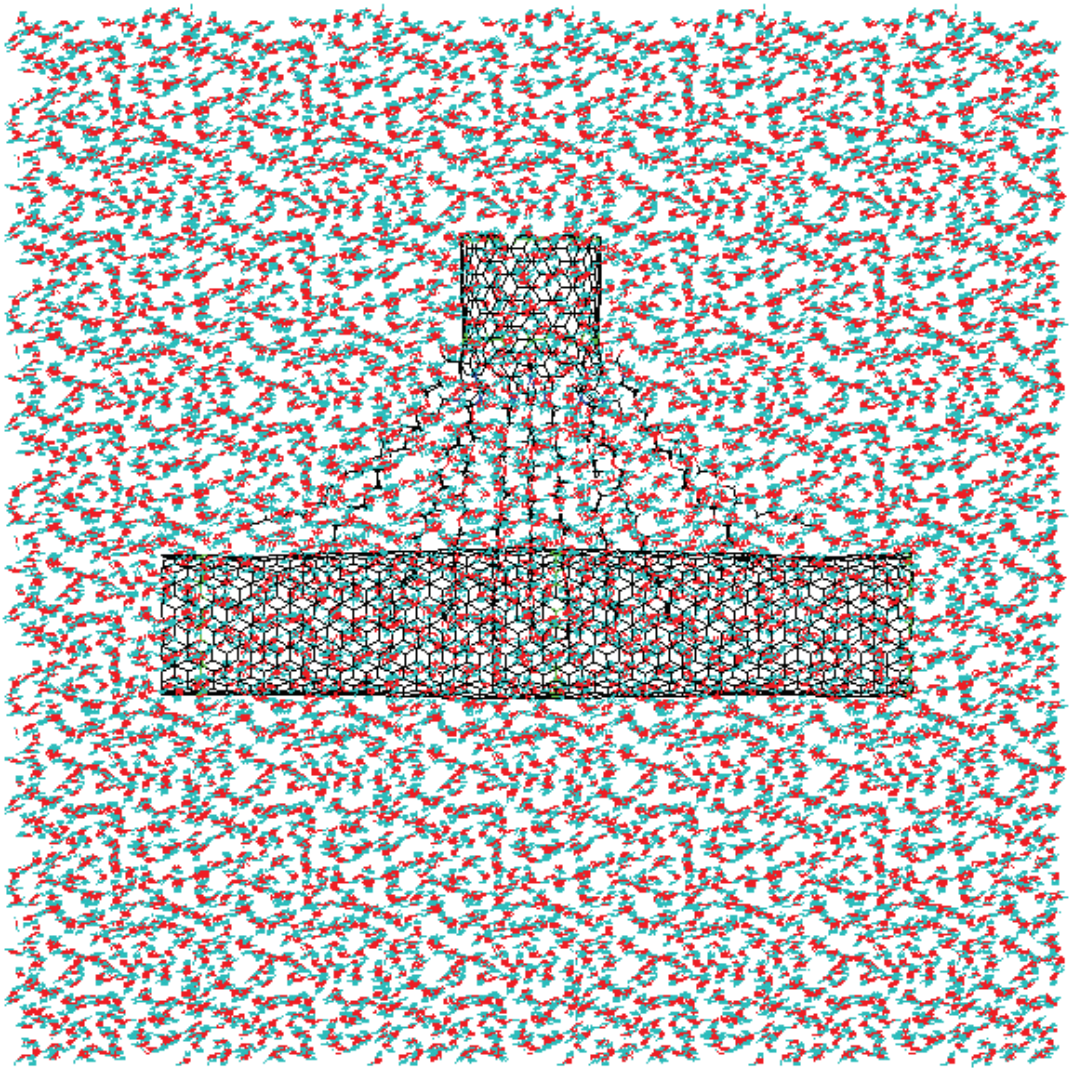

Figure 5.5. Example system containing one nanotube body segment and one nanotube end segment in water. The distance between two nanotube segment centers is 3.1 nm. The carbon atoms are shown in black, the oxygen atoms are shown in red, the hydrogen atoms are shown in cyan. Each atom is represented as a bead.

The PMFs are plotted in Figure 5.6. The HER-HER curve is re-plotted from Figure 5.3. The HSR-HSR interaction has a potential well depth (–15 kJ/mol) at a distance of 1.67 nm, which is ~10% of that for the HER-HER interaction in forming the cluster. The HSR-HSR interaction is short-ranged because of the lack of polymer

chain extensions. The HSR-HER potential reaches –53 kJ/mol at a distance of 2.57 nm. The HSR-HER interaction potential falls between the HER-HER potential and HSR-HSR potential, which is as expected.

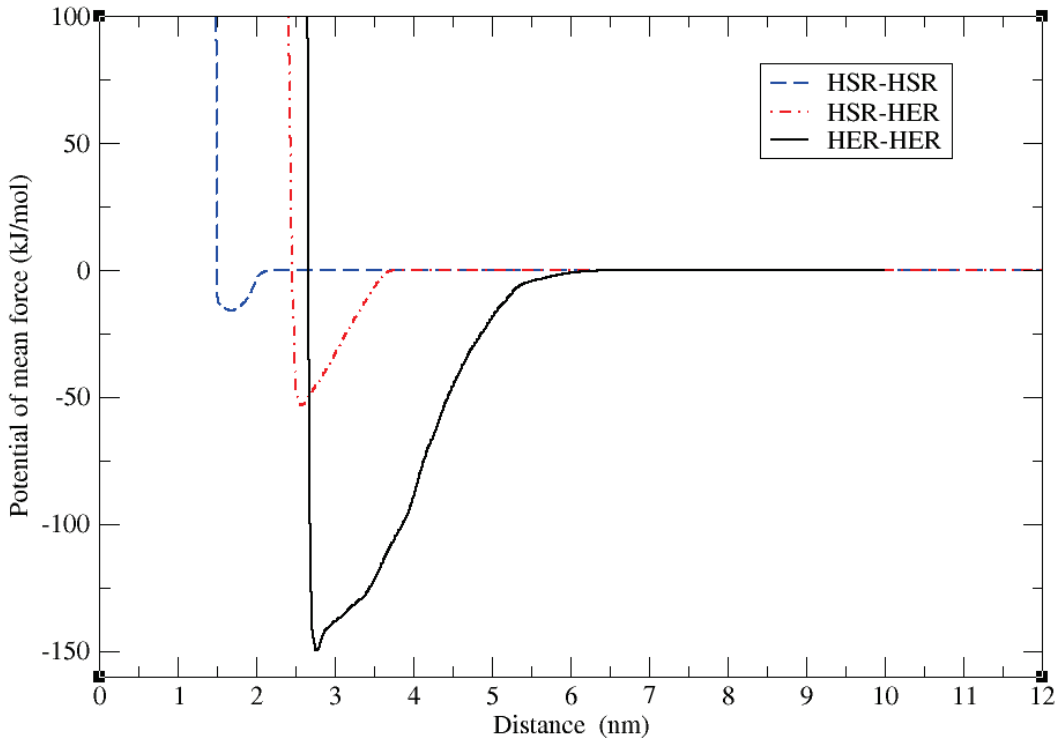

Figure 5.6. Potentials of mean force between HSR-HSR (dashed line in blue), HSR-HER (dash-dot-line in red), and HER-HER (solid line in black).

5.3. Configurational entropy of SWCNTs network structure

The configurational entropy ($\Delta S_{configuration}$) for SWCNTs is divided into a distributional part ($\Delta S_{distrib}$) and a clustering part ($\Delta S_{clustering}$).

$$\Delta S_{configuration} = \Delta S_{distrib} + \Delta S_{clustering} \tag{5}$$

$\Delta S_{distrib}$ represents the entropy increase by distributing nanotubes such that every p nanotubes are close to each other in a space volume. $\Delta S_{cluster}$ represents the entropy increase by arranging already closely placed p nanotubes into a radially shaped structure within that space volume. Both terms are evaluated from probabilities. Note that $\Delta S_{clustering}$ is not included in $\Delta U_{cluster}$, which was evaluated when constraining small nanotube segments in the small cluster domain.

To evaluate $\Delta S_{configuration}$, consider placing N nanotubes into M volume elements (VE) in a system of total volume V. Each VE has a volume V_{VE}, which can accommodate p radially clustered SWCNTs. The diameter of the spherical domain is approximated by L_{CNT}, the length of SWCNTs. Assume that the VEs and nanotubes are distinguishable.

The SWCNTs networking procedure is formulated in accordance with two steps. First consider a simple case where there are (1) n_p VEs ($n_p \le N$), each containing p nanotubes ($p \ge 2$ is an integer), and (2) other $M - n_p$ VEs, each containing one or zero nanotubes. The probability of having this state contributes to the distributional entropy. Second, for one VE that contains p nanotubes, the probability of arranging p nanotubes into an end-jointed radial structure contributes to the clustering entropy. A schematic illustration is provided in Figure 5.7 for the above configurational approach. VEs and nanotubes are considered distinguishable.

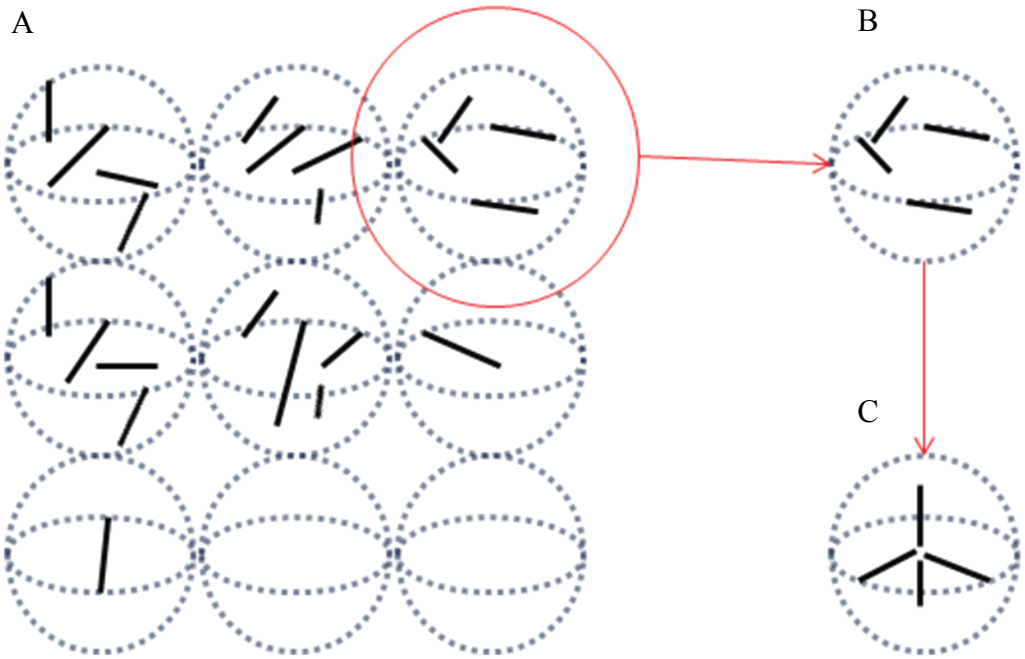

Figure 5.7. Schematic illustrations of (A) Distribute N nanotubes into M volume elements (Each volume element contains 4, 1 or 0 nanotubes. Only one layer of volume elements is filled with nanotubes.); and (C) Arrange the 4 nanotubes into end-jointed radial structure in the volume element. (B) Represents a single volume element accommodating 4 randomly distributed nanotubes. The scheme is not drawn to scale.

5.3.1 Distributional probability and associate entropy ($\Delta S_{distrib}$)

The distribution of N nanotubes is performed via two steps. First pn_p nanotubes are placed in n_p VEs, each containing p nanotubes. Then put $N - pn_p$ nanotubes in $N - pn_p$ VEs, each containing one nanotube.

Step 1. Place pn_p nanotubes in n_p VEs, each containing p nanotubes

First choose n_p VEs from M VEs. The number of methods is

$$A_{11} = \frac{M!}{(M - n_p)! n_p!} \tag{6a}$$

Then choose pn_p nanotubes from N nanotubes. The number of methods is

$$A_{12} = \frac{N!}{(N - pn_p)!(pn_p)!} \tag{6b}$$

Finally place pn_p nanotubes into pn_p slots in n_p VEs, each having p nanotubes. The number of methods is

$$A_{13} = \frac{(pn_p)!}{(p!)^{n_p}} \tag{6c}$$

Note that the permutation of p nanotubes in one VE is not counted at the distribution stage.

The total number of methods for putting pn_p nanotubes in n_p VEs is then

$$A_1 = A_{11}A_{12}A_{13} = \frac{M!}{(M - n_p)!n_p!}\frac{N!}{(N - pn_p)!(p!)^{n_p}} \tag{6d}$$

Step 2. Place $N - pn_p$ VEs from $N - pn_p$ VEs, each containing one nanotube

First choose $N - pn_p$ VEs from $M - n_p$ VEs. The number of methods is

$$A_{21} = \frac{(M - n_p)!}{(M - n_p - N + pn_p)!(N - pn_p)!} \tag{7a}$$

Second, choose $N - pn_p$ nanotubes from the rest $N - pn_p$ nanotubes. The number of methods is

$$A_{22} = 1 \tag{7b}$$

Finally place $N - pn_p$ nanotubes in $N - pn_p$ VEs, each has one nanotube. The number of methods is

$$A_{23} = \frac{(N - pn_p)!}{(1!)^{n_p}} = (N - pn_p)! \tag{7c}$$

The total number of methods for putting $N - pn_p$ nanotubes in $N - pn_p$ VEs is then

$$A_2 = A_{21}A_{22}A_{23} = \frac{(M - n_p)!}{(M - n_p - N + pn_p)!} \tag{7d}$$

The total number of methods (states) for orderly nanotube distribution is then

$$A_{orderly} = A_1 A_2 = \frac{M!}{n_p!} \frac{N!}{(N - pn_p)!(p!)^{n_p}} \frac{1}{(M - n_p - N + pn_p)!} \tag{8}$$

The total number of methods (states) to place N nanotubes in M VEs, each containing p nanotubes, is

$$A_{total} = \frac{(pM)!}{(pM - N)!} \tag{9}$$

Generally $A_{orderly} \ll A_{total}$, and random distribution is the most favorable state for the SWCNTs. Here we assume

$$A_{random} \approx A_{total} = \frac{(pM)!}{(pM - N)!} \tag{10}$$

Based on the well-known Boltzmann's equation, the increase in entropy from random status to orderly distributed status is calculated.

$$\begin{aligned} \Delta S_{distrib} &= S_{orderly} - S_{random} \\ &= k \ln(A_{orderly}) - k \ln(A_{random}) = k \ln(\frac{A_{orderly}}{A_{random}}) = k \ln P_{distrib} \end{aligned} \tag{11a}$$

$$S_{orderly} = k \ln\left(A_{orderly}\right) \tag{11b}$$

$$S_{random} = k \ln\left(A_{random}\right) \tag{11c}$$

$$P_{distrib} = \frac{A_{orderly}}{A_{random}} = \frac{M!}{n_p!} \frac{N!}{\left(N - pn_p\right)!(p!)^{n_p}} \frac{\left(pM - N\right)!}{\left(M - N + \left(p-1\right)n_p\right)!\left(pM\right)!} \tag{11d}$$

$S_{orderly}$ and S_{random} are the entropies of SWCNTs orderly distributed state and randomly distributed state, respectively. $P_{distrib}$ is the distributional probability. Note that both entropies are for the SWCNTs in space volume V. Note also that $P_{distrib} \ll 1$ and $\Delta S_{distrib}$ is negative.

$\Delta S_{distrib}$ in equation (11) can be further simplified based upon Stirling's approximation, assuming M, N, $n_p \gg 1$.

$$\begin{aligned}\Delta S_{distrib} = k \ln P_{distrib} \approx k\{&M \ln M + N \ln N + \left(pM - N\right)\ln\left(pM - N\right) \\ &-\left(N - pn_p\right)\ln\left(N - pn_p\right) - \left(M - N + \left(p-1\right)n_p\right)\ln\left(M - N + \left(p-1\right)n_p\right) \\ &-pM \ln\left(pM\right) - n_p \ln n_p - n_p \ln(p!)\}\end{aligned} \tag{12}$$

Denote $\gamma_p = \frac{n_p}{N}$. Then $p\gamma_p$ is the percentage of the nanotubes that form p-tube clusters. Denote $\alpha = \frac{N}{M}$, which relates to SWCNTs concentration in the volume V. After separation of variables, equation (12) may be expressed as a function of p, γ_p and α.

$$\Delta S_{distrib} = Nk\left\{\frac{1}{\alpha}\ln\frac{1}{\alpha}+\ln\frac{\alpha}{p}+\left(\frac{p}{\alpha}-1\right)\ln\left(1-\frac{\alpha}{p}\right)-\left(1-p\gamma_p\right)\ln\left(1-p\gamma_p\right)\right.$$
$$\left.-\gamma_p\ln\gamma_p-\left(\frac{1}{\alpha}-1+\left(p-1\right)\gamma_p\right)\ln\left(\frac{1}{\alpha}-1+\left(p-1\right)\gamma_p\right)-\gamma_p\ln(p!)\right\} \quad (13)$$

5.3.2 Clustering probability and associate entropy ($\Delta S_{clustering}$)

The clustering probability for p nanotubes in a radial formation in a VE is evaluated by two steps. First, position one end of the nanotubes together at the VE center (small cluster domain at nanotube ends). Then distribute the remaining nanotube ends over a spherical surface.

Step 1. Position the cluster domain that contains p nanotube ends at the VE center

The cluster domain that contains p nanotube ends is placed at the VE center. A spherical interaction volume ($V_i^{(p)}$) is used to describe the cluster domain that accommodates the entangled polymer chains, ions, and associated p tube-end segments. The spherical interaction domain for the cluster formed by a pair of nanotubes has a diameter ($d_i^{(2)}$) of 2.76 nm, at which the atomistic simulations exhibited the largest attraction potential. The interaction volume increases when more nanotube ends form a cluster. Assume that each HEG functionalized nanotube end contributes equally to the interaction volume of the cluster domain. $V_i^{(p)}$, interaction volume for the cluster formed by p nanotube ends, is then estimated as

$$V_i^{(p)} = p\frac{V_i^{(2)}}{2}, \qquad V_i^{(2)} = \frac{4}{3}\pi\left(d_i^{(2)}\right)^3 \tag{14a,b}$$

Note that $V_i^{(2)}$ is the interaction volume for the cluster domain formed by two nanotubes.

The spatial probability ($P_{clustering}^{(1)}$) of having p nanotube ends in the interaction volume is calculated as the ratio of the interaction volume over the volume of the VE, where p nanotubes are accommodated.

$$P_{clustering}^{(1)} = \frac{V_i^{(p)}}{V_{VE}} = \frac{\frac{p}{2}\frac{4}{3}\pi\left(d_i^{(2)}\right)^3}{\frac{4}{3}\pi\left(L_{CNT}\right)^3} = \frac{p}{2}\left(\frac{d_i^{(2)}}{L_{CNT}}\right)^3 \tag{15}$$

Here L_{CNT} is the length of the nanotubes. Note both volumes are spherical.

Step 2. Distribute un-clustered ends of the nanotubes over a spherical surface

After joining p nanotubes ends together in the small cluster domain, uniform angular orientations are the preferred configuration of the nanotubes. Figure 5.7 (C) provides an example for the uniform angular orientation of 4 SWCNTs in a VE. As further illustrated in Figure 5.8, this work defines the orientation of a nanotube that originates from the cluster center along the nanotube axis towards its un-joined end (black arrow head). The angles between any two adjacent nanotube orientations (θ_p) are equivalent for the p -nanotube configuration. In this scenario, the un-joined ends of nanotubes are distributed over a spherical surface with radius L_{CNT} . The probability is evaluated separately for n_p=2 and n_p>2. Note that θ_p equals to 120°, 109.47° and

90° when p =3, 4 and 6, respectively. As shown in Figure 5.9, θ_p for other values of θ_p are estimated by fitting a curve with these three cases.

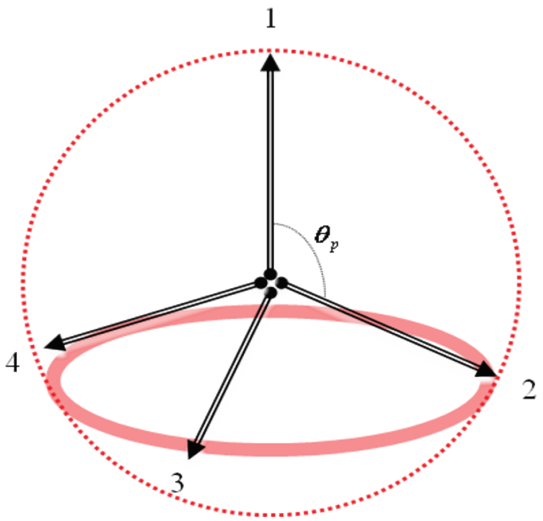

Figure 5.8. An illustration of arranging 4 nanotubes into a end-joined radial configuration in a volume element. θ_p is the angle between two most adjacent nanotubes. After fixing the nanotube 1, nanotube 2 is free to rotate around nanotube 1 at an angle θ_p (ring in red). After the first two nanotubes are fixed, the entire radial structure is determined. The dimensions are not drawn to scale.

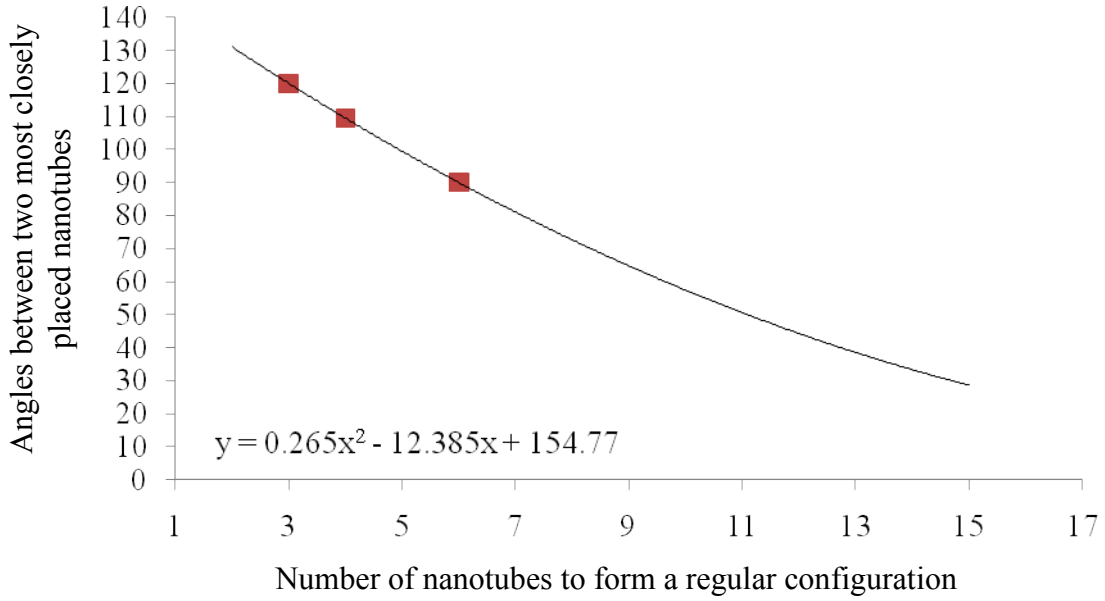

Figure 5.9. Angles between two most closely placed nanotubes for a regular configuration formed by p nanotubes. The squares (■) are the real values for p =3,4 and 6. The black curve is fitted with a polynomial shown in the figure.

Case 1. $n_p = 2$, $\theta_2 = \pi$. When two nanotubes form a radially clustered structure at their ends, the first nanotube is free to place its un-joined end. Note $\theta_2 = \pi$. Once the position of the first nanotube's un-joined end is chosen, the orientation of the second nanotube is determined to be opposite to the first tube. In this study, $L_{CNT} \gg D_{CNT}$ and $S_{Sphere} \gg S_{CNT\_section}$. The probability ($P_{clustering}^{(2-2)}$) for this configuration could be evaluated from the ratio of the area of nanotube cross-section to the area of the sphere surface.

$$P_{clustering}^{(2-2)} = \frac{S_{CNT\_section}}{2S_{Sphere}} = \frac{\pi\left(\frac{D_{CNT}}{2}\right)^2}{8\pi L_{CNT}^2} = \frac{1}{2}\left(\frac{D_{CNT}}{4L_{CNT}}\right)^2 \qquad (16)$$

Here $S_{CNT\_section}$ is the cross-section area of a SWCNT, S_{Sphere} is the sphere surface area, and D_{CNT} is SWCNT diameter. Note that a factor of 2 in the denominator is to remove the repeat count due to the two ends of a SWCNT.

Case 2. n_p>2, $\theta_p < \pi$. When more than two nanotubes form radially clustered structure at their ends, the first nanotube is free to place its un-joined end. The second nanotube is oriented at θ_p angle from the orientation of the first nanotube. Note that the second nanotube is free to rotate around the axis of the first nanotube, as illustrated in Figure 5.8 (The bold red ring). The possibility to orient the first two nanotubes is

$$P_{clustering}^{(2-p-I)} = \frac{S_{ring}^{(p)}}{2S_{Sphere}} = \frac{2\pi L_{CNT}\left(D_{CNT}\sin\theta_p\right)}{8\pi L_{CNT}^2} = \frac{D_{CNT}\sin\theta_p}{4L_{CNT}} \tag{17}$$

After fixing the first two nanotubes, the entire radial structure inside the volume element is indeed determined, given the uniform angular distribution condition. The remaining task is to fill the remaining $p-2$ nanotubes into the already-fixed $p-2$ orientations. There are $(p-2)!$ methods. Each of the $p-2$ nanotubes occupies an area of the nanotube cross-section. The probability of arranging the remaining $p-2$ nanotubes is evaluated as following:

$$\begin{aligned} P_{clustering}^{(2-p-II)} &= \frac{1}{(p-2)!}\left(\frac{S_{CNT\_section}}{2S_{Sphere}}\right)^{p-2} = \frac{1}{(p-2)!}\left(\frac{\pi\left(D_{CNT}/2\right)^2}{8\pi L_{CNT}^2}\right)^{p-2} \\ &= \frac{1}{(p-2)!}\left(\frac{D_{CNT}}{4\sqrt{2}L_{CNT}}\right)^{2p-4} \end{aligned} \tag{18}$$

The probability ($P_{clustering}^{(2-p)}$) for orienting n_p (n_p >2) nanotubes in a volume element equals to the product of equations (17) and (18).

$$P_{clustering}^{(2-p)} = P_{clustering}^{(2-p-I)} P_{clustering}^{(2-p-II)} = \frac{\sqrt{2}\sin\theta_p}{(p-2)!}\left(\frac{D_{CNT}}{4\sqrt{2}L_{CNT}}\right)^{2p-3} \tag{19}$$

Combine the cases when n_p>2 or n_p=2. This provides a complete expression to describe the probability ($P_{clustering}^{(2)}$) of step 2 to orient p nanotubes in a volume element, based on equations (16) and (19).

$$P_{clustering}^{(2)} = \begin{cases} \frac{1}{2}\left(\frac{D_{CNT}}{4L_{CNT}}\right)^2, p = 2 \\ \frac{\sqrt{2}\sin\theta_p}{(p-2)!}\left(\frac{D_{CNT}}{4\sqrt{2}L_{CNT}}\right)^{2p-3}, p > 2 \end{cases} \tag{20}$$

Based on steps 1 and 2 in this sub-section, the clustering probability ($P_{clustering}$) of arranging p nanotubes into a radially clustered configuration in a volume element is calculated from equations (15) and (20).

$$P_{clustering} = P_{clustering}^{(1)} P_{clustering}^{(2)} = \begin{cases} \frac{\pi p}{3}\left(\frac{d_i^{(2)}}{L_{CNT}}\right)^3\left(\frac{D_{CNT}}{4L_{CNT}}\right)^2, p = 2 \\ \frac{2\sqrt{2}\pi p}{3}\frac{\sin\theta_p}{(p-2)!}\left(\frac{d_i^{(2)}}{L_{CNT}}\right)^3\left(\frac{D_{CNT}}{4\sqrt{2}L_{CNT}}\right)^{2p-3}, p > 2 \end{cases} \tag{21}$$

Similar to the distributional entropy calculation, the clustering entropy is expressed as

$$\Delta S_{clustering} = n_p k \ln P_{clustering} = n_p k \begin{cases} \ln\left[\dfrac{\pi p}{3}\left(\dfrac{d_i^{(2)}}{L_{CNT}}\right)^3\left(\dfrac{D_{CNT}}{4L_{CNT}}\right)^2\right], p = 2 \\ \ln\left[\dfrac{2\sqrt{2}\pi p}{3}\dfrac{\sin\theta_p}{(p-2)!}\left(\dfrac{d_i^{(2)}}{L_{CNT}}\right)^3\left(\dfrac{D_{CNT}}{4\sqrt{2}L_{CNT}}\right)^{2p-3}\right], p > 2 \end{cases} \tag{22}$$

Note that there are n_p radial clustered structures in the SWCNTs network.

5.4. Gibbs free energy of SWCNTs network structure

After obtaining both energetic and entropic parts, the Gibbs free energy for SWCNTs network structure in equation (2) is rewritten here in equation (23).

$$\Delta G_{network} = n_p \Delta U_{cluster}^{(p)} - T\left(\Delta S_{distrib} + \Delta S_{clustering}\right) \tag{23}$$

Here $\Delta U_{cluster}^{(p)}$, the total energy of the small cluster domain containing p nanotube ends, is evaluated from the PMF data obtained in the atomistic simulations. Note $kT \approx 2.5$ kJ/mol at T =300 K, where k is Boltzmann constant. Denote $\overline{\Delta U}_{cluster}^{(p)} = \dfrac{\Delta U_{cluster}^{(p)}}{kT}$ the kT normalized Helmholtz free energy of the cluster of p nanotubes. N is the total number of SWCNTs in the network. Denote $\overline{\Delta G}_{network} = \dfrac{\Delta G_{network}}{NkT}$ the NkT averaged Gibbs free energy. Denote $\overline{\Delta S}_{configuraion} = \dfrac{\Delta S_{configuration}}{Nk}$, $\overline{\Delta S}_{distrib} = \dfrac{\Delta S_{distrib}}{Nk}$, $\overline{\Delta S}_{clustering} = \dfrac{\Delta S_{clustering}}{Nk}$ the Nk averaged configurational, distributional and clustering entropies, respectively. Equation (23) is expressed as follows:

$$\overline{\Delta G}_{network} = \gamma_p \overline{\Delta U}^{(p)}_{cluster} - \left(\overline{\Delta S}_{distrib} + \overline{\Delta S}_{clustering} \right) \tag{24a}$$

$$\overline{\Delta G}_{network} = \frac{\Delta G_{network}}{NkT} \tag{24b}$$

$$\overline{\Delta U}^{(p)}_{cluster} = \frac{\Delta U^{(p)}_{cluster}}{kT} \tag{24c}$$

$$\begin{aligned} \overline{\Delta S}_{distrib} = \frac{\Delta S_{distrib}}{Nk} = \frac{1}{\alpha}\ln\frac{1}{\alpha} + \ln\frac{\alpha}{p} + \left(\frac{p}{\alpha} - 1\right)\ln\left(1 - \frac{\alpha}{p}\right) - \gamma_p \ln(p!) - \gamma_p \ln\gamma_p \\ - \left(\frac{1}{\alpha} - 1 + (p-1)\gamma_p\right)\ln\left(\frac{1}{\alpha} - 1 + (p-1)\gamma_p\right) - \left(1 - p\gamma_p\right)\ln\left(1 - p\gamma_p\right) \end{aligned} \tag{24d}$$

$$\overline{\Delta S}_{clustering} = \frac{\Delta S_{clustering}}{Nk} = p\gamma_p \begin{cases} \ln\left[\frac{\pi}{3}\left(\frac{d_i^{(2)}}{L_{CNT}}\right)^3 \left(\frac{D_{CNT}}{4L_{CNT}}\right)^2\right], p = 2 \\ \ln\left[\frac{2\sqrt{2}\pi p}{3}\frac{\sin\theta_p}{(p-2)!}\left(\frac{d_i^{(2)}}{L_{CNT}}\right)^3 \left(\frac{D_{CNT}}{4\sqrt{2}L_{CNT}}\right)^{2p-3}\right], p > 2 \end{cases} \tag{24e}$$

Note that all the state functions in (24a) are dimensionless, and are averaged by N, the total number of nanotubes in the network of volume V.

Equation (24) was used to analyze the relationship between the Gibbs free energy and the number of nanotubes per cluster. D_{CNT} =1.4 nm is the SWCNT diameter. For a single-walled carbon nanotube, the molecular weight (MW_{SWCNT}) can be calculated as follows:

$$MW_{SWCNT} = L_{CNT}\rho + 2N_{end}MW_{HEG} \tag{25}$$

Here $\rho = 2.212 \times 10^3 g/nm/mol$ is the linear density of 1.4 nm diameter SWCNTs, $N_{end} = 46$ is the number of possible functionalization sites at each of the two nanotube ends, $MW_{HEG} = 340 g/mol$ is the molecular weight of the attached hexaethylene glycol linker, and L_{CNT} = 65 nm is the average SWCNTs length taken from the length distribution in Chapter 3 (Figure 3.2). A 65 nm long SWCNT with 1.4 nm diameter and end functionalities has a molecular weight (MW_{SWCNT}) of 175060 g/mol, as calculated from equation (25). Effective $\Delta U_{cluster}^{(p)}$ is estimated from the potential of mean force (PMF) of the atomistic simulations in Figure 5.3. The diameter ($d_i^{(p)}$) of the effective spherical interaction volume ($V_i^{(p)}$) is used to evaluate the effective energy contribution from each nanotube in the cluster domain. $\alpha = \frac{N}{M}$ is calculated based on the SWCNTs concentration.

$$\alpha = \frac{N}{M} = \frac{c_{SWCNTs} \times 10^{-3} / MW_{SWCNT} \times A_{mol}}{1 \times 10^{-6} / \left(\frac{4}{3} \pi L_{CNT}^3\right)} \tag{26}$$

Here c_{SWCNTs}, with a unit of mg/mL, is the concentration of SWCNTs in water. $A_{mol} = 6.022 \times 10^{23} / mol$ is the Avogadro constant.

For a small SWCNTs concentration, 0.01 mg/mL, $\alpha = 0.039$. When all nanotubes form clusters ($pn_p = N$), the calculated Gibbs free energy and its components are plotted (Figure 5.10) verses p, the number of SWCNTs per cluster.

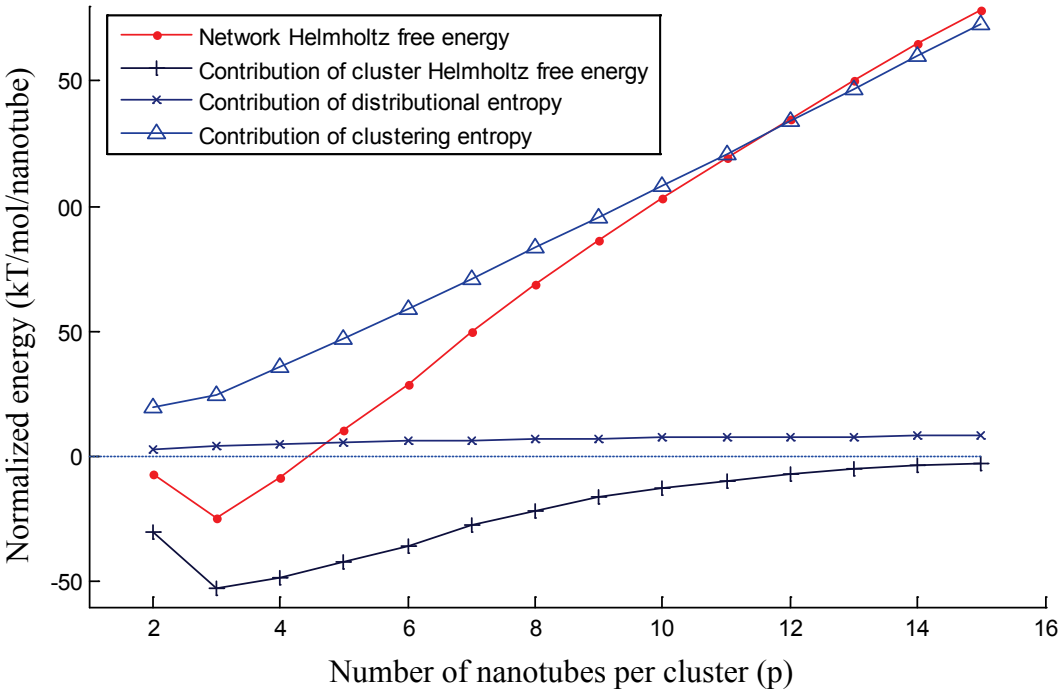

Figure 5.10. Helmholtz free energy and its energetic and entropic components (0.01 mg/mL). A horizontal dashed line (x=0) is drawn as reference.

The network Gibbs free energy is most negative when the cluster is formed by three nanotubes, indicating the most stable configuration. When only a few nanotubes form a radially clustered shape, the energetic contribution from the cluster is larger than the entropic counterparts combined. The Gibbs free energy is negative when p =2, 3 and 4, indicating stable network structures. This agrees with the experimental observations that 72% of the joints (clusters) are formed by 3 nanotubes. Note that the experimental result was counted from the 2D network structure that formed when the 3D network structure collapsed. When more nanotubes join together, their interaction volume increases, resulting in the decrease of energetic portion. The entropic energies increase quickly, on the contrary, when more nanotubes form the radially clustered

shape in one volume element. The network Gibbs free energy becomes positive when $p \geq 5$.

The contributions to $\overline{\Delta G}_{network}$ from both distributional entropy and clustering entropy increase when more nanotubes form a radially clustered structure, as expected. The clustering entropy is over ten times larger than the distributional entropy, as seen from the graph. One reason for this could be due to the large aspect ratio (~48) of the 1D nanotube. Entropically, arranging p nanotubes into a radially clustered shape is much less favorable compared with distributing every p nanotubes closely together in a volume element. The influence of the SWCNTs concentration is discussed in the following section.

5.5. Effect of SWCNTs concentration on the Gibbs free energy

Now we discuss the effect of SWCNTs' concentration on the SWCNTs' network Gibbs free energy ($\overline{\Delta G}_{network}$). When SWCNTs' concentration (c_{SWCNTs}) varies, only the distributional entropy will change, as can be seen from equation (24). The energetic contribution from cluster domains and the clustering entropy do not vary with SWCNTs' concentration, the effect of which on distributional entropy is discussed in the following.

Note that SWCNTs concentration (c_{SWCNTs}) may increase such that $\alpha = \frac{N}{M}$ is larger than 1, indicating a saturated state when placing N nanotubes into M volume

elements. When $n \le \alpha = \frac{N}{M} < n+1$, where n is integer, the SWCNTs status is defined as the n^{th} saturated state of SWCNTs. In the n^{th} saturated state, each volume element is expected to accommodate at least $n+1$ nanotubes, otherwise the SWCNTs will precipitate. Hence, in n^{th} saturated state, the free energy change is studied when $p = n+1$ or more nanotubes form a cluster in each volume element. Hence $p > \frac{N}{M}$.

When $\alpha = \frac{N}{M} \gg 1$, SWCNTs are likely to precipitate until a lower concentration is reached.

Note that the entropies are state functions. The distributional entropy ($\Delta S_{distrib}$) obtained in equation (11a) is calculated by subtracting the random-state entropy from the orderly-distributed entropy. Equations (11) and (13) are rewritten here as equation (27).

$$\begin{aligned}\Delta S_{distrib} &= S_{orderly} - S_{random} \\ &= Nk\left\{\frac{1}{\alpha}\ln\frac{1}{\alpha} + \ln\frac{\alpha}{p} + \left(\frac{p}{\alpha}-1\right)\ln\left(1-\frac{\alpha}{p}\right) - \left(1-p\gamma_p\right)\ln\left(1-p\gamma_p\right)\right. \\ &\left. -\gamma_p \ln\gamma_p - \left(\frac{1}{\alpha}-1+\left(p-1\right)\gamma_p\right)\ln\left(\frac{1}{\alpha}-1+\left(p-1\right)\gamma_p\right) - \gamma_p \ln(p!)\right\}\end{aligned} \quad (27a)$$

$$S_{random} = k\ln\left(A_{random}\right) = k\ln\left(\frac{(pM)!}{(pM-N)!}\right) \quad (27b)$$

Note when SWCNTs' concentration changes, the entropies should be compared with regard to the same space volume. However, when the concentration (c_{SWCNTs}) changes, the total number (N) of SWCNTs changes for the given volume.

For SWCNTs in a certain volume V, the random-state entropy (S_{random}), used as a reference state, changes with N, as indicated by equation (27b). Hence S_{random} changes with c_{SWCNTs}, which is undesired. To analyze the distributional entropy change as a function of SWCNTs concentration, it is necessary to have a constant reference.

Equation (27b) is recalculated for different SWCNTs concentrations. Denote $c_{SWCNTs}^{(0)}$ as a reference SWCNT concentration. Denote a as a concentration parameter, such that

$$c_{SWCNTs} = a \cdot c_{SWCNTs}^{(0)} \tag{28}$$

Denote N_0 as the total number of SWCNTs in the volume V for the reference concentration ($c_{SWCNTs}^{(0)}$). Then $N = aN_0$ is the total number of SWCNTs in the same volume V for a concentration c_{SWCNTs}.

S_{random} may be expressed as a function of a.

$$S_{random}(c_{SWCNTs}) = k \ln\left(\frac{(pM)!}{(pM - aN_0)!}\right) \tag{29a}$$

Recall that $\alpha = \frac{N}{M} = a\alpha_0$ is a function of a. After the Stirling approximation and separation of variables, equation (29a) becomes

$$S_{random}(c_{SWCNTs}) = Nk\left\{\frac{p}{\alpha}\ln\left(\frac{p}{\alpha}\right) - \left(\frac{p}{\alpha} - 1\right)\ln\left(\frac{p}{\alpha} - 1\right) + \ln a + \ln N_0\right\} \tag{29b}$$

Here α and a are both functions of c_{SWCNTs}. Note that for n^{th} saturated state, the only cases considered are when $p = n + 1$ or more nanotubes form a cluster in each

volume element. So $pM - aN_0 \gg 1$, although $pM \sim aN_0$. $M \sim 10^{15}$ for 65 nm long SWCNTs in a volume of 1 mL.

Dividing equation (29b) by Nk provides the average random state entropy per nanotube $\overline{S}_{random}(c_{SWCNTs})$.

$$\overline{S}_{random}(c_{SWCNTs}) = \frac{S_{random}(c_{SWCNTs})}{Nk} = \frac{p}{\alpha}\ln\left(\frac{p}{\alpha}\right) - \left(\frac{p}{\alpha} - 1\right)\ln\left(\frac{p}{\alpha} - 1\right) + \ln a + \ln N_0 \tag{30}$$

Denote $\overline{\Delta S}_{random}(c_{SWCNTs}) = \overline{S}_{random}(c_{SWCNTs}) - \ln N_0$.

$$\overline{\Delta S}_{random}(c_{SWCNTs}) = \frac{p}{\alpha}\ln\left(\frac{p}{\alpha}\right) - \left(\frac{p}{\alpha} - 1\right)\ln\left(\frac{p}{\alpha} - 1\right) + \ln a \tag{31}$$

Now there is an expression for the random state entropy change due to the SWCNTs concentration change.

Combine this with the distributional entropy change in equation (24d), and the revised distributional entropy change ($\overline{\Delta S}^{*}_{distrib}(c_{SWCNTs})$) of SWCNTs' network structure for different concentrations may be compared.

$$\overline{\Delta S}^{*}_{distrib}(c_{SWCNTs}) = a\overline{\Delta S}_{distrib} + a\overline{\Delta S}_{random}(c_{SWCNTs}) \tag{32}$$

Note that both $\overline{\Delta S}_{distrib}$ and $\overline{\Delta S}_{random}(c_{SWCNTs})$ are per nanotube. However, when SWCNTs concentration changes, the number of SWCNTs per unit volume changes by a factor of a, where $a = c_{SWCNTs} \big/ c^{(0)}_{SWCNTs}$.

The energy contribution of the revised distributional entropy ($\overline{\Delta S}^{*}_{distrib}(c_{SWCNTs})$) and its components ($a\overline{\Delta S}_{random}(c_{SWCNTs})$ and $a\overline{\Delta S}_{distrib}$) for different SWCNTs' concentrations are calculated and plotted in Figure 5.11 (A), (B) and (C), respectively.

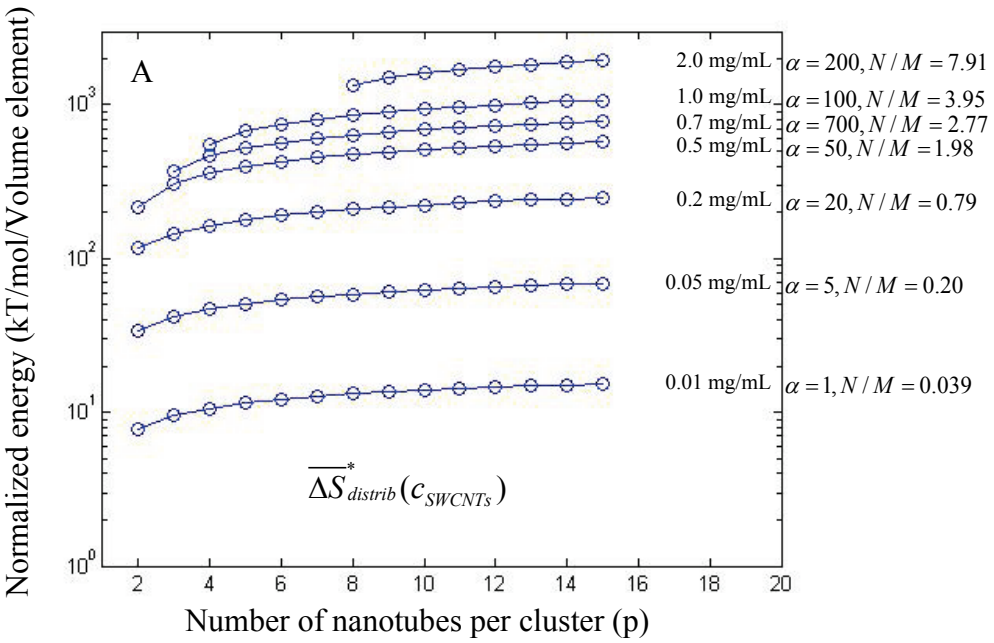

Figure 5.11. Energy contribution of (A) distributional entropies ($\overline{\Delta S}^{*}_{distrib}(c_{SWCNTs})$) and its components (B) $\overline{\Delta S}_{distrib}$ and (C) $\overline{\Delta S}_{random}(c_{SWCNTs})$ for different SWCNTs concentrations. The entropies are defined in equation (32).

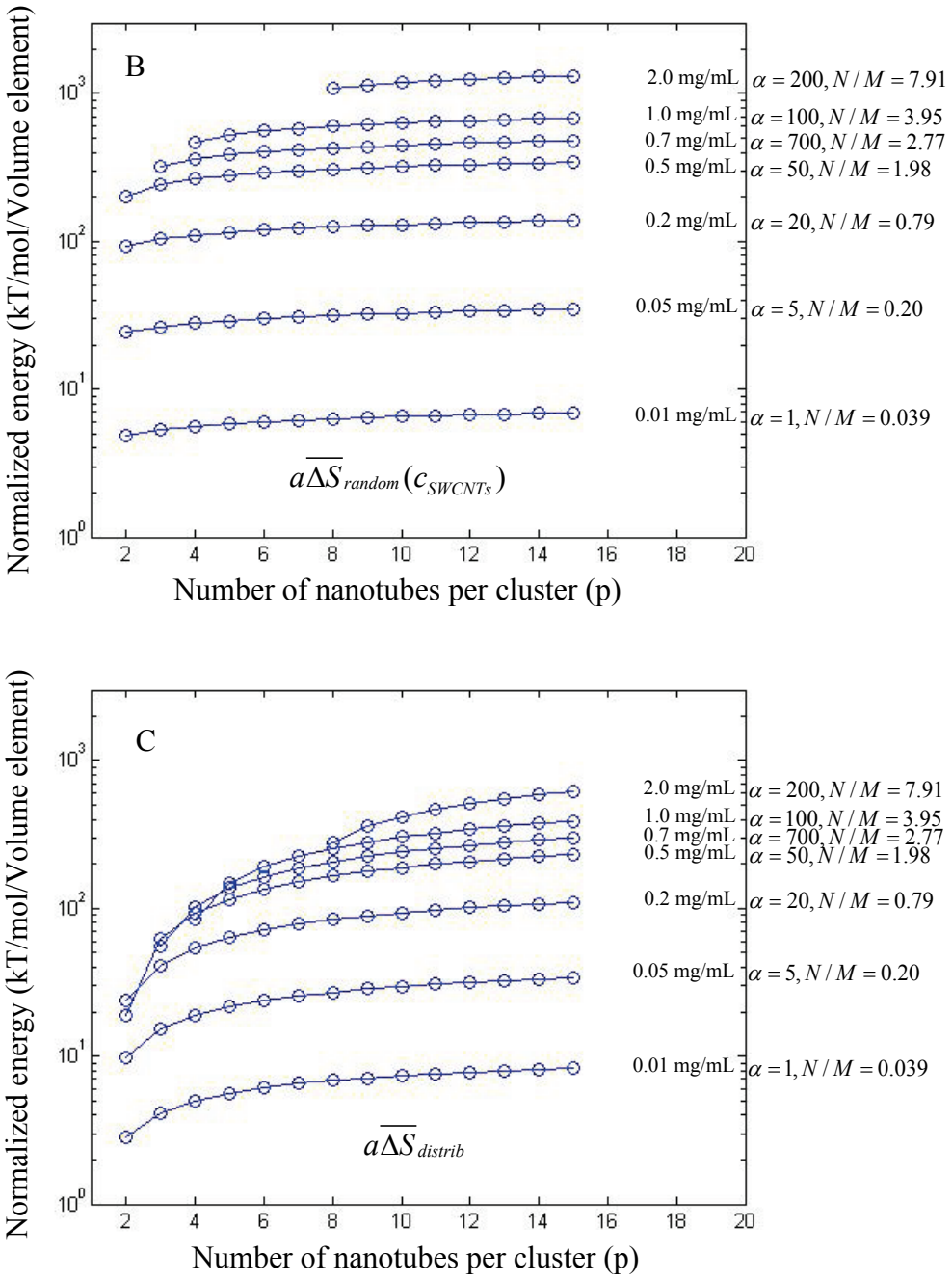

Figure 5.11. Continued.

Figure 5.11 (A) reveals the revised change in distributional entropy ($\overline{\Delta S}^{*}_{distrib}(c_{SWCNTs})$) of SWCNTs for different concentrations. $\overline{\Delta S}^{*}_{distrib}(c_{SWCNTs})$ increases

with c_{SWCNTs} and p. Note the number of SWCNTs increases by a factor of a in the volume. For large concentrations, when $n \le \alpha = \frac{N}{M} < n+1$, and n is integer, only the situations with $p \ge n+1$ are calculated. $\overline{\Delta S}_{random}(c_{SWCNTs})$ is generally larger than $\overline{\Delta S}_{distrib}$ for same set of c_{SWCNTs} and p, as indicated by Figure 5.11 (B) and (C). Figure 5.11 (B) illustrates $\overline{\Delta S}_{random}(c_{SWCNTs})$ also increases with c_{SWCNTs} and p. The increase in SWCNTs results in the increase of the random state entropy, as expected.

$\overline{\Delta S}_{distrib}$ generally increases with c_{SWCNTs} and p, as exhibited in Figure 5.11 (C). However, it reveals an interesting behavior when $\frac{N}{M}$ approaches an integer value, indicating a saturated state. For example, when $\frac{N}{M} = 1.98$ (0.5 mg/mL) and $p = 2$, the corresponding $\overline{\Delta S}_{distrib}$ is smaller than that when $\frac{N}{M} = 0.79$ (0.2 mg/mL). This indicates a local entropy minimum at $\frac{N}{M} = 2$. The reason is that, when $\frac{N}{M} = 1.98$ (0.5 mg/mL), placing every 2 nanotubes in one volume element promotes a state very similar to their random distributions. Hence, the distributional entropy change ($\overline{\Delta S}_{distrib}$) from the random state is small. In the other case when $\frac{N}{M} = 0.79$ (0.2 mg/mL), placing every 2 nanotubes in one volume element deviates substantially from the random distributed state, and is thus less favored. Similar trends are observed when $\frac{N}{M}$ =2.77, 3.95 and 7.91. Note that $\frac{N}{M} = 2.77$ corresponds to a SWCNTs'

concentration of 0.7 mg/mL, which was used in the experiments. This result indicates that, for 0.7 mg/mL SWCNTs, a stable radially clustered structure could form by three nanotubes, in agreement with experimental observations (Figure 3.3).

5.6. Attempts to coarse-grain SWCNTs and associate Monte Carlo simulations

Preliminary Monte Carlo simulations were conducted to facilitate understanding of many-SWCNTs behavior. SWCNTs were modeled with a coarse-graining method using the PMF obtained from atomistic simulations.

A single-walled carbon nanotube was treated as a set of beads with radius R. The geometry is indicated in Figure 5.12. The beads are divided into two groups: wall bead (WB) and end bead (EB). A wall bead represents a 1.357 nm nanotube sidewall segment. An end bead represents a 1.357 nm nanotube end segment and the attached functional groups. In this example, 48 WBs and 2 EBs are linearly fixed to represent a rigid, 66.5 nm long single-walled nanotube with end functional groups. The beads are closely placed next to each other and are centered at the nanotube axis.

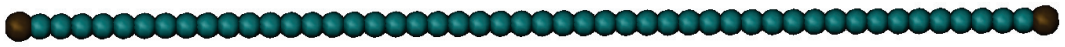

Figure 5.12. Schematic illustration of a coarse-grained SWCNT. The two beads at the ends represent the functionalized nanotube segments. Other beads represent the carbon nanotube sidewalls.

In a preliminary approach, three major types of interactions are described among the two types of beads: the interaction between two WBs is described by the HSR-HSR PMF obtained from atomistic simulations in section 5.2 (Figure 5.6); the interaction between two EBs is described by the HER-HER PMF; and, the interaction between a EB and a WB is described by the HER-HSR PMF.

The total interaction energy of many SWCNTs in a simulation box, U_{tot}, is given by the sum of inter-bead potentials:

$$U_{tot} = \sum_{i,j>i} U_{i,j} \tag{32}$$

Here $U_{i,j}$ is the interaction potential between beads i and j belonging to the different nanotubes.

To understand SWCNTs behavior, randomly distributed nanotubes are subject to Monte Carlo movements: displacement and rotation. In the displacement move, one nanotube is randomly chosen, and all the beads of the nanotube are displaced along a random vector. The x, y and z components of the displacement vector are sampled from a uniform distribution ranging from –0.2 nm to +0.2 nm. In the rotation move, one nanotube is randomly chosen to rotate a small random angle ($\Delta\varphi$) around either the x or y axis. $\Delta\varphi$ is sampled from a uniform distribution $-4.4° < \Delta\varphi < +4.4°$. All beads of the nanotube are rotated around the center of the nanotube. The sample sizes for both displacement and rotations are small due to the large aspect ratio of SWCNTs. The move is accepted using the standard Metropolis acceptance criterion:

$$p_{acc} = \min\left[1, \exp\left(-\Delta U_{tot}/kT\right)\right] \tag{33}$$

Here ΔU_{tot} is the change in the total energy upon movement, k is Boltzmann constant, and T is absolute temperature.

A molecular simulation package was adopted (Maitra, 2008) for the MC simulations. A Monte Carlo integrator code was integrated into the simulation package to study the coarse-grained SWCNTs behavior. Periodic boundary conditions for the nanotube mass center were applied to the simulation box.

In a typical MC procedure, 74 coarse-grained SWCNTs are generated and randomly distributed in a 300 × 300 × 300 nm^3 box, representing a 0.7 mg/mL concentration. The system was simulated for 1×10^7 MC steps. The total energy is plotted in Figure 5.13.

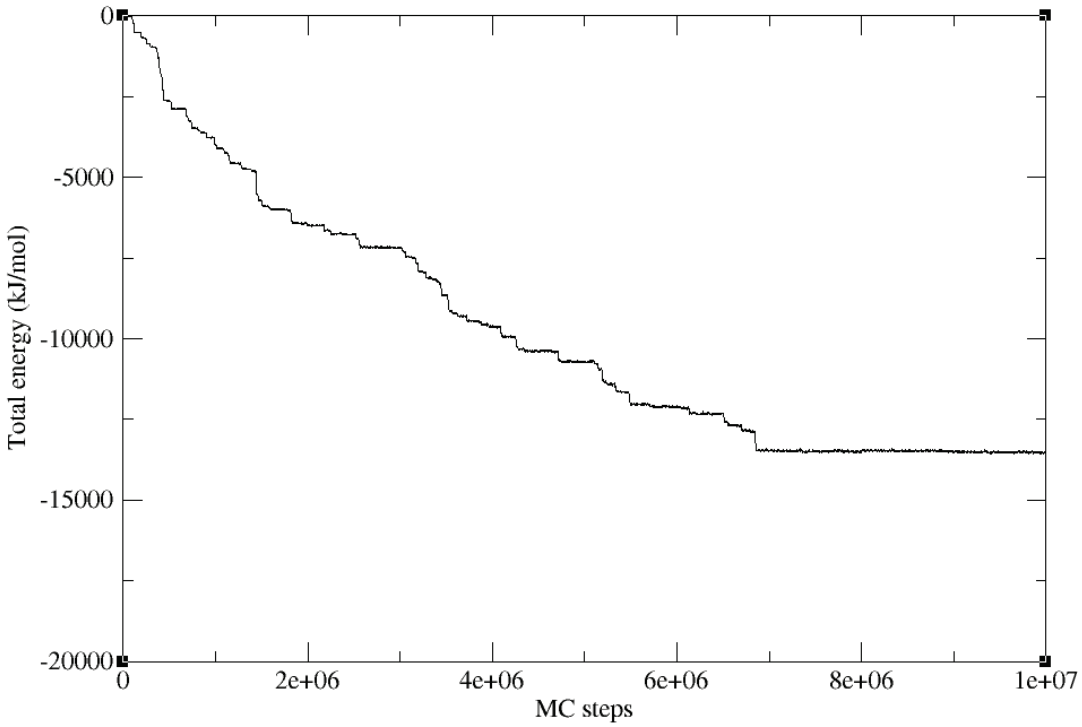

Figure 5.13. Total energy of the SWCNTs system in a MC simulation.

The system total energy decreases gradually and becomes constant after ~7×10^6 MC steps, indicating the SWCNTs system experienced a long equilibration period. After 7×10^6 MC steps SWCNTs structural configuration becomes stable, as compared with their behavior at the beginning of the simulation. After the SWCNTs reach equilibrium, the *NkT* averaged total energy of the SWCNTs is about -73 $mol^{-1}nanotube^{-1}$. The normalized total energy is comparable to -52 $mol^{-1}nanotube^{-1}$, the energetic contribution from the inter-nanotube interaction as calculated from energy analysis in section 5.4. The difference may due to the SWCNTs bundling, which will lower the total energy.

After the SWCNTs configuration reaches equilibrium, the majority of nanotubes are clustered. Several bundles and isolated nanotubes are identified. The majority of clusters are formed by two or three nanotubes, as seen from the snapshot in Figure 5.14. Different types of clusters were observed: those formed at the ends of individual nanotubes; those formed with bundled or semi-bundled nanotubes; and those not formed at the associated ends of the nanotubes. Interconnections were observed between clusters. The complexity of the nanotube interactions renders the configuration characterization and quantitative analysis very difficult. The preliminary MC simulations in this dissertation focus on the qualitative characteristics of the SWCNTs clustering and interconnection.

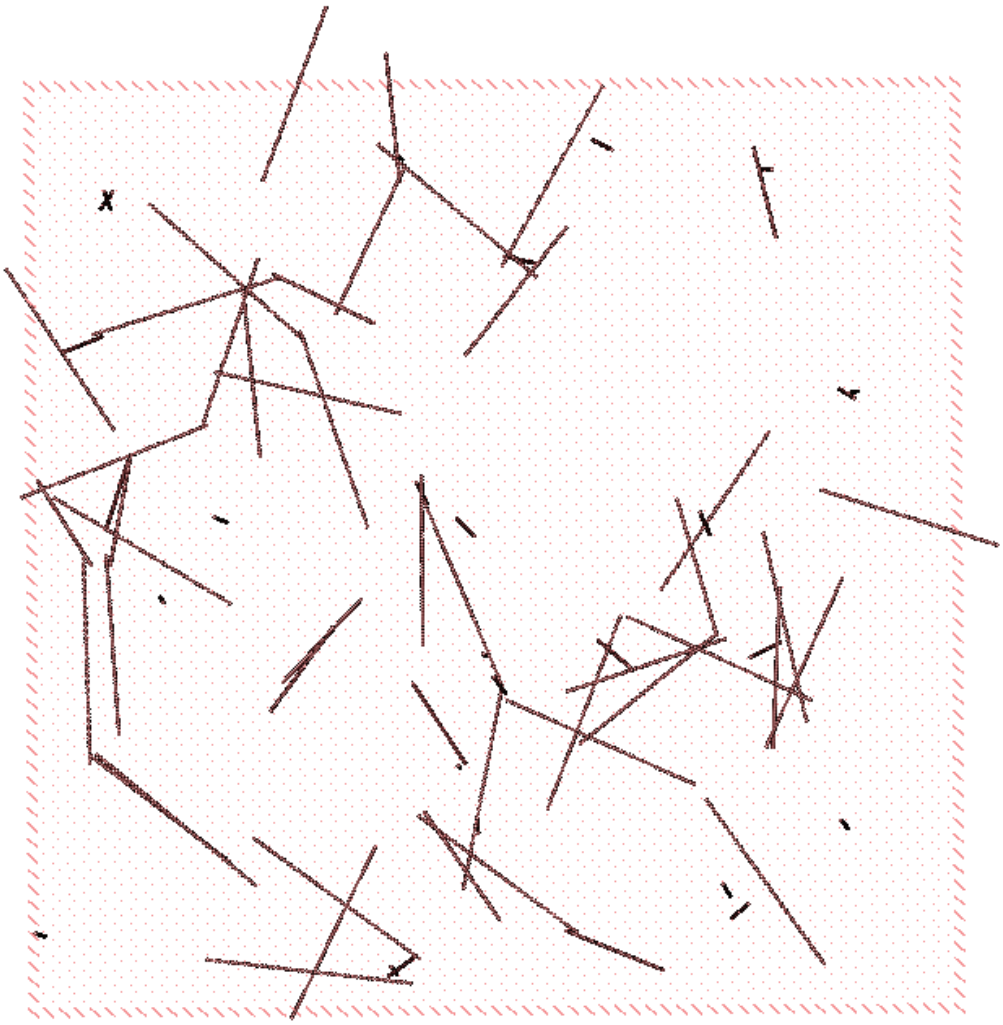

Figure 5.14. 2D projection of the snapshot of 74 SWCNTs in 300×300×300 nm^3 box after 7×10^6 MC steps. The thick lines are the SWCNTs. The small dots represent the simulation box, keeping periodic boundary condition in mind. Both clusters and bundles are observed.

5.7. Concluding remarks

In summary, Chapter 5 systematically analyzed the Gibbs free energy of SWCNTs' network structures. Both analytical tools and numerical simulations were

applied to facilitate the analysis. The results indicate that, when 2, 3 or 4 SWCNTs joined together and form a cluster at their ends, the resulting network was energetically stable. When a cluster is formed by more than 4 nanotubes, the entropic influence dominates and prevents the formation of a stable network structure. The analysis agrees with the experiment observation that 72% of the clusters were formed by 3 nanotubes. The effect of SWCNTs' concentration to the network Gibbs free energy is also discussed.

Coarse-graining models were attempted to describe SWCNTs, and preliminary Monte Carlo simulations were conducted for many nanotubes. Clustering was observed as SWCNTs primary configurations after system equilibration. Most of the clusters are formed by two or three nanotubes.

5.8. Acknowledgement

I would like to thank Dr. Arijit Maitra for providing me with his molecular simulation codes upon which the Monte Carlo integrator was built. I am grateful to Dr. Arijit Maitra for many helpful discussions regarding the molecular modeling and numerical simulations. Finally, I would like to express my most sincere appreciation to Dr. Alireza V. Amirkhizi for many helpful discussions regarding the Gibbs free energy analysis. The author acknowledges computer time on the Granite supercomputing cluster of the Bioengineering Department at UCSD.

5.9. References

G. Arya (2009). "Energetic and entropic forces governing the attraction between polyelectrolyte grafted colloids." Phys. Chem. B, Vol.113, 15760-15770.

T. Jue (2010). "Biomedical Applications of Biophysics (Handbook of Modern Biophysics), first edition." Humana Press, New Jersey.

A. D. Mackerel (2004). "Empiracol force fields for biological macromolecules: overview and issues." J. Comput. Chem., Vol.25, 1584-1604.

S. O. Nielsen, C. F. Lopez, G. Srinivas and M, L (2004). "Coarse grain models and the computer simulation of soft materials." J. Phys.: Condens. Matter., Vol.16, R481-R512.

U. Burkert and N. L. Allinger (1989). "Molecular Mechanics." American Chemical Society, Washington, DC.

M. Van Voorst Tot Voorst (2008). "Large-Scale Disasters: Prediction, Control and Mitigation ." Mohamed Gad-el-Hak (ed.). Cambridge University Press , NY.

E. Nativ-Roth, R. Shvartzman-Cohen, C. Bounioux, M. Florent, D. Zhang, I. Szleifer and R. Yerushalmi-Rozen (2007). "Physical Adsorption of Block Copolymers to SWNT and MWNT: A Nonwrapping Mechanism." Macromolecules, Vol.40(10), 3676-3685.

E. J. Wallace, M. S. P. Sansom (2007). "Carbon Nanotube/Detergent Interactions via Coarse-Grained Molecular Dynamics." Nano Lett., Vol.7(7), 1923-1928.

C. Song, Y. Xia, M. Zhao, X. Liu, B. Huang, F. Li and Y. Ji (2005). "Self-assembly of base-functionalized carbon nanotubes." Phys. Rev. B, Vol.72, 165430.

T. Duren and F. J. Keil (2001). "Molecular Modeling of Adsorption in Carbon Nanotubes."Chem. Eng. Technol., Vol.24(7), 698-702.

I. Gurevitcha and S. Srebnik (2008). "Conformational behavior of polymers adsorbed on nanotubes." J. Chem. Phys. Vol.128, 144901.

S. Zou, D. Maspoch, Y. Wang, C. A. Mirkin and G. C. Schatz (2007). "Rings of Single-Walled Carbon Nanotubes: Molecular-Template Directed Assembly and Monte Carlo Modeling." Nano Lett., Vol.7(2), 276-280.

P. Angelikopoulos and H. Bock (2008). "Directed Self-Assembly of Surfactants in Carbon Nanotube Materials." J. Phys. Chem. B, 2008, Vol.112(44), 13793–13801.

W. L. Jorgensen and J. Tirado-Rives (1988). "The OPLS Force Field for Proteins. Energy Minimizations for Crystals of Cyclic Peptides and Crambin." J. Am. Chem. Soc., Vol.110, 1657–1666.

W. L. Jorgensen, D. S. Maxwell and J. Tirado-Rives (1996). "Development and Testing of the OPLS All-Atom Force Field on Conformational Energetics and Properties of Organic Liquids." J. Am. Chem. Soc., Vol.118(45), 11225–11236.

O. Borodin, G. D. Smith and R. Douglas (2003). “Force Field Development and Molecular Dynamics Simulations of Poly(ethylene Oxide)/LiF4 Polymer Electrolytes.” J. Phys. Chem. B, Vol.107, 6824-6837.

O. Borodin, R. Douglas, G. D. Smith, F. Trouw and S. Petrucci (2003). “Molecular Dynamics Simulations and Experimental Study of Structure, Dynamics and Thermodynamics of Poly(ethylene Oxide) and Its Oligomers.” J. Phys. Chem. B, Vol.107, 6813-6823.

J. T. Frey and D. J. Doren, TubeGen 3.3, University of Delaware, Newark DE, 2005. (web-interface, http://turin.nss.udel.edu/research/tubegenonline.html)

D. Tom, Y. Darrin and P. Lee (1993). "Particle mesh Ewald: an N [center-dot] log(N) method for Ewald sums in large systems." J. Chem. Phys., Vol.98, 10089–10092.

S. Nose (1984). "A unified formulation of the constant temperature molecular-dynamics methods." J. chem. phys., Vol.81(1), 511–519.

W. G. Hoover (1985). "Canonical dynamics: Equilibrium phase-space distributions." Phys. Rev. A, Vol.31(3), 1695–1697.

B. Hess, H. Bekker, H. J. C. Berendsen and J. Fraaije (1997). "LINCS: a linear constraint solver for molecular simulations." J. Comp. Chem., Vol.18, 1463–1472.

A. Maitra (2008). Molecular simulation program package, unpublished work.

Chapter 6

Conclusions and Future Research

6.1. Self-assembled SWCNTs in aqueous electrolyte solution

The results presented in this dissertation have illustrated the novel self-assembling behavior of short， end-functionalized single-walled carbon nanotubes (SWCNTs). Short SWCNTs (50–100 nm) have been functionalized with hexaethylene glycol (HEG) chains at the ends. The other termini of the HEG chains were modified to bear carboxylic anions. When the functionalized short SWCNTs were placed in aqueous electrolyte (sodium ion), they automatically clustered at the ends via ionic driving force and self-assembled into network structures. A simple model was built based on essential physical factors to understand SWCNTs self-assembling behavior and to provide guidance for the fabrication. The existence of the network structure has been established by electron microscopy. A free energy analysis has been implemented, and excellent agreement has been obtained with the experiment observations. Molecular simulations have been conducted to assist the free energy analysis. Monte Carlo simulations have been attempted to understand SWCNTs self-assembling behavior.

The presented set of theoretical, experimental and numerical tools may offer a solution to systematically establish mass manipulation of single-walled carbon nanotubes, which has been a bottleneck for practical applications of SWCNTs.

6.2. Future work

This section briefly touches on a few areas for future research on this topic.

The electron tomography method may be improved to better characterize the three-dimensional (3D) network structures of SWCNTs. Low electron contrast of the carbon nanotubes embedded in polymer resin is the major obstacle for a clear 3D profile. Heavy metal staining could provide additional electron contrast to the carbon nanotubes. However, it blurs the nanotubes themselves due to the small diameter of the SWCNTs. One may think of alternate embedding material or staining methods to help distinguish single-walled carbon nanotubes from surrounding materials during the electron imaging process.

Monte Carlo simulations of coarse-grained SWCNTs could be extended to reflect more physical conditions. For example, the interaction between two nanotube ends could vary according to their angular relationships. A finer coarse-graining approach might be performed for the nanotube end functionalization domain to provide more accurate results.